IMPROVING REGIONAL HYDROLOGICAL SIMULATIONS BY ACCOUNTING FOR CLIMATE FORCING UNCERTAINTY AND HUMAN IMPACTS

By

Tamanna Kabir

A DISSERTATION

Submitted to
Michigan State University
in partial fulfillment of the requirements
for the degree of

Civil Engineering – Doctor of Philosophy

2023

ABSTRACT

Advancing the understanding of the changes in various water budget components is crucial for improved water resource assessment and management at the global, continental, and river basin scales. This is important, especially because the intensified hydrologic dynamics due to climate change and accelerated human activities are altering the terrestrial water cycle in unprecedented ways and over a range of scales. Land surface models (LSMs) are widely used to investigate the changes in water resources resulting from natural and human-induced alterations. However, these models are subject to inherent uncertainties, including those associated with climate forcing and model parameterizations. Therefore, there is an urgent need to address climate forcing induced uncertainties in hydrological simulations using process based LSMs. In addition, representing human impacts such as irrigation and groundwater pumping in LSMs is critical for improving hydrological simulations. This dissertation advances regional hydrological simulation, addressing climate forcing uncertainty, by leveraging the potential of emerging satellite data and using an advanced LSM. A comprehensive analysis is conducted using a fully-process based LSM to examine the propagation of precipitation uncertainty into hydrological simulations over the Mekong River Basin (MRB). The Community Land Model version 5 (CLM5) at a relatively high spatial resolution of 0.05° (~5 km) and without any parameter calibration is implemented. Simulations conducted using different precipitation datasets are compared to investigate the discrepancies in streamflow, terrestrial water storage (TWS), soil moisture, and evapotranspiration (ET). Furthermore, this dissertation advances the simulation of basin wide groundwater dynamics in the MRB, providing key insights on the evolving groundwater system and improving process-based groundwater modeling capabilities by implementing CLM5 with groundwater and irrigation parameterizations. An in-depth analysis is

conducted to examine groundwater mechanisms in the MRB, focusing on groundwater flow processes that are modulated by climate variability and physiographic features, and primary drivers of groundwater-surface water interactions. Further, the influence of extensive irrigation and groundwater pumping on groundwater dynamics is quantified. Finally, global drought recovery and its drivers across different climate zones and biodiversity hotspots are investigated using multi-model hydrological simulations, enhancing the understanding of future drought risk and ecosystem resilience. The key findings from the aforementioned multi-scale analyses are: (1) precipitation is a key determinant of simulated streamflow and peak flow is particularly sensitive to precipitation input; notable differences are also found among TWS, soil moisture, and ET simulated using different precipitation products. (2) Precipitation data with a higher spatial resolution did not improve the simulations, contrary to the common perception that using meteorological forcing with higher spatial resolution would improve hydrological simulations. (3) High spatial heterogeneity in groundwater recharge and discharge across the MRB is governed by climate and subsurface characteristics; a pronounced seasonality is found in groundwater recharge; with substantial carryover to the consecutive dry season that alleviates soil moisture. (4) Groundwater discharge is a dominant source of streamflow all year round, and irrigation pumping is directly altering groundwater flows and storages. (5) Climate variability smoothens pumping effects over long times, but the model simulates region-wide groundwater depletion in the Mekong Delta during dry years. (6) The drought recovery time varies considerably across different climate regions globally, and there has been a notable increase in drought recovery time over the last few decades. This dissertation provides crucial insights on precipitation-induced uncertainties in hydrological modeling, also advancing process-based groundwater modeling capabilities for regional scale application.

Dedicated to my beloved parents and husband.

ACKNOWLEDGEMENTS

I would like to express my gratitude to all who have contributed to my Ph.D. research. First and foremost, I am deeply grateful to my Ph.D. advisor, Dr. Yadu Pokhrel, for his great mentoring, support, illuminating guidance and encouragement throughout my doctoral program. This dissertation would not have been possible without his help, and I am grateful that I had the opportunity to work with him. I would also like to express my great appreciation to my committee members, Dr. Shu-Guang Li, Dr. Phanikumar Mantha, and Dr. Jiaguo Qi for their persistent help and meticulous comments and suggestions. This dissertation was partially supported by the National Science Foundation (Awards #: 1752729 and 2127643) and NASA (Award # 80NSSC17K0259). I gratefully acknowledge the high-performance computing support from the Institute for Cyber Enabled Research at Michigan State University and Cheyenne provided by NCAR's Computational and Information Systems Laboratory (doi:10.5065/D6RX99HX). I thankfully acknowledge Dr. Farshid Felfelani, my co-author in Chapter 2 and chapter 3, for being critical to my research and providing helpful comments. I am thankful to Mekong River Commission for providing streamflow data. I am thankful to my dear friends and colleagues Sanghoon Shin, Suyog Chaudhari, Mateo Burbano, Huy Dang, Omid Bagheri, Amar Deep Tiwari, Ahmed Elkouk and Tanjila Akhter for their fruitful discussions and spending cheerful time together. I wish to express my most special appreciation to my dear parents, Kabir and Kamrunnahar, and to my lovely sister, Tanha and brother Nadbi, for all the love they have given me and for helping me to shape my life.

TABLE OF CONTENTS

Chapter 1. Introduction

1.1 Research Motivation

1.1.1 Addressing Climate Forcing Uncertainty in Land Surface Models (LSM)

An improved understanding of water balance is crucial for water resources assessment and management at the global, continental, and river basin scales, especially in light of the changing hydrologic dynamics due to climate change and accelerated human activities (e.g., land use land cover change, irrigation water withdrawal, and flow regulations) that have left a large footprint on the terrestrial water cycle (Haddeland et al., 2011; Pokhrel et al., 2016). The lack of long-term and continuous observations of water and energy states and fluxes, however, limits our ability to understand the interaction between hydrology, human interventions, and climate change and how they affect freshwater availability (Döll et al., 2016). The state-of-the-art land surface models (LSMs) bridge this gap by providing spatially complete and temporally continuous hydrological simulations that allow for the assessment and prediction of water availability by taking into account human activities and climate change (Biemans et al., 2009; Bierkens et al., 2015; Hanasaki et al., 2017; Huang et al., 2017; Kumar et al., 2006; Schilling et al., 2008; Schmied et al., 2014). The growing interest in using LSM has led to both the improvement of process representations and the addition of new processes and functionalities (Lawrence et al., 2011, 2016, 2019). Physically-based LSMs with explicit representation of soil moisture dynamics, canopy processes, surface, and subsurface runoff parameters as well as human impacts such as dynamic vegetation and crop and irrigation has led to improved simulation of streamflow, terrestrial water storage, soil moisture, and other states and fluxes (Liang et al., 2003; Pokhrel et al., 2014; Zeng et al., 2018). Most LSMs, however, have been developed and applied primarily for large-scale applications (e.g., globally) at relatively coarse spatial resolutions (e.g., 0.5º×0.5º) (Lawrence et al., 2011; Schilling et al., 2008; Zaherpour et al., 2018).

To adequately address critical issues related to water resources, models need to be implemented regionally at high spatial resolution that can explicitly represent the effects of topography, soils, and vegetation on hydrological dynamics at the regional scale (Keith J. Beven & Cloke, 2012; Merz et al., 2009) accounting for the underlying non-linear dynamics in a way fundamentally different than in lumped parameter models. The usage of fully physically based LSM on a regional scale will have significant long-term benefits for the assessment of available water resources and future changes. When using LSM to assess water resources, it is critical to consider modeling uncertainties (Biemans et al., 2009; Di et al., 2014; Schmied et al., 2014; Schreiner-McGraw & Ajami, 2020). Models suffer from a variety of sources of uncertainty, including hydrological process representation, choice of model parameters, representation of human influences, and water use (Schmied et al., 2014). Another, and yet more important, source of uncertainty is the input data (Biemans et al., 2009). LSMs are driven by climate forcing input data sets (hereafter "climate forcing"), based on station observations, reanalysis (global circulation models), and/or remote sensing products. Within the last two decades, numerous climate forcing data have been developed, providing data from as early as 1901 until recent years (Raimonet et al., 2017; Weedon et al., 2014). These climate forcings differ from each other and thus may lead to varying estimations of water and energy fluxes (Beck, Van Dijk, De Roo, et al., 2017; Biemans et al., 2009; Clark et al., 2015a; Schreiner-McGraw & Ajami, 2020; Thompson et al., 2014). Precipitation is one of the key variables in climate forcing and a major driver of hydrological simulation that has dominant control over fluxes and states such as streamflow, terrestrial water storage (TWS), soil moisture, and evapotranspiration (Biemans et al., 2009;

Chen et al., 2018; Fan & Luo, 2019; Lauri et al., 2014; Schreiner-McGraw & Ajami, 2020; Wang et al., 2016). For river basins such as the Mekong, over 65% of the streamflow variations in parts of the basin is caused by the variations in precipitation alone (Fan & He, 2015).

Precipitation uncertainty can propagate through various processes simulated, eventually translating to similar or even greater uncertainty in the output variables such as river discharge (Fekete et al., 2004). Therefore, the use of reliable and accurate precipitation data is crucial for hydrological modeling. Many recent studies have characterized precipitation uncertainty on a regional scale. Some studies have compared different precipitation products to in-situ observations, and others have adopted modeling techniques to investigate precipitation uncertainty over Mekong River Basin (MRB) (Fan & Luo, 2019; Lauri et al., 2014; Li et al., 2019; Luo et al., 2019; Tang et al., 2019; Wang et al., 2016) primarily with a common goal of finding a precipitation dataset that can best reproduce the temporal dynamics of observed streamflow. These studies have provided important insights on the role of precipitation data in hydrological modeling but lack the quantification of the uncertainty arising from precipitation data. Also, most of the studies used basin-scale models using parameter calibration which often enables improved model performance for a specific variable, but this could come at the cost of reduced accuracy of other variables due to unrealistic partitioning of precipitation between runoff and other water balance terms (Biemans et al., 2009). This challenge could be overcome by using LSMs, with minimal parameters involved in combination with reliable precipitation data. Thus, assessment of precipitation uncertainty using a LSM is crucial in order to depict the hydrologic behavior at regional scale.

1.1.2 Improving LSM simulations in data-scarce regions by representing missing processes and human impacts

LSMs have undergone significant developments over the years, with advancements made in both the model structure and the representation of various physical processes. Some of the major advancements in LSMs include improvements in soil and vegetation processes representations (Bonan et al., 2011), incorporation of biogeochemical cycles to better represent ecosystem dynamics (D. M. Lawrence et al., 2019; P. J. Lawrence et al., 2012), as well as nutrient and pollutant transport. Furthermore, progress has been made in improving the irrigation parameterizations (Leng et al., 2013, 2014, 2014; Nie et al., 2018, 2021; Pokhrel et al., 2012; Pokhrel, Koirala, et al., 2014; Pokhrel et al., 2016), as well as incorporating groundwater and water table dynamics (Fan et al., 2013; Yeh & Eltahir, 2005) and lateral flow (Felfelani et al., 2021; de Graaf et al., 2017; de Graaf & Stahl, 2022). Notably, there has also been an effort to include water regulations, such as those representing dams and reservoirs (Pokhrel, Shin, et al., 2018a; Shin et al., 2019), to better represent anthropogenic influences. These developments have substantially improved our understanding of the hydrological system under the influence of natural climate, climate change and variability, and anthropogenic stressors. Thus, the use of LSMs has increased significantly, and these models have been used in many global and regional watersheds to address critical water related issues (De Graaf et al., 2014; Liu et al., 2016; Pokhrel et al., 2013; Schmied et al., 2014; Wada et al., 2014, 2016, 2017). However, most of these model development studies have focused on data-rich regions such as the US basin where issues are rapidly emerging due to increased anthropogenic stressors such as water regulations through dams and reservoirs and pumping for irrigation (Maxwell et al., 2015; Nie et al., 2019, 2021, 2022; Doll et al., 2014; Pokhrel et al., 2015), leaving major gaps that come with challenges, toward using the models in regions where water related issues are rapidly emerging, but data are scarce particularly for groundwater study.

Groundwater is a crucial component of the global water cycle (Bierkens & van den Hurk, 2007; Condon et al., 2020; Condon & Maxwell, 2015; Gleeson et al., 2012, 2016; R. M. Maxwell et al., 2015; Miguez-Macho & Fan, 2012a). It is the world's largest source of freshwater that provides clean water to billions of people, forms an integral part of irrigated agriculture, and contributes to the health of many ecosystems (Döll, 2009; Scanlon et al., 2012; Stefan Siebert & Döll, 2010). Recently, new areas have emerged with heightened groundwater issues, yet they pose significant challenges for study due to the notoriously complex and heterogeneous behavior of groundwater systems (Condon et al., 2021). The groundwater flow and transport processes is highly intricate, and a multitude of factors, such as geological and hydrological properties, can significantly influence the behavior of groundwater systems. Moreover, data on groundwater is often limited, incomplete, or difficult to obtain. As a result, investigating and modeling these systems is an ongoing scientific challenge that requires innovative approaches and advanced methodologies particularly for data limited regions.

The MRB is a prime example of a region where increased groundwater pumping for domestic and irrigation purposes is rapidly altering groundwater dynamics. However, basin-scale groundwater studies in this region are scarce or non-existent, with inadequate attention given to understanding the natural dynamics of groundwater, let alone the growing anthropogenic influence (Lacombe et al., 2017). Process-based models can offer promising avenues to simulate these changes, resolving the interactions among various governing processes, and identifying the key drivers (Koirala et al., 2014; Pokhrel, et al., 2014). Fundamentally, little advancement has been made in understanding the critical controls of climate, physiography, and anthropogenic drivers on the dynamics of groundwater over many such data limited regions. Thus, it is necessary to leverage our efforts towards utilizing process-based modeling to enhance our understanding of groundwater processes, particularly in data limited basins. This approach allows for the incorporation of small-scale processes, such as lateral groundwater flow, while reducing parameterizations and better representing the subsurface. Moreover, process based LSMs have undergone substantial improvements to enable their application across diverse geographic and climate settings, while incorporating better parameterizations of human impacts such as irrigation development and groundwater extraction (Felfelani et al., 2021; 2015; Swenson et al., 2019; Wada et al., 2016).

Thus, basin-scale and long-term (e.g., decadal evolutions) groundwater modeling at high spatial resolution using advance groundwater and irrigation scheme considering climatic and anthropogenic drivers can enhance our understanding of evolving groundwater systems over many data limited regions across the globe. This has implications on reliable future projections of water resource availability and use under climate change and intensified anthropogenic activities (Jasechko et al., 2014). Besides, recent development of satellite-based observations of crop and irrigation areas can be utilized to better constrain irrigation simulations in LSMs. However, to my best knowledge, the potential of using advanced groundwater and irrigation schemes constraining the model with emerging datasets has not yet been examined.

1.1.3 Global Drought Recovery and its Linkage to Potential Drivers

Large-scale models have been widely used to investigate the effects of climate change and human impacts on terrestrial hydrology and evaluate their consequences on global changes such as droughts, floods, and other associated phenomena. However, the ability of the hydrological system to recover from drought, such as restoring groundwater recharge and runoff, as well as surface water flow, remains poorly understood (Peterson et al., 2021; Sheffield et al., 2012; Wen Wang et al., 2016). This knowledge gap limits our understanding of the risks and impacts of drought, hindering our ability to develop effective drought mitigation and adaptation strategies. Therefore, advancing our understanding of drought recovery and underlying mechanisms is crucial for developing more comprehensive and accurate assessments of drought risk and impacts, eventually informing more effective drought management strategies in different regions of the world. Drought recovery—the time it takes for a system to bounce back to pre-drought conditions after a drought event—is a complex and multi-faceted process that is influenced by a range of hydrological, ecological, and socio-economic factors (Jiao et al., 2021; Yang Li et al., 2023; Liu et al., 2019; Schwalm et al., 2017; Guy Davidesko1,2, Amir Sagy1, 2014; Wu et al., 2019, 2020).

Droughts exhibit considerable variability in their characteristics, including severity, duration, and spatial extent, with recovery mechanisms likely to differ across diverse geographical and climatic settings (Yuting et al., 2017). Thus, understanding drought recovery can be exceedingly complex. Recovery time can vary significantly due to a range of factors, influenced by soil moisture (Samaniego et al., 2013; Sheffield et al., 2004; Sheffield & Wood, 2008) and precipitation patterns (Anne F. Van Loon et al., 2016), vegetation dynamics and plant phenology (Yang Li et al., 2023), catchment characteristics (Anne F. Van Loon et al., 2016), and water management practices (J. Wu et al., 2018). Understanding of drought recovery requires comprehensive assessments of interplay of these factors that drive drought recovery across various regions and climatic zones. However, such studies over the global scale are largely lacking, hindering our ability to fully understand global drought risk across different regions with varying climatic and geographic settings. This is particularly critical to understand given the expected increase in frequency and intensity of droughts due to climate change.

Despite the significant progress made in recent years, challenges and opportunities remain in using large-scale hydrological models (LHMs) or LSMs for drought studies. One of the main challenges is the considerable variation in hydrological process representation and parameterization among models. Differences in water partitioning, runoff generation, groundwater processes, and soil hydrologic parameterization can lead to varying degrees of change in energy and water balances associated with climate impacts. Moreover, uncertainty can arise due to variations in human impacts parameterization in the models, which can result in inaccurate estimation of hydrological states and fluxes. To overcome these challenges, it is crucial to integrate a large ensemble of global hydrological models to provide a range of possible drought recovery scenarios in response to climate change, land management, and human impacts. Leveraging multi-model simulations of hydrological variables can provide a comprehensive understanding of drought recovery across global basins, climate regions, and biodiversity hotspots. This approach can provide insights into the diverse traits of drought recovery under the impacts of climate change and variability and human activities.

1.2 Research Goal, Objectives, and Science Questions

As discussed above, there are both gaps and opportunities for reducing uncertainty in hydrological modeling through improved hydrological process representation, accurate climate forcing, integration of satellite remote sensing data, and utilization of multi-model ensembles. The necessity of addressing climate forcing uncertainty (section 1.1.1) and utilizing advanced LSMs in regions with limited data availability (section 1.1.2) lead me to pursue the overarching goal of my Ph.D. dissertation. Substantial improvement in hydrological simulation can be achieved by addressing climate forcing uncertainty. The explicit representation of groundwater processes and irrigation representation in the LSMs is expected to enhance the simulation of groundwater dynamics in the data limited regions. Further, the study has broader implications on climate extremes such as monitoring drought as well as on environmental sustainability. The overarching scientific questions are: (1) How does climate forcing uncertainty impact the simulation of hydrological states and fluxes? (2) What is the potential of utilizing advanced LSMs with improved representation of land surface processes and human impacts, along with emerging irrigation and crop data, to enhance our understanding of regional groundwater dynamics, particularly in data-limited regions? (3) How does drought recovery time evolve over decadal timescale and how do climate change and variability and human interventions affect drought recovery across different climate regions? These overarching questions are addressed by answering the following specific science questions under different chapters.

Chapter 2. Analysis of precipitation uncertainty at the regional scale

Q1. How do uncertainties in the precipitation datasets propagate into hydrological simulation and affect various streamflow signatures?

Q2. How sensitive are other water budget components (i.e., TWS, soil moisture, and ET) to the uncertainties in precipitation data?

Chapter 3. Understanding groundwater dynamics under the influence of natural climate variability and human interventions

Q3. Can we enhance the representation of groundwater dynamics and human interventions in LSMs using emerging data on anthropogenic impacts, specifically irrigation areas and groundwater pumping?

Q4. How do the interplays between long-term climate variability and groundwater extraction affect groundwater dynamics?

Chapter 4. Analysis of drought recovery under the influence of climate change and human impacts.

Q5. How is drought recovery time affected by climate variability and human impacts on different global regions?

Q6. What is the impact of prolonged drought recovery time on ecosystem sustainability in various climate zones and biodiversity hotspots?

To investigate how global LSM performs in regional-scale modeling with high spatial resolution, the MRB is chosen as a study area for regional scale study. Regional-scale CLM5 is first implemented and validated across the MRB. Climate forcing uncertainty particularly, precipitation uncertainty, is examined by using different precipitation datasets at varying resolutions. Then, CLM5 with an advanced groundwater model coupled with the irrigation scheme is implemented constraining the model with new irrigation datasets. Further, multiple hydrological models with explicitly varying hydrological process representation are used in identifying drought events and analyzing drought recovery time and mechanisms in different climate zones.

1.3 Dissertation Outline

The remainder of the dissertation is organized as follows.

Chapter 2. Precipitation-induced uncertainty in hydrological simulation: A regional Analysis of streamflow, TWS, soil moisture, and ET using LSM at high spatial resolution.

Chapter 3. Groundwater dynamics in the MRB under natural climate variability and under the influence of human impacts such as irrigation and groundwater pumping are investigated.

Chapter 4. A multi-model assessment of global drought recovery and its drivers in different climate zones.

Chapter 5. Summary and Conclusion.

Chapter 2. On the Precipitation-Induced Uncertainties in Process-Based Hydrological Modeling in the Mekong River Basin

Based on: Kabir, T., Pokhrel, Y., & Felfelani, F. (2022). On the precipitation-induced uncertainties in process-based hydrological modeling in the Mekong River Basin. Water Resources Research, 58, e2021WR030828. https://doi.org/10.1029/2021WR030828

2.1 Introduction

Many large global river basins are undergoing rapid hydrological alterations due to climate change and variability, land use and land cover change, and modification of natural hydrological systems due to land-water management activities (Júnior et al., 2015; Schilling et al., 2008; Veldkamp et al., 2018). The Mekong River basin (MRB) in Southeast Asia is one of such basins where the hydrological regime had been relatively stable historically but has recently begun to transform (Nilsson et al., 2005) due to ongoing climate change and a recent acceleration in land-water management activities including basin-wide dam construction (Pokhrel et al., 2018a; Shin et al., 2020; Yun et al., 2021). The MRB is a transboundary basin shared by six nations (China, the Lao PDR, Myanmar, Thailand, Cambodia, and Vietnam), and provides critical water resources in the region, especially for over 60 million people living in the five downstream countries (MRC, 2005; Pokhrel et al., 2018a). Further, the MRB is the second most hydrologically and ecologically diverse river basin in the world, after the Amazon basin (Ziv et al., 2012); the basin hosts one of the most productive inland fisheries in the world (Ziv et al., 2012). Therefore, the hydrological changes within the MRB have important implications on the livelihood of millions and the functioning of critical ecosystems that depend on the unique river flood pulse (Arias et al., 2013; Kummu & Sarkkula, 2008) that provides a timely supply of water and nutrients for agriculture, fishery, and riverine ecosystems (Pokhrel et al., 2018a).

The hydrology of the MRB has been increasingly studied in the recent past. Numerous studies have used observed data to examine the change in streamflow patterns and attribute the observed changes to natural and human factors (i.e., Li et al., 2017; Wang et al., 2017; Yun et al., 2020). Other studies have focused on modeling to characterize the past and provide future projections under climate change (Arias et al., 2012, 2013; Fan & He, 2015; Han et al., 2019; Hoang et al., 2019; Lauri et al., 2012, 2014; Hoang et al., 2016; Pokhrel et al., 2018a; Räsänen et al., 2012, 2017; Shin et al., 2020; Sridhar et al., 2019). However, even some of the fundamental questions regarding the cause of observed changes in streamflow remain unanswered. Crucially, outstanding challenges and opportunities exist in developing a comprehensive assessment of the ongoing hydrological changes and quantifying the uncertainties in modeling the complex hydrology and hydrodynamics of the basin (Bierkens et al., 2015). In terms of hydrological modeling, notable progress has been made in basin-wide and sub-basin level modeling of streamflow (Johnston & Kummu, 2012); however, there is still a lack of models that mechanistically simulate various surface hydrological, soil, groundwater, and river processes on a full physical basis and over the entire basin. The complex topographic, geographic, and hydrological characteristics of the MRB that originates in the Tibetan Plateau and runs through vast topographic gradients across different climate zones make the surface and subsurface characterizations in the model extremely challenging (Pokhrel et al., 2018a). The challenges in process representation are further compounded by the lack of observed data for the entire MRB and the short record of available data (X. Luo et al., 2019). While observed data to constrain and evaluate model simulations are vital to ensure the reliability of model results, it is even more important to use reliable climate forcing data, especially precipitation, because the uncertainties in climate forcing directly impact hydrological simulations (Lauri et al., 2014; Raimonet et al., 2017; Tang et al., 2019).

Numerous studies used global and regional scale hydrological models to quantify the spatiotemporal variability of hydrological fluxes and states in the MRB. While some have simulated the hydrology of the entire basin (e.g., Kite, 2001), others have focused on parts of the basin such as the upper Mekong river basin (UMRB) (Dang et al., 2020; Zhongying Han et al., 2019b), lower Mekong river basin (LMRB), Tonle Sap Lake (TSL), or the Mekong delta (Arias et al., 2014; Han et al., 2019). Models used for basin-wide simulations include the land-use runoff process (SLURP) (Kite, 2001), Mac-PDM.09, and MIKE SHE (Thompson et al., 2014), Soil Water Assessment Tool (SWAT), Variable Infiltration Capacity (VIC), VMOD (Lauri et al., 2012), CaMa-Flood (Yamazaki et al., 2011, 2014) and HiGW-MAT (Pokhrel et al., 2014). Among these, SWAT, VIC, and VMOD have been commonly used by many studies (e.g., Haddeland et al., 2006; Hoang et al., 2019; Lauri et al., 2014; Tatsumi & Yamashiki, 2015), demonstrating satisfactory performance in reproducing streamflow and in some cases sediment transport (B. Shrestha et al., 2013; Sok et al., 2020). Some studies have also used the VIC model to examine the effects of irrigation on energy balance (Haddeland et al., 2006; Tatsumi & Yamashiki, 2015) and others used HiGW-MAT and CaMa-Flood to understand the effects of dams on flood pulse and inundation dynamics (Pokhrel et al., 2018b; Shin et al., 2019, 2020).

However, the models like VIC and SWAT employ calibration and validation techniques where streamflow observations are used to calibrate model simulation. Such tuning of model parameters enables improved model performance for a specific variable, typically streamflow, but this could come at the cost of inaccurate process representation leading to unrealistic partitioning of precipitation between runoff and other water balance terms (Biemans et al., 2009).

This is particularly so when the forcing data contain large uncertainties. Further, the performance of calibrated models can degrade for periods outside of the calibration window, hence the models may fail to capture the non-linear hydrological dynamics (Biemans et al., 2009), for example, under future climate (Kumarasamy & Belmont, 2018). Because many of the calibrated models are not fully distributed and/or process-based, it is challenging to assess whether any uncertainty in the simulations is caused by missing process representation or due to uncertainties in input datasets. Therefore, the uncertainty in simulation arising from climate forcing and model structure is incorrectly inferred. This challenge could be overcome by using physically-based models, referred to as the land surface models (LSMs), that represent a wide range of interconnected processes, explicitly accounting for the underlying non-linear dynamics in a way fundamentally different than in lumped parameter models (Drewry et al., 2010; Fisher & Koven, 2020; Kuppel et al., 2018) that adopt a more conceptual approach for process representation (Wei Wang et al., 2016).

Some studies have used LSMs to simulate the hydrology of the entire MRB; however, these studies have relied on global models with a relatively coarse resolution of 0.5º or ~50 km at the equator (Haddeland et al., 2006; Tatsumi & Yamashiki, 2015). Amongst those include our recent studies (Pokhrel et al., 2018b; Shin et al., 2020) in which we used a global LSM to simulate runoff (~50 km resolution) over the entire MRB and routed it using a high resolution (~5 km) river-floodplain hydrodynamics model. This enables a more realistic representation of the river-floodplain processes compared to the global model, which is crucial in the MRB where surface water processes dominate hydrologic dynamics (Pokhrel et al., 2018b). However, such an approach only enables improvements in streamflow and flood simulations through a better representation of only the river and floodplain processes. Various other surface and subsurface processes (e.g., surface and subsurface runoff generation, evapotranspiration (ET)) are still simulated at the coarse resolution, which may impact the overall simulation outcome (S. V. Kumar et al., 2006; Vanderkwaak & Loague, 2001; Yuan et al., 2014). Recently, global LSMs have been improved and used in regional scale studies at high resolution. For example, Felfelani et al. (2021) used a high-resolution version of the Community Land Model version 5 (CLM5) over the continental US. Some other studies have also used CLM5 at continental to regional scales at high spatial resolution (i.e., ~1-5 km) (Leng et al., 2014; Zeng et al., 2016, 2018). However, such advanced LSMs have not been used regionally for the MRB at such high resolution.

Additionally, and more crucially, uncertainties in hydrological simulation over the MRB caused by the uncertainties in climate forcing have not been examined using process-based models, which has further limited our understanding of the cause of uncertainties in modeling the hydrology of the MRB. Calibrated models could misrepresent the uncertainty as the calibration process may disguise such uncertainty in forcing dataset (Biemans et al., 2009; Schmied et al., 2014). Precipitation is amongst the most important forcing data that is subject to major uncertainties due to climate and topographic complexities (Faridzad et al., 2018; Imerg-v et al., 2020; Iui & Yang, 1991; Tang et al., 2018) and directly affects water balance (Bárdossy & Das, 2008; Nilsson et al., 2005; Wei Wang et al., 2016). Particularly for the MRB, studies have suggested that over 65% of the streamflow variations in parts of the basin can be attributed to the variations in precipitation alone (Fan & He, 2015). Precipitation uncertainty can eventually translate to similar or even greater uncertainty in simulated hydrological variables (Fekete et al., 2004). Therefore, an in-depth understanding of the role of precipitation data is crucial for improved hydrological modeling in the MRB.

Many recent studies have characterized precipitation uncertainty in the MRB (Dinh et al., 2020; Tian et al., 2021). Some studies have compared different precipitation products to in-situ observations, but such comparisons have been limited in scope for the MRB due to the sparse gage network. Others have adopted modeling techniques to investigate precipitation uncertainty over MRB (Fan & Luo, 2019; Lauri et al., 2014; Li et al., 2019; Luo et al., 2019; Tang et al., 2019; Wang et al., 2016) primarily with a common goal of finding a precipitation dataset that can best reproduce the temporal dynamics of observed streamflow. These studies have provided important insights on the role of precipitation data in hydrological modeling but lack the quantification of the exact uncertainty arising from precipitation data. More crucially, a comprehensive assessment of the precipitation uncertainty on other hydrological variables than streamflow (e.g., terrestrial water storage (TWS), soil moisture, and ET) using high-resolution, fully distributed process-based models is largely lacking.

These issues underscore the need for fully distributed, process-based models that simulate various surface and subsurface processes on a full physical basis, such that the uncertainties in various simulated fluxes and storages caused by precipitation uncertainty can be explicitly quantified. Specifically for the MRB, it is equally important to use high-resolution models to capture the effects of high contrast in hydrological and topographic characteristics between the UMRB and LMRB (Wei Wang et al., 2016). The goal of this study is to address these gaps and limitations through hydrological simulations using a state-of-the-art LSM, the CLM5, driven by multiple precipitation datasets. CLM5 is set up regionally for the MRB and simulations are used to compare key hydrological variables including mean monthly streamflow, low flow, high flow, TWS anomaly, soil moisture, and ET from the multiple simulations. The study is driven by the following key science questions. (1) How do uncertainties in the precipitation datasets propagate into hydrological simulation and affect different streamflow signatures? (2) How sensitive are other water budget components (i.e., TWS, soil moisture, and ET) to the uncertainties in precipitation data?

The remainder of the paper is organized as follows. Study area, model description, data used, and simulation settings are described in section 2; results and discussions are provided in section 3; and summary and concluding remarks are presented in section 4.

2.2 Study Area and Methods

2.2.1 Study Area

The study domain is the MRB with a total drainage area of 769,500 km^2 (MRC, 2005). The MRB is characterized by diverse topography, dense drainage networks, and complex geomorphology, with distinct climatic and topographic features in the upper and lower portions of the basin (Pokhrel et al., 2018a). The UMRB is narrow with steep topography while the LMRB spreads across a wider region and is characterized by a large tributary river system (X. Luo et al., 2019). The UMRB makes up 21% of the total area and contributes to 15–20% of the river discharge at the outlet of the Mekong river (MRC, 2005; Piman et al., 2013). The streamflow in the UMRB is governed by snowmelts in the Tibetan Plateau and plays an important role in the low flow hydrology of the MRB, contributing to ~30% of the average dry season flow (MRC, 2005). The streamflow in the LMRB is primarily driven by the high-intensity monsoonal rainfall that accounts for 85%-90% of annual precipitation (X. Luo et al., 2019). The Mekong river is the 10th largest river in the world in terms of mean annual streamflow, with average streamflow of ~14,500 m^3/s (MRC, 2005). The streamflow in the Mekong is strongly modulated by the tropical monsoon (Tian et al., 2021) with distinct flood and dry season. The streamflow during the flood season that extends from June to November contributes to 80% to

90% of the annual flow volume. Temperate to tropical climate exists in the MRB with relatively high annual precipitation (Tang et al., 2019); the UMRB and LMRB receive average annual precipitation of ~600 mm and ~3,000 mm, respectively.

2.2.2 Model

We use CLM5 (D. M. Lawrence, Fisher, Koven, Oleson, Zeng, et al., 2019a), the latest version of CLM (D. M. Lawrence et al., 2011; K. Oleson & Lawrence, 2013) which is the land component of the Community Earth System Model (CESM). CLM5 is a fully distributed global LSM that resolves various surface and subsurface hydrological processes (e.g., soil and plant hydrology, snow physics, river routing, crop modeling) coupled with energy and biogeochemical (carbon and nitrogen) cycles on a full physical basis at the typical spatial resolution of 0.5°×0.5°. A complete description of CLM5 can be found in previous literature (D. M. Lawrence et al., 2011; D. M. Lawrence, Fisher, Koven, Oleson, Zeng, et al., 2019a) and technical documentation (NCAR, 2019). For completeness, here we provide a brief description of the key surface and subsurface parameterizations.

CLM5 represents the spatial land surface heterogeneity as a nested sub-grid hierarchy in which grid cells are composed of smaller units (i.e., land units, columns, and patches) (NCAR, 2019). The subsurface has a high vertical resolution for improved simulation of soil water. Soil thickness is 8.5 m with 20 active soil layers of varying depth. The depth to bedrock is derived from spatially explicit soil thickness data (Tan et al., 2015). The water table depth is determined by identifying the first soil layer above the bedrock when the soil water saturation fraction is less than a threshold. The threshold is set to 0.9 in standard CLM5 (NCAR, 2019). CLM5 includes an irrigation scheme that simulates irrigation requirements based on the soil moisture deficit in the root zone (Felfelani et al., 2018; Mutlu Ozdogan, Yang, et al., 2010). When an irrigation scheme is enabled, crop areas are split into irrigated and rainfed fractions based on the dataset of areas equipped for irrigation (Portmann et al., 2010). Irrigation is applied to the irrigated portion of a grid cell when the crop leaf area index is greater than zero, and the available soil water falls below a specified threshold. The details of the irrigation scheme can be found in NCAR (2019).

Surface runoff is parameterized based on the SIMTOP model (Niu et al., 2005), a simplified version of the TOPMODEL developed for large-scale applications (K. J. Beven & Kirkby, 1979). In SIMTOP, surface runoff discharges from the saturated portion of the grid cell (f_{sat}) as a function of topographic characteristics and soil moisture. f_{sat} is a function of maximum saturated fraction (f_{max}), water table depth and a decay factor (f_{over}). f_{max} involves an extensive computational process because it is calculated globally at 0.125° spatial resolution and interpolated to model resolution; f_{over} is determined from sensitivity analysis. Subsurface runoff is estimated as a linear function of soil saturated thickness i.e., $q_{sub} = \Theta_{ice}\, K_{base}\, \tan(\beta)\, (z_{bedrock} - z_{wt})$; where, Θ_{ice} is ice impedance factor, K_{base} is a calibration parameter, β is the mean grid cell slope, z_{wt} is water table depth, and $z_{bedrock}$ is the bedrock (Pelletier et al., 2016). Finally, streamflow is simulated using a process-based Model for Scale Adaptive River Transport (MOSART) that routes runoff using kinematic wave formulations (Li et al., 2015). We use MOSART hydrography dataset available globally at 0.125° spatial resolution. Topographic parameters such as flow direction, channel length and, channel slope are derived using the Dominant River Tracking (DRT) algorithm (Li et al., 2015).

2.2.3 Data

2.2.3.1 Atmospheric Forcing Data

We use WATCH Forcing Data methodology applied to the ERA-Interim reanalysis data (WFDEI) dataset (Weedon et al., 2014) as the baseline forcing data. WFDEI data are available at

0.5×0.5° spatial resolution since 1979. WFDEI data have been widely used in many global and regional hydrological modeling studies (Beck et al., 2017; Felfelani et al., 2017; Hanasaki et al., 2017; Schmied et al., 2014) and found to well reproduce observed streamflow (Chaudhari et al., 2019; Monteiro et al., 2016). The forcing variables in WFDEI data include longwave radiation, shortwave radiation, surface pressure, air temperature, wind speed, and specific humidity. To investigate uncertainty arising from precipitation data, we use four additional precipitation datasets, namely the Multi-Source Weighted-Ensemble Precipitation (MSWEP) version 2.1 at 0.1×0.1° spatial resolution (Beck et al., 2017), Tropical Rainfall Measuring Mission (TRMM-3B42V7) (X. Luo et al., 2019), Precipitation Estimation from Remotely Sensed Information using Artificial Neural Networks - Climate Data Record (PERSIANN-CRD) (Beck et al., 2017) and ECMWF Reanalysis 5th Generation (ERA5) at 0.25×0.25° spatial resolution. The temporal resolution of all datasets is 3-hour. The precipitation data are selected based on the availability period and temporal resolution that is consistent with CLM5 requirements.

2.2.3.2 Observed Streamflow

To evaluate streamflow simulations, we use daily discharge data obtained from the Mekong River Commission (MRC) for eight gauging stations across the basin. The gauging stations are selected with the criteria that at least 20 years of observational data are available during the 1979-2016 period.

2.2.3.3 TWS and Soil Moisture Data

We use TWS data derived from the Gravity Recovery and Climate Experiment (GRACE) satellite mission to validate the simulated TWS anomaly for the 2002-2016 period. GRACE provides global monthly TWS anomaly by measuring the Earth's gravity field changes (Felfelani et al., 2017a; S. C. Swenson & Lawrence, 2015). In this study, we use the TWS from GRACE mass concentration block (mascon) because the mascon products are found to better capture TWS anomaly signals in many regions globally (Scanlon et al., 2018). Two mascon products from the Centre of Space Research (CSR) and the Jet Propulsion Laboratory (JPL) are used. The original JPL mascon products are provided at 3×3° grids but have been resampled to 0.5×0.5° (Wiese et al., 2016). Basin averaged TWS anomaly is calculated by taking account of the varying grid cell area (Chaudhari et al., 2019). TWS anomaly from CLM5 simulations is calculated using the base period of 2004-2009, consistent with GRACE products (Landerer & Swenson, 2012).

We use Soil Moisture Active Passive (SMAP) L4 data, available globally at 9 km spatial resolution to validate simulated soil moisture. We compare SMAP with simulated soil moisture for the year 2016 which is the only complete overlapping year with SMAP. SMAP is chosen over other soil moisture products as SMAP is a widely used, state-of-the-art soil moisture product. Further, SMAP product is available as volumetric soil moisture (mm^3/mm^3) that is consistent with CLM5 simulation.

2.2.4 Simulation Settings

CLM5 is set up for the entire MRB at the spatial resolution of 0.05°×0.05° (~5×5 km at the equator). First, the model is spun up for 100 years from a cold start and by using WFDEI forcing data repeatedly for the year 1979. Then, five different simulations are conducted: a baseline simulation for the 1979-2016 period using WFDEI forcing data, and four additional simulations by replacing precipitation in the WFDEI forcing data with the four precipitation products (Section 2.3.1). All other forcing variables in the latter four simulations remain the same as in the baseline simulation. Hereafter, the additional simulations are termed as MSWEP, TRMM, ERA5, and PERSIANN-CDR simulations, which are conducted for a shorter period because the objective is to examine the uncertainties arising from precipitation data, rather than long-term changes. The simulation period is 1998-2016, chosen to include average, dry, and wet years (Section 3.3), except for the PERSIANN-CRD simulation that is conducted for the 2000-2016 period since PERSIANN-CDR data are not available before 2000. Since the climatological equilibrium may vary across precipitation products, an additional spin up of five years is conducted for each precipitation data by starting from the 100-year spin up conducted with WFDEI forcing. The irrigation module is activated in the simulations. The WFDEI forcing data and the four precipitation products, available at varying spatial resolution are spatially interpolated to the model resolution (0.05°) within CLM5 using bilinear interpolation.

2.3 Results and Discussions

2.3.1 Evaluation of Simulated Streamflow

Figure 2-1 presents the long-term (1979-2016) average streamflow and its seasonal variation from the simulation driven by the WFDEI forcing data. The seasonal patterns of streamflow are reasonably captured by the model with expected upstream-downstream and tributary-mainstream contrasts. Importantly, the high seasonal variability in streamflow that represents the unique Mekong flood pulse is distinctly reproduced by the model (Figure 2-1; right panels). Further, the general streamflow patterns in the major tributary systems including the Mun-Chi sub-basin and the 3S river system (Sekong, Sesan, and Sre Pok) are also captured. These sub-basins contribute to ~15% and ~17% of the Mekong annual streamflow, respectively (Xue et al., 2011). The tributary system connected to the TSL is also captured by the model. Validation of these results at the selected gauging stations (red scatters in Figure 2-1) is provided in Figure 2-2.

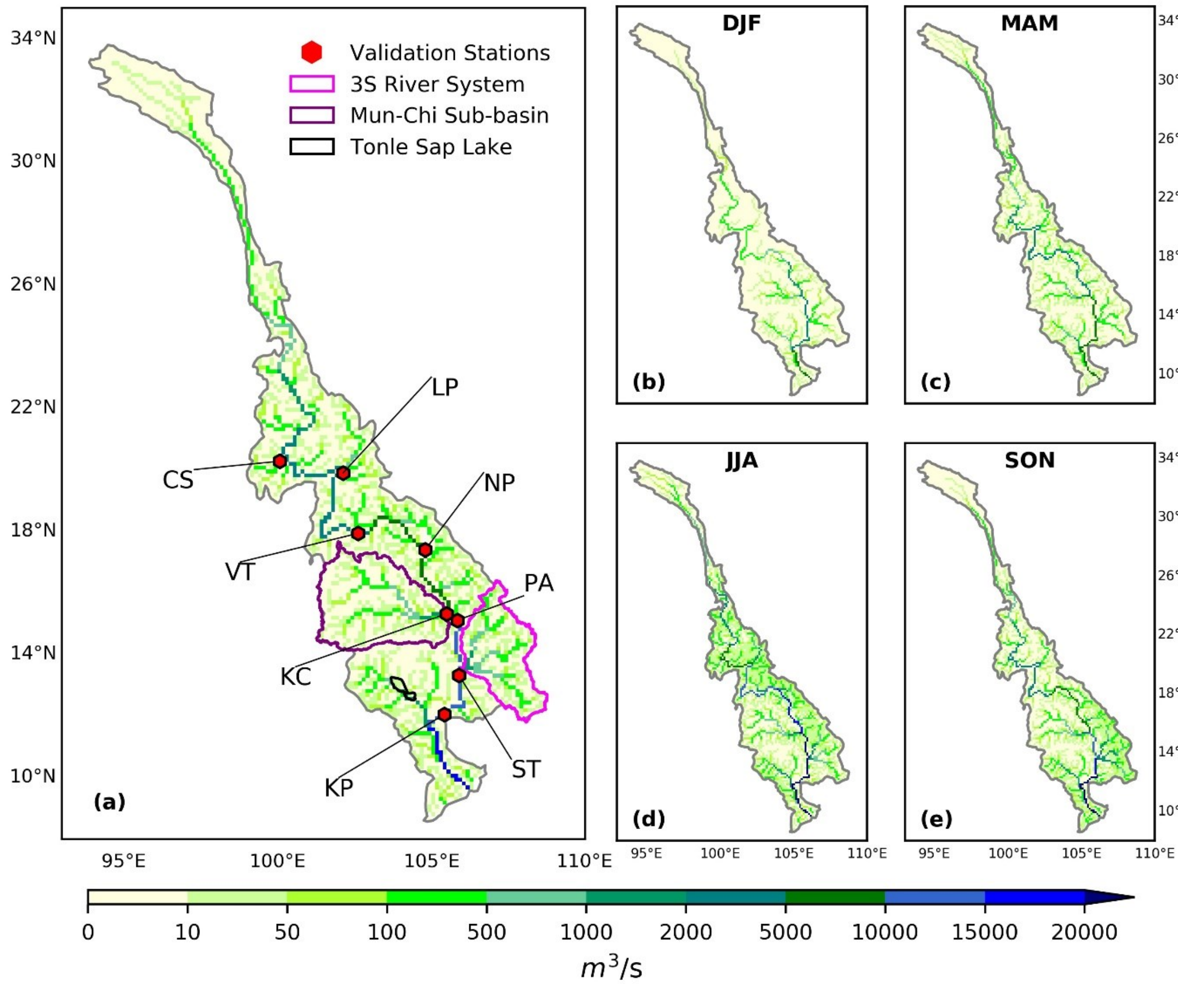

Figure 2-1. Long-term mean streamflow (a) and its seasonal variation (b-e) for the 1979-2016 period from the baseline simulation (with WFDEI forcing). DJF, MAM, JJA, SON denote December-February, March-May, June-August, and September-November. The eight gauging stations selected for streamflow validation are marked by red hexagon: CS (Chiang Saen), LP (Luang Prabang), VT (Vientien), NP (Nakhon Phenom), KC (Kong Chiam), PA (Pakse), ST (Stung Treng), KP (Kampong Cham). Mun-Chi sub-basin, 3S river system, and Tonle Sap Lake (TSL) boundaries are delineated with different colors.

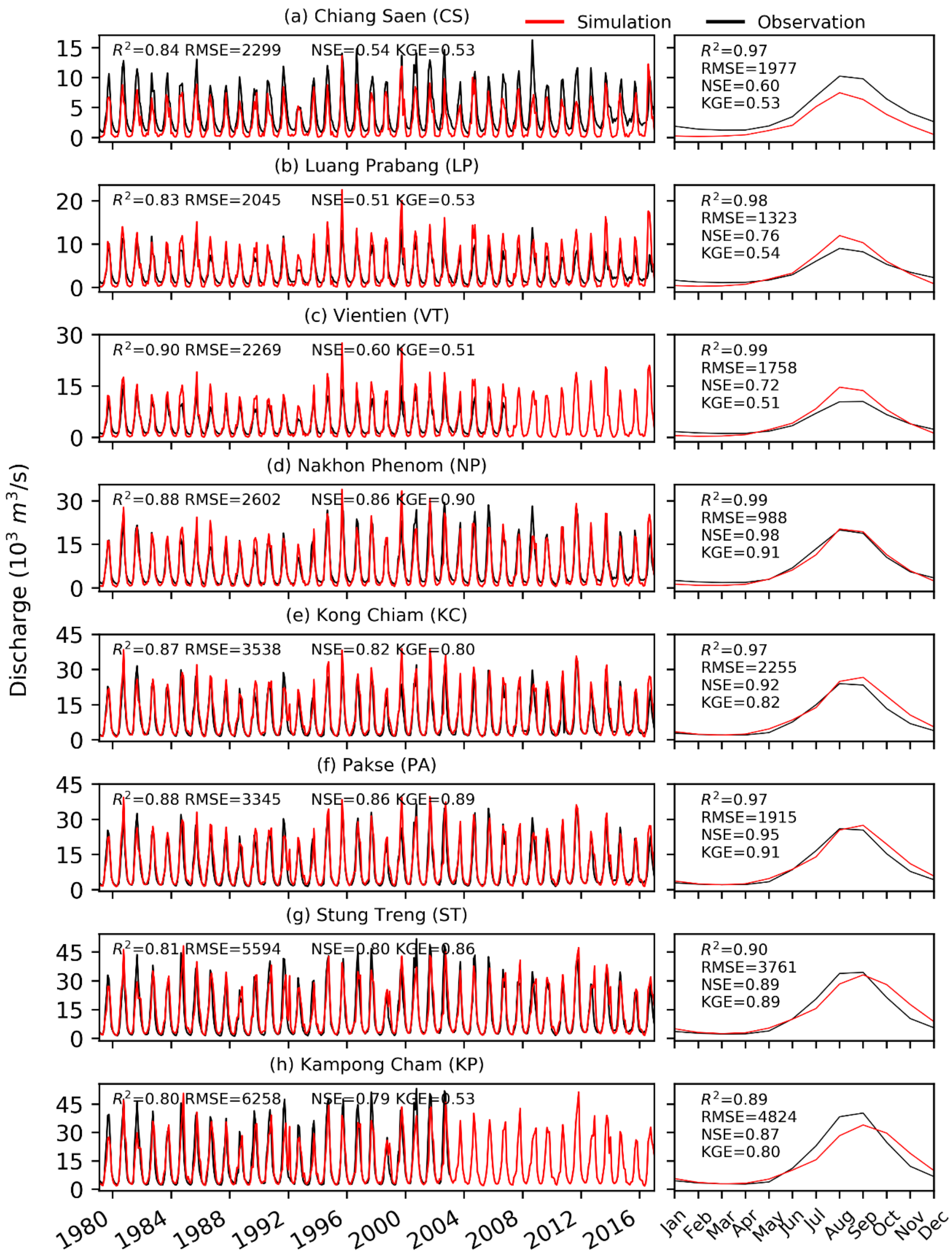

Figure 2-2. Evaluation of monthly streamflow (1979-2016) from the baseline simulation at eight gauging stations marked in Figure 2-1. Panels on the right show the mean seasonal cycle. Observed data (obtained from the MRC) are shown for only the period available. R^2, RMSE, NSE, and KGE are shown in each panel. The right and left panels share the same y-axis labels.

At most of the selected stations, the model captures the observed long-term trend and variability as well as the seasonal variations in streamflow remarkably well (see R^2 in Figure 2-

2). The low flow is generally well reproduced at most stations with an exception of CS, the most upstream station in the LMRB. Flood peaks are also simulated reasonably well with varying accuracies from year to year. Some discrepancies can be seen, which could be partly attributed to missing effects of dams, especially the Lancang cascade dams in the UMRB, and partly to CLM5 parameterizations (e.g., snowmelt and groundwater) as well as input forcing (discussed later). Previous studies have shown that the impacts of the Lancang cascade dams have already been observed at the CS station (Han et al., 2019; Li et al., 2017; Räsänen et al., 2017) but the impacts are pronounced only after the year 2010 (Shin et al., 2020).

Dams are not simulated in the present study because CLM5 does not include a reservoir operation scheme. Our results indicate that the accuracy is generally higher in the downstream stations (see Nash–Sutcliffe Efficiency (NSE) and Kling-Gupta Efficiency (KGE) in Figure 2-2), particularly for low flow. In general, the effects of upstream dams are offset in the downstream by the substantial flow accumulation from downstream tributaries. The increased downstream accuracy is, however, contrary to some previous findings (e.g., Wang et al., 2016) on higher accuracies in the upstream. In our study, no adjustment is done to the subsurface runoff parameterizations (i.e., CLM5 employs a linear representation of the subsurface runoff which is a function of saturated soil thickness as explained in Section 2.2) that could technically be calibrated for improved performance (Bisht et al., 2018; Felfelani et al., 2021) especially at the upstream location of the MRB where the topography is relatively complex.

The long-term average seasonal cycle of the simulated streamflow also compares well with observations both in terms of magnitude and timing (Figure 2-2 right panels). Again, the largest discrepancy among all stations can be seen at the most upstream station (i.e., CS); the performance improves toward the downstream with the simulated seasonal cycle comparing extremely well with observation at the middle reach (NP, KC, and PA). Further downstream, the performance is not as good, likely due to missing representation of predominant floodplain processes including channel bifurcation. In particular, both the timing and magnitude of peak are not as accurately reproduced by the model at KP where the mainstream flow could have been affected by floodplain processes. Overall, the results provide confidence that CLM5 accurately simulates the long-term temporal dynamics as well as the seasonality of streamflow and could be used to examine the uncertainties caused by precipitation data discussed in the subsequent sections.

2.3.2 Evaluation of Simulated TWS with GRACE Data

Figure 2-3 depicts a comparison of simulated and GRACE-based TWS anomaly averaged over the entire MRB and for the GRACE-simulation data overlap period of 2002-2016. Similar to streamflow, CLM5 reasonably captures the temporal variability of basin-averaged TWS anomaly. In particular, the temporal variability is accurately reproduced, along with the historical wet and dry cycles in the MRB even though there are certain discrepancies. For example, the TWS amplitude during the relatively dry (e.g., 2005, 2007, and 2015) and wet (e.g., 2011 and 2013) years are in good agreement with GRACE even though the model missed some events such as the low TWS in 2010. Figure 2-3 also includes the surface and subsurface components of the simulated TWS anomaly but those could not be evaluated because GRACE data does not provide the individual components.

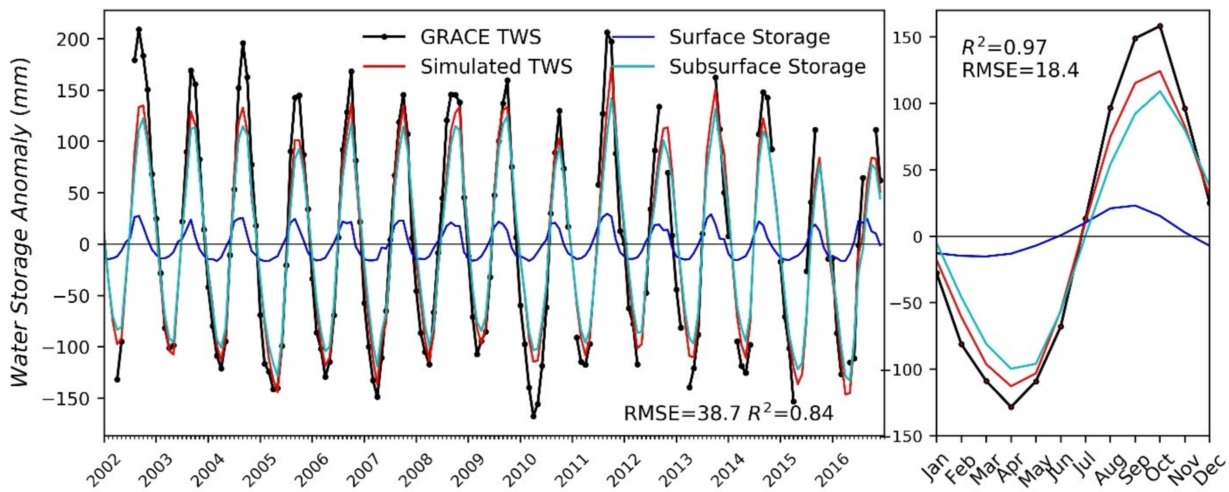

Figure 2-3. Comparison of simulated and GRACE-based monthly TWS anomaly averaged over the entire MRB for the 2002-2016 period. Simulated surface and subsurface water storage components are also shown. Surface water storage includes water stored in rivers, small sub-grid scale water bodies, snow, and canopy whereas subsurface water storage includes water stored in the soil column. The right panel shows the seasonal cycle. R^2 and RMSE are also shown in each panel.

The simulated seasonal cycle of TWS also matches well with the GRACE data with slightly underestimated peak amplitude (Figure 2-3; right panel), likely due to lack of flood processes such as the two-way flow in the Tonle Sap River and wet-season storage in the TSL that plays a role of natural detention reservoir during the flood season. The seasonal cycle of the simulated TWS components suggests that when averaged over the entire MRB, ~16% of the seasonal TWS amplitude is explained by the amplitude of seasonal surface water storage, in line with the findings of Pokhrel, et al., (2018b) who reported this contribution to be ~13% based on a global LSM HiGW-MAT that is similar to CLM5 in process representation. Using the results from a hydrodynamic model (CaMa-Flood) that explicitly simulates floodplain processes, the same study found the surface water contribution to be ~27% of the seasonal TWS amplitude. These findings underscore the importance of representing flood inundation processes in the models. Further, the remarkably well reproduced streamflow in the middle reaches indicates that the discrepancies in TWS simulations could have come primarily from missing floodplain storage in the TSL and Mekong Delta regions where the hydrology is modulated primarily by substantial seasonal surface water storages in rivers, floodplains, and wetlands. Overall, these TWS comparisons add further confidence that CLM5 reasonably simulates the fundamental hydrological processes over the entire basin.

2.3.3 Propagation of Precipitation Uncertainty in Streamflow

Figure 2-4 presents the simulated and observed daily climatological mean streamflow at six selected gauging stations where continuous observations are available during the simulation period, for five different time windows: 1998-2016 mean (Figure 2-4a), dry years (1998 and 2015; Figures 2-4b, c), and wet years (2000 and 2011; Figures 2-4d, e). It is readily discernible in the figure that streamflow simulated using different precipitation datasets varied substantially at all stations as a direct result of the large difference between the precipitation products.

The following key observations can be made from Figure 2-4. First, the timing of peak flow in the long-term mean (Figure 2-4a) is captured well in most simulations, especially in the stations downstream of CS; however, peak magnitude is substantially overestimated in all but the baseline simulation. For the long-term mean (Figure 2-4a) and when averaged across all stations except CS, the peak magnitude is overestimated by ~30% in the MSWEP simulation and ~50% in TRMM, ERA5, and PERSIANN-CDR simulations, compared to only 15% in the baseline simulation. Because all other forcing variables and experimental settings are identical among different simulations, these differences are a direct result of the differences in precipitation data.

A comparison of the precipitation data indicates that the total precipitation during the wet season (i.e., June-November) in the four datasets is 10-25% higher than in the WFDEI data; on an annual basis, the difference ranged between 7-19%. That is, the difference in the magnitude of peak flow is generally larger than the difference in total precipitation during the wet season, implying that the propagation of precipitation uncertainty into streamflow simulations could amplify in terms of the magnitude of peak flow. These findings highlight the need for reliable precipitation data to accurately simulate the flood pulse in the MRB. Choice of certain parameters in CLM5 including f_{over} and K_{base} (see Section 2.2.2 for details) could also be linked to the uncertainty and nonlinear response of streamflow to varying precipitation datasets. Understanding such dynamic linkages between model parameters and forcing data requires a detailed sensitivity analysis, which is beyond the scope of the present study. Second, the low flow is generally well captured in most simulations with relatively small differences among the five simulations. This is reasonable because the MRB receives a substantial portion of the total annual precipitation (~70%) during the wet season (Chen et al., 2018), hence the dry season flow is less influenced by precipitation even though the water storage during the dry season—directly influenced by precipitation—can buffer dry season flows.

Third, results indicate that the use of higher resolution precipitation data would not necessarily lead to improved streamflow results for the MRB. It is evident from Figure 2-4a and validation provided in Section 3.1 that the baseline simulation with WFDEI data (0.5°) produces better results compared to the other simulations with higher resolution precipitation data (0.25°-0.1°; see Section 2.3.1), particularly in terms of the wet-season flow patterns and the peak magnitude. All four simulations with higher resolution precipitation data produce comparable long-term daily simulations, which cluster away from the baseline simulation and do not compare well with observations. Detailed statistics of the comparison of all simulations with observation are provided in Table 2-1. At the upstream stations (CS and LP), relatively larger discrepancies can be seen between all simulations and observations (see Section 3.1). These results indicate that the spatial resolution of precipitation data is not the primary cause of uncertainties in streamflow simulations; instead, the spatial distribution of precipitation and its total amount is important. A direct evaluation of all precipitation datasets with ground observations would provide further insights but this is not possible due to lack of observed data.

Fourth, large differences are found between different simulations for wet and dry years (Figures 2-4b-e). In general, there is a large and systematic overestimation of wet season flow during dry years in all simulations (Figures 2-4b,c) but, again, the baseline simulation outperforms the others. The overestimation in peak magnitude in the baseline simulation ranges between 2-28% and 15-51% for 1998 and 2015, respectively; the overestimation in the MSWEP simulation is similar with the range being 2-28% and 14-51%, respectively. The overestimation is much larger in TRMM, ERA5, and PERSIANN-CDR simulations ranging between 42-79%, 114-115%, and 51-85%, respectively for 2015. Overall, the systematic wet bias during the wet season even in dry years could suggest a potential tendency in CLM5 to overestimate streamflow; however, and importantly, the relatively better comparison of the baseline simulation with observations indicates that the overestimation is due to overestimated precipitation amount. Also, the untimely secondary streamflow peak observed in 1998 in the baseline simulation, particularly in the downstream stations (i.e., KC, PA, and ST), mostly reflects the precipitation pattern in that year (Figure 2-5), suggesting that precipitation uncertainty is directly affecting the magnitude and timing of flow.

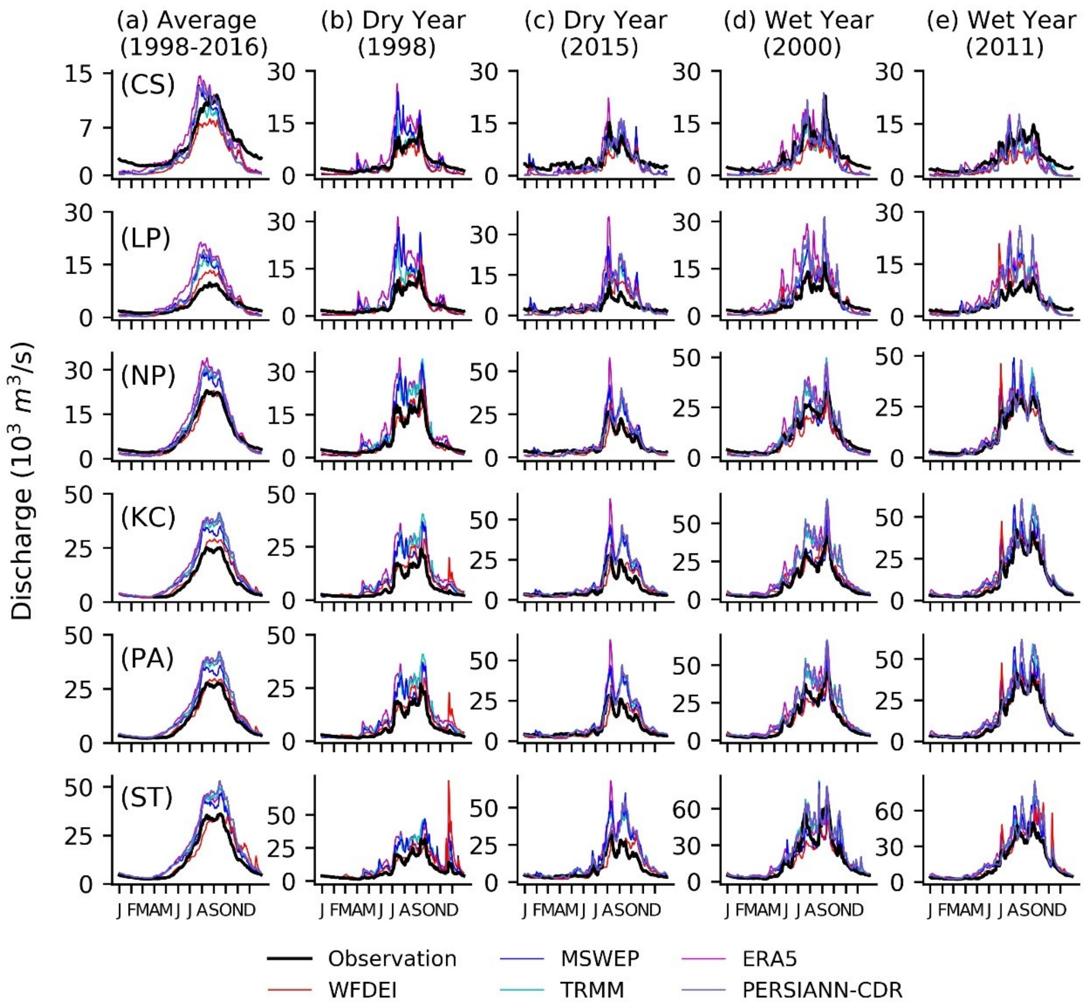

Figure 2-4. Simulated and observed daily streamflow climatology at six selected gauging stations and for five different periods. The simulated results shown are from the baseline simulation and four additional runs using different precipitation datasets. The station abbreviations are indicated in Figure 2-1.

Table 2-1. R2 and RMSE calculated for different periods as shown in Figure 2-4.

	Long term average (R^2)					Long term average (RMSE)				
	WFDEI	**MSWEP**	**TRMM**	**ERA5**	**PERSIANN-CDR**	**WFDEI**	**MSWEP**	**TRMM**	**ERA5**	**PERSIANN-CDR**
CS	0.96	0.86	0.92	0.86	0.88	2075	1728	1654	1828	1835
LP	0.98	0.91	0.95	0.90	0.93	1737	3332	2913	5184	3908
NP	0.98	0.98	0.99	0.98	0.99	1293	2514	3012	4534	3402
KC	0.90	0.95	0.96	0.96	0.94	3159	4236	5793	6377	6704
PA	0.89	0.95	0.96	0.96	0.94	3225	3105	4453	4871	5390
ST	0.81	0.93	0.95	0.96	0.93	6028	3859	4517	4212	5735
	1998 (R^2)					**1998 (RMSE)**				
	WFDEI	**MSWEP**	**TRMM**	**ERA5**	**PERSIANN-CDR**	**WFDEI**	**MSWEP**	**TRMM**	**ERA5**	**PERSIANN-CDR**
CS	0.91	0.80	0.85	0.80		1565	2784	1672	3619	
LP	0.89	0.82	0.90	0.85		1520	4312	2958	5627	
NP	0.91	0.89	0.96	0.94		1915	3692	4114	5424	
KC	0.84	0.88	0.96	0.94		3735	5165	6610	7529	
PA	0.83	0.89	0.96	0.95		3643	4590	5971	6824	
ST	0.53	0.83	0.94	0.93		8022	7281	7235	7613	
	2015 (R^2)					**2015 (RMSE)**				
	WFDEI	**MSWEP**	**TRMM**	**ERA5**	**PERSIANN-CDR**	**WFDEI**	**MSWEP**	**TRMM**	**ERA5**	**PERSIANN-CDR**
CS	0.76	0.79	0.80	0.84	0.76	2401	2160	1931	2423	2285
LP	0.80	0.87	0.89	0.91	0.79	2477	4276	3427	6135	4235
NP	0.84	0.95	0.95	0.95	0.84	2808	4573	4221	6297	4451
KC	0.78	0.93	0.94	0.93	0.81	3525	6661	6538	8299	6831
PA	0.82	0.95	0.95	0.95	0.85	3240	6033	5955	7736	6216
ST	0.78	0.95	0.95	0.96	0.87	4308	8668	7566	9497	8342
	2000 (R^2)					**2000 (RMSE)**				
	WFDEI	**MSWEP**	**TRMM**	**ERA5**	**PERSIANN-CDR**	**WFDEI**	**MSWEP**	**TRMM**	**ERA5**	**PERSIANN-CDR**
CS	0.86	0.88	0.88	0.81	0.87	3295	2344	2353	2306	2300
LP	0.88	0.93	0.91	0.85	0.92	1852	2469	3293	5967	4273
NP	0.95	0.94	0.93	0.95	0.93	3486	2950	3761	4862	4140
KC	0.92	0.93	0.77	0.95	0.92	3213	2868	9393	8823	9077
PA	0.92	0.93	0.94	0.95	0.92	3600	3331	6385	6895	7358
ST	0.90	0.83	0.91	0.94	0.87	7681	7263	7445	5538	8949
	2011 (R^2)					**2011 (RMSE)**				
	WFDEI	**MSWEP**	**TRMM**	**ERA5**	**PERSIANN-CDR**	**WFDEI**	**MSWEP**	**TRMM**	**ERA5**	**PERSIANN-CDR**
CS	0.91	0.75	0.62	0.73	0.71	3230	2639	3121	2201	2776
LP	0.88	0.93	0.91	0.85	0.92	2874	3460	3101	4622	4308
NP	0.91	0.94	0.95	0.92	0.92	3118	3583	3382	3852	3785
KC	0.92	0.94	0.94	0.91	0.91	4034	5105	5750	5580	6909
PA	0.94	0.95	0.95	0.93	0.91	3617	4966	5588	4999	6906
ST	0.85	0.96	0.95	0.94	0.89	7405	7172	7222	6363	9768

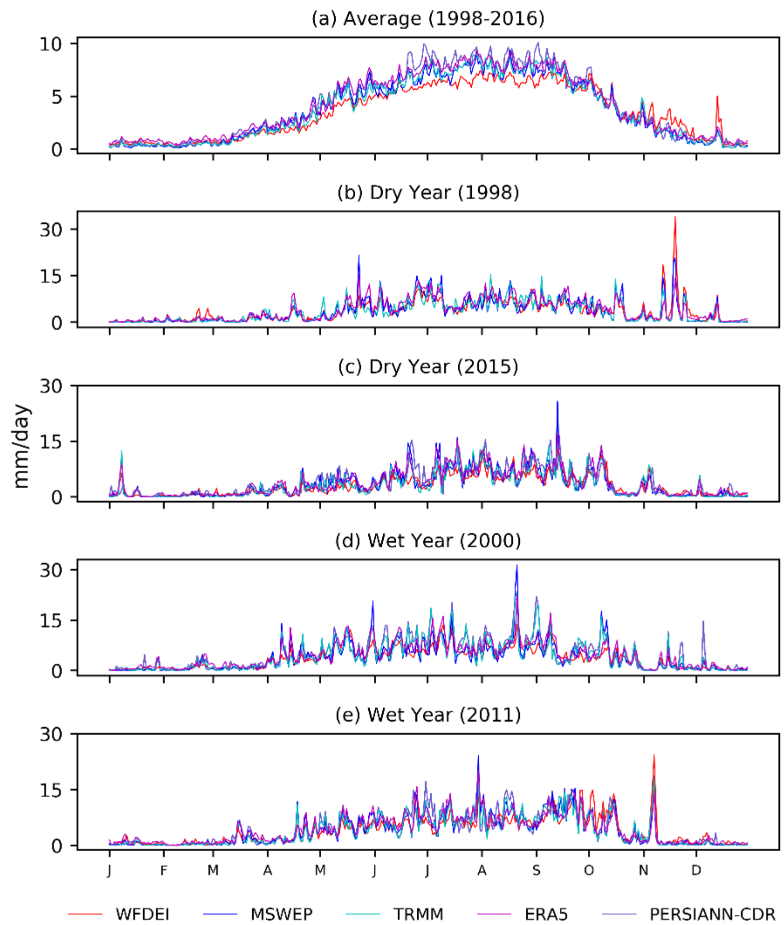

Figure 2-5. Mean annual precipitation climatology for the period of 1998-2016. Simulated results for the same period are analyzed to examine precipitation uncertainty.

Results for the wet years (Figures 2-4d, e) also suffer from overestimation as during dry years, especially during the wet season. The results from the baseline simulation show different traits with underestimation of 1-18% and overestimation of 10-40% in the years 2000 and 2011, respectively. The overestimation is much larger in the other four simulations ranging from 15-47%, 33-76%, 20-75%, and 26-88% for MSWEP, TRMM, ERA5, and PERSIAN-CDR simulations, respectively, for the year 2000. For 2011, these overestimates range between 35-101%, 36-76%, 19-122%, and 44-135% for MSWEP, TRMM, ERA5, and PERSIAN-CDR simulations, respectively. Similar to the peak flow, precipitation uncertainty has a substantial impact on the high (Q5) and low (Q95) flows (Figure 2-6). The low flow indicator is underestimated in all simulations, particularly in the upstream and some intermediate stations. This is likely because of the missing reservoirs in the model—reservoirs generally augment dry season flow.

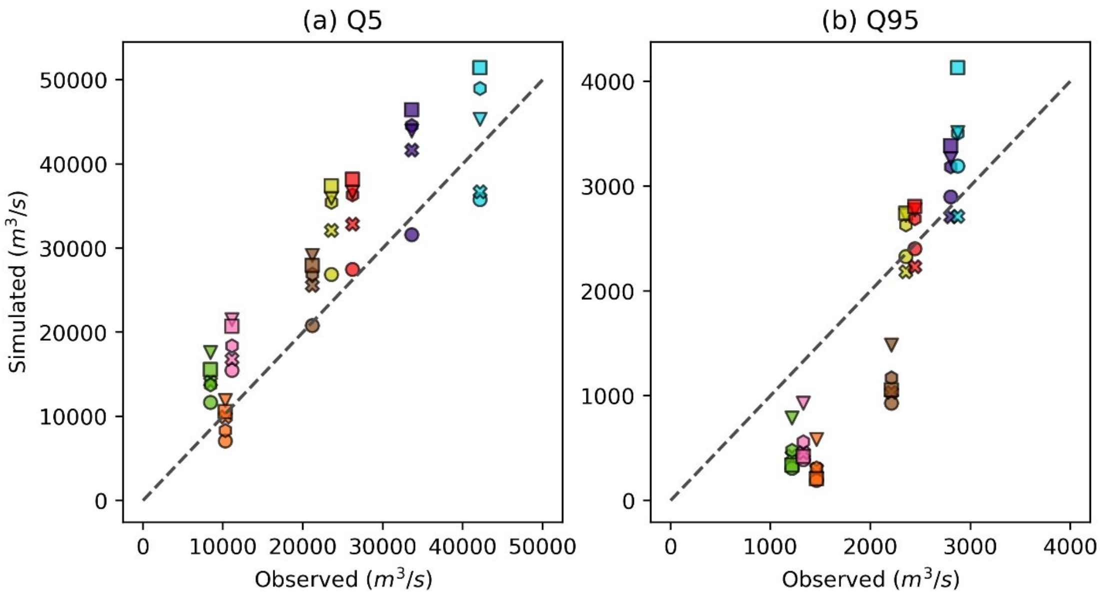

Figure 2-6. Comparison of simulated and observed high flow indictor (Q5) and low flow indicator (Q95) for eight stations for the 1998-2016 period. Markers denote different simulations and colors indicate different stations as consistent with Figures 2-4 and 2-5.

The above results demonstrate that precipitation is a major source of uncertainty for streamflow simulations in the MRB. In particular, precipitation data choice tends to substantially affect the magnitude of the peak flow—the flood pulse in the MRB—implying that the choice of precipitation data may largely govern flood pulse simulations regardless of model parameterizations and other input datasets. Models could be calibrated to still match simulated streamflows with observations, but such a calibration would lead to the right results for the wrong reasons.

Figure 2-7 presents a more detailed evaluation of streamflow at all stations using the Taylor diagram and four widely-used statistical measures, namely the NSE, KGE (Gupta et al., 2009), Percent Bias (PBIAS), and Mean Percent Error (MPE). The Taylor diagram summarizes simulation errors in terms of the ratio of standard deviation (SD) of the simulated streamflow to the observed streamflow as radial distance and their correlation as an angle in the polar axis (Figure 2-7a).

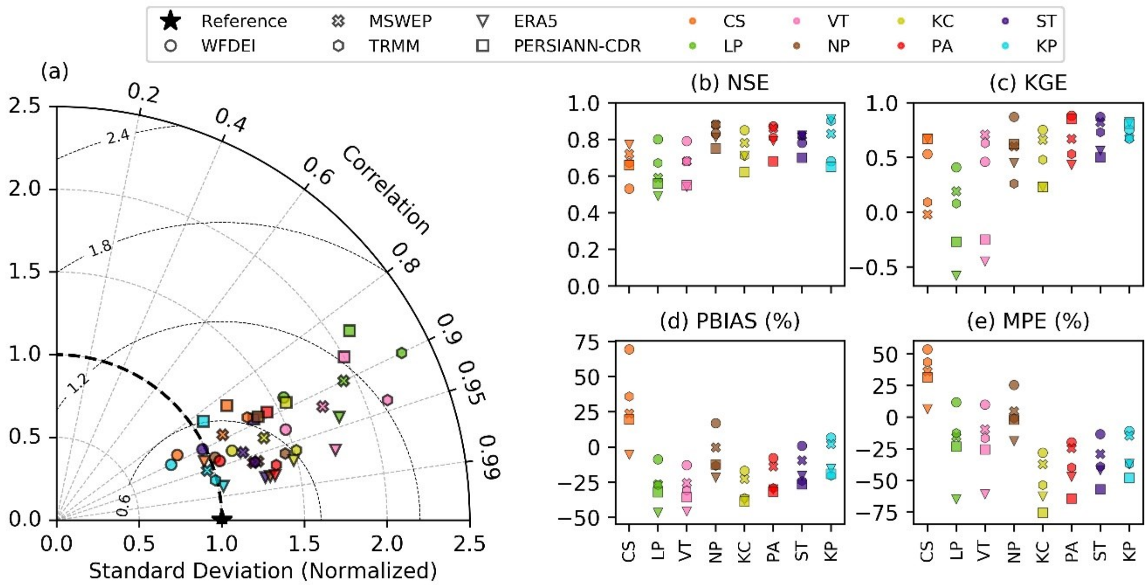

Figure 2-7. The performance of different simulations in capturing monthly streamflow during 1998-2016 at the eight gauging stations marked in Figure 2-1. The result for PERSIANN-CDR is shown for the 2000-2016 period. Simulations are indicated with markers and gauging stations are color-coded. The Taylor diagram on the left (a) illustrates the normalized standard deviation (SD) on vertical and horizontal axis and the correlation on the radial axis. The reference point (black star) is situated where correlation and normalized SD are both unity. Four panels on the right: Nash–Sutcliffe efficiency (NSE) (b), Kling-Gupta Efficiency (KGE) (c), Percent Bias (PBIAS) (d), and Mean Percent Error (MPE) (e) statistical measures. Figures 2-7b-e share the same x-axis labels.

It is evident from Figure 2-7a that the baseline simulation (i.e., WFDEI) outperforms all other simulations in producing the temporal dynamics of streamflow at most stations (correlation > 0.9), as also discussed in Section 3.1 (Figure 2-2). Note that the evaluation period here is different than that in Figure 2-2. Performance varies between stations and across simulations. For example, the normalized SD at the upstream stations (CS, LP, and VT) varies substantially across simulations where high ratios (i.e., >1.5) are evident for all simulations but the baseline.

Such relatively inferior performance in these stations is also discussed in Section 3.1 and Figure 2-2. While there are differences in the flow variability ratio (based on the spread of SD in the Taylor diagram), most of the simulations capture the temporal dynamics of streamflow with a correlation ratio between 0.8 and 0.99. The correlation for the downstream stations is generally better (Figure 2-7a). Further, the PERSIANN-CDR and ERA5 simulations form the lower bound (lowest correlation) and upper bound (highest correlation), respectively, in the Taylor diagram. A more detailed evaluation of the variations in performance across stations and simulations is presented in Figures 2-7b-e using additional statistical measures such as the NSE, KGE, PBIAS, and MPE. These measures provide insights into how various streamflow signatures are reproduced. For example, NSE rates the simulations' predictive skill in capturing the observed streamflow, KGE decomposes NSE into its components (Correlation, variability term and, bias ratio) (Knoben et al., 2019), PBIAS measures the tendency of the simulated streamflow to be larger or smaller than the observed streamflow, and MPE provides the error of each simulation.

Varying predictive skills can be seen in terms of NSE and KGE scores across different simulations. NSE scores demonstrate that simulation performance improves towards downstream stations, with a minimum NSE of 0.6 that ramps up to 0.9 in most downstream stations (Figure 2-7b). PERSIANN-CDR simulation shows relatively poor performance in terms of NSE whereas ERA5 underperforms according to KGE scores. There is, however, a wide range in KGE at some stations, particularly at CS, LP, VT, and NP (Figure 2-7c), even though the NSE does not vary substantially. Varying KGE score between simulations is a result of the different bias ratios (ratio of simulated mean to observed mean), in addition to the difference in flow variability error and correlation, as shown in the Taylor diagram (Figure 2-7a). According to the KGE score, WFDEI simulations perform the best while ERA5 simulation perform poorly across the

MRB. As evident from the varying KGE, performance varies across simulations to capture the mean flow for many stations. As other forcing variables and model parameterizations are consistent across simulations, such differences in predictive skills could be directly attributed to the uncertainty in the precipitation data. PBIAS (Figure 2-7d) indicates that the tendency to underestimate streamflow is relatively high in CS, while it is overestimated at the intermediate stations (PBIAS < 0). The minimum bias is achieved toward the downstream and especially in the WFDEI simulation. Further, streamflow simulation error differs substantially between stations and simulations based on MPE (Figure 2-7e). The absolute MPE in the ERA5 simulation is the highest in CS to NP stations and substantially large compared to other simulations whereas PERSIANN-CDR simulation shows the highest absolute MPE in further downstream stations.

Some other sources of uncertainty such as wind-induced under-catch tend to underestimate precipitation in the mountainous part of the UMRB and the difficulty in interpolating input data in the narrow-stretched parts of the basin could possibly add additional uncertainty in streamflow simulation. These effects could have affected different precipitation products at varying degrees, leading to varied propagation to streamflow simulations. In general, the detailed statistical analyses indicate that high spatial resolution of the precipitation data would not necessarily improve the simulation efficiency. Specifically, WFDEI and MSWEP show nearly similar efficiency at all stations although the spatial resolution of these two datasets is substantially different (Section 2.3.1). In contrast, TRMM, ERA5, and PERSINN-CDR have varying efficiency (different NSE and KGE) even though they have the same—and relatively higher—spatial resolution. Overall, all precipitation except WFDEI and MSWEP show relatively poor efficiency across stations (e.g., 0.5>KGE>0; Kling et al. (2012)). Such varying scores of different statistical measures further suggest that caution should be taken when using lumped parameter model with parameter tuning using such statistical measures as objective functions to improve simulation accuracy.

2.3.4 Uncertainty in TWS, Soil Moisture, and ET

Figure 2-8 presents the uncertainty in simulated TWS resulting from the uncertainty in precipitation input by comparing TWS anomaly from different simulations with GRACE data. The broad spatial patterns and seasonal variations of TWS are captured in all simulations, although differences are evident in the seasonal amplitude. In terms of timing, basin-wide discrepancies among simulations and GRACE are notable in some seasons. Examples include DJF where none of the simulations could capture the seasonal mean in GRACE data, showing disagreement even in the direction of change in some areas. GRACE, for instance, detects negative anomaly in the areas around TSL whereas WFDEI, MSWEP, and ERA5 simulations show positive anomaly. Some differences are also found in the Mekong delta during MAM when GRACE detects relatively small negative TWS anomaly compared to all simulations. The differences between GRACE and simulations are likely caused by missing floodplain processes as well as uncertainty in forcing datasets as it is evident that precipitation uncertainty largely affects streamflow simulation discussed earlier (Section 3.3). Coarse-resolution (i.e., ~0.5-3 degrees) and lack of fine-scale details in GRACE data limit a fully consistent comparison with high resolution (~5km) TWS simulations especially over the narrow-stretched portion of the basin.

While simulations show notable spatial discrepancies (Figure 2-8) as a result of using different precipitation datasets, the basin-averaged TWS anomaly largely agrees across simulations (Figure 2-9). Spatially, the agreement between simulations is generally good in the UMRB as opposed to differences in the LMRB. For example, during DJF, the WFDEI simulation shows positive anomaly over a sizable portion of the LMRB, while other simulations except PERSIANN-CDR show positive anomaly at a relatively small magnitude only in some parts of the LMRB. The differences within the simulations are also quite evident during MAM, with TRMM and PERSIANN-CDR demonstrating strong negative anomaly in the Mun-Chi sub-basin and delta regions, while other simulations produce negative anomaly only around the mainstream of the Mekong River. There are also large basin-wide variations in precipitation during MAM (Figure 2-10), which can be linked to variations in simulated TWS during that season.

Also in JJA, there are differences between the simulations, particularly in the 3S river system. MSWEP and ERA5 produce different spatial patterns than WFDEI, TRMM, and PESIANN-CDR. Conversely, all simulations produce a similar spatial variation of TWS during SON. Also, the attributional analysis (discussed later) suggests a relatively small TWS response to precipitation during SON. The highest variation in TWS can be seen (Figure 2-8) on the Mun-Chi sub-basin, areas around TSL, and delta regions where the hydrology is strongly modulated by the amount of precipitation in the basin (Figure 2-10). The results indicate that accurate spatial distribution of precipitation is crucial to capture the basin-wide changes in TWS. Spatially, the mean annual precipitation amount also substantially varies among different datasets, particularly in LMRB (Figure 2-11), affecting TWS variations over long terms. Overall, TWS anomaly among simulations varies, particularly exhibiting large variations during JJA, following the patterns of wet season streamflow, which can be attributed to the variations in mean seasonal precipitation amount among five precipitation products (Figure 2-11).

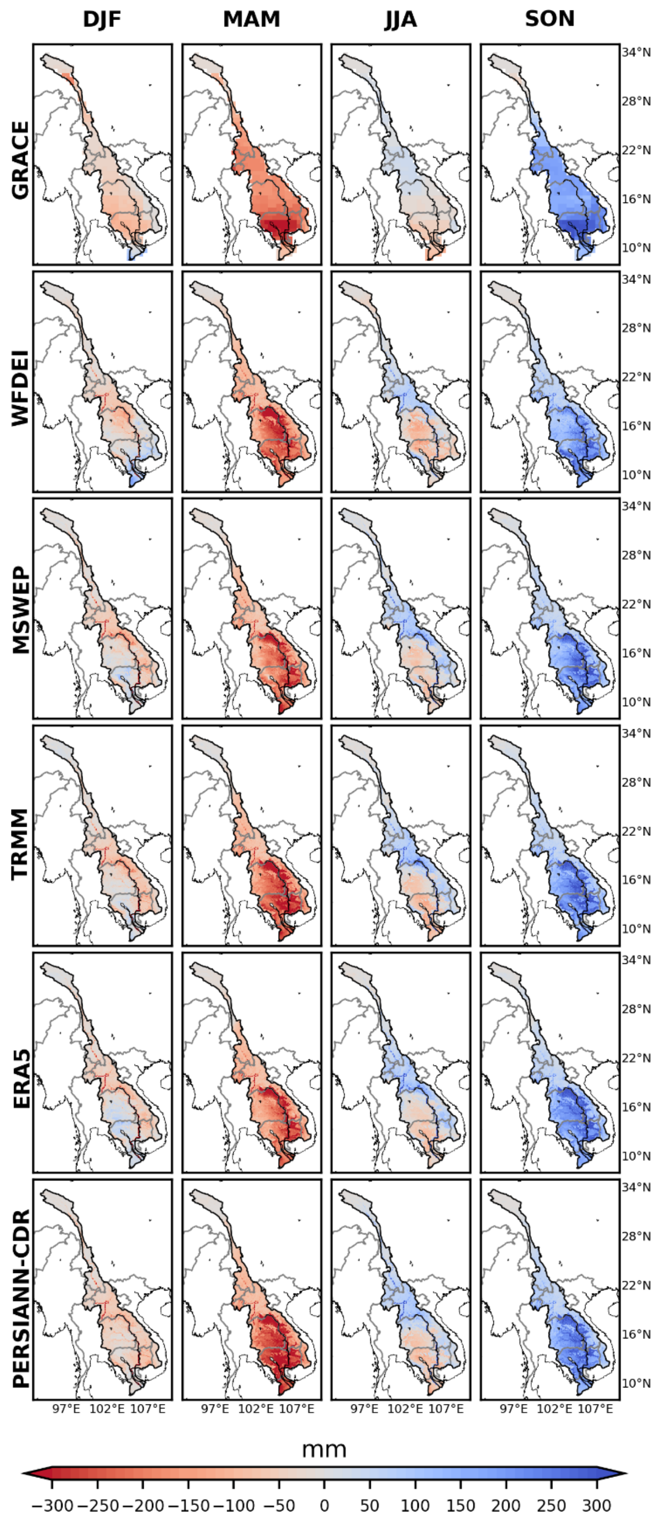

Figure 2-8. Spatial variability of the seasonal average of TWS anomaly from five different simulations and GRACE data for the 2002-2016 period. GRACE results are shown as the mean of mascon solutions from two different processing centers (i.e., CSR and JPL).

Simulations driven by different precipitation datasets capture the broad spatial pattern of soil moisture seen in SMAP data, and the contrast between UMRB and LMRB, particularly during DJF and MAM (Figure 2-12). However, some discrepancies are also evident, especially during JJA and SON during which precipitation uncertainty could have substantially affected soil moisture simulations. A comparison of soil moisture from different simulations with observed soil moisture could provide further insights on the role of precipitation uncertainty in soil moisture simulations; however, such an exercise is not possible due to the lack of observed soil moisture products for the MRB. Further, even the comparison with SMAP data should be interpreted with caution, especially in the southeastern part of the LMRB, because SMAP data likely include substantial uncertainties in these densely vegetated and forested areas (Mousa & Shu, 2020; Zhang et al., 2019).

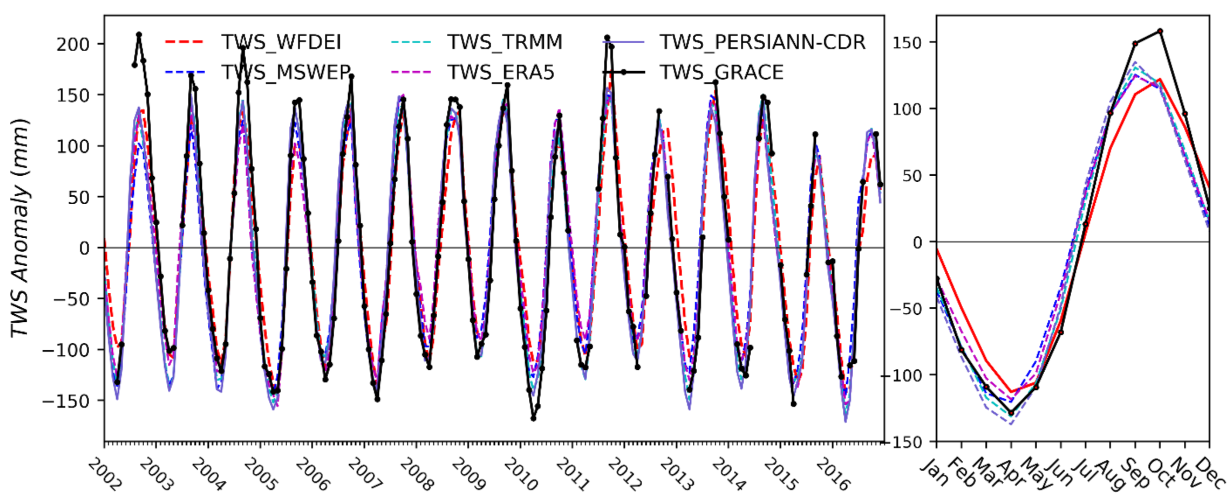

Figure 2-9. Comparison of TWS anomaly from multiple precipitation driven simulations for the 2002-2016 period. In the right panel of the figure comparison of the monthly seasonal cycle of TWSA from all simulations and GRACE is also shown.

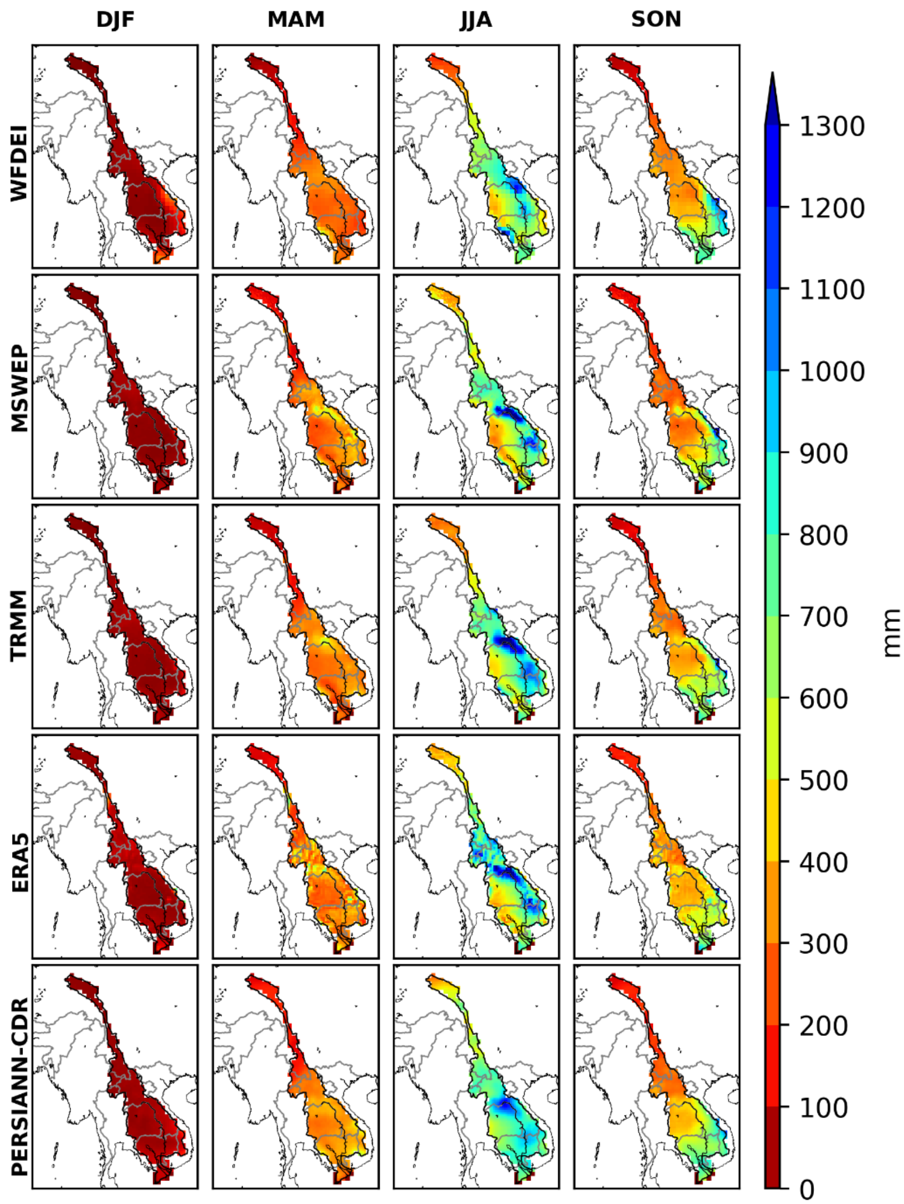

Figure 2-10. Mean seasonal precipitation for the period of 1998-2016. Simulations for the same period are analyzed to examine precipitation uncertainty.

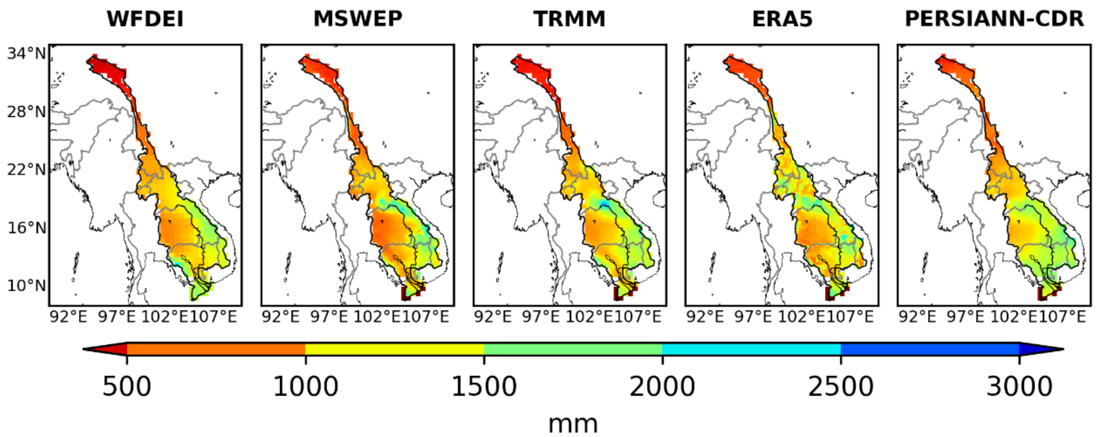

Figure 2-11. Mean annual precipitation for the period of 1998-2016. Simulated results for the same period are analyzed to examine precipitation uncertainty.

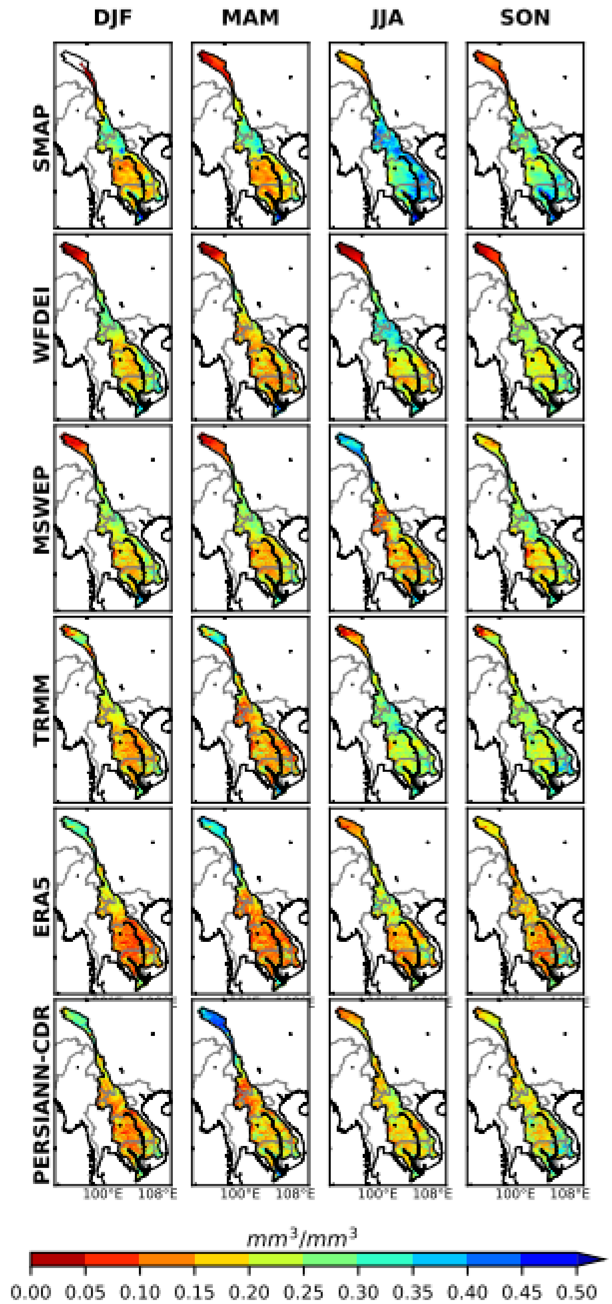

Figure 2-12. Comparison of seasonal soil moisture with SMAP data for the year 2016.

Nonetheless, the comparison of soil moisture among simulations (Figure 2-12; left panels) suggests that soil moisture can vary considerably between simulations and across the basin as a direct result of the uncertainty in seasonal precipitation (Figure 2-10). Spatially, the variations in grid-level soil moisture are considerable during DJF and MAM, with results from the WFDEI simulation showing the lowest soil moisture estimates and ERA5 showing the highest (Figure 2-7; left panels). Similarly, attributional analysis (Figure 2-14) shows the highest disagreement in precipitation between WFDEI and ERA5 during MAM and thereby the highest soil moisture response, suggesting that precipitation uncertainty can substantially affect soil moisture simulations. The disagreement in the LMRB is pronounced in the wet season, similarly to streamflow. For example, soil moisture simulations from WFDEI, MSWEP, and TRMM show relatively better agreement with each other in DJF and MAM, but show large differences in JJA and SON—especially in the LMRB—during which the total precipitation amount largely varies among different precipitation products (Figure 2-11). Discrepancies among simulations suggest that the degree of precipitation uncertainty varies spatially across the basin and substantially impacts soil moisture simulation at the grid level, which further highlights that accurate precipitation data with realistic spatial distribution are critical for consistent simulation of soil moisture in the MRB.

To examine the effect of precipitation on seasonal ET we compare simulated ET from different simulations (Figure 2-13; right panels), highlighting how precipitation biases impact other water cycle components. Despite differential ET rates among simulations at the grid level, all simulations produce a similar pattern of basin-wide ET variations (Figure 2-13; right); this includes the contrast between UMRB, LMRB, and the Mekong delta. Results indicate that ET variations in the MRB are less sensitive to precipitation than other variables such as TWS and soil moisture, likely because there is an upper limit for ET due to energy limitations during the wet season. Overall, simulated TWS, soil moisture, and ET differ in their sensitivity to different precipitation inputs. Attributional analysis (Figure 2-14) provides further insights on the sensitivity of different variables to change in precipitation.

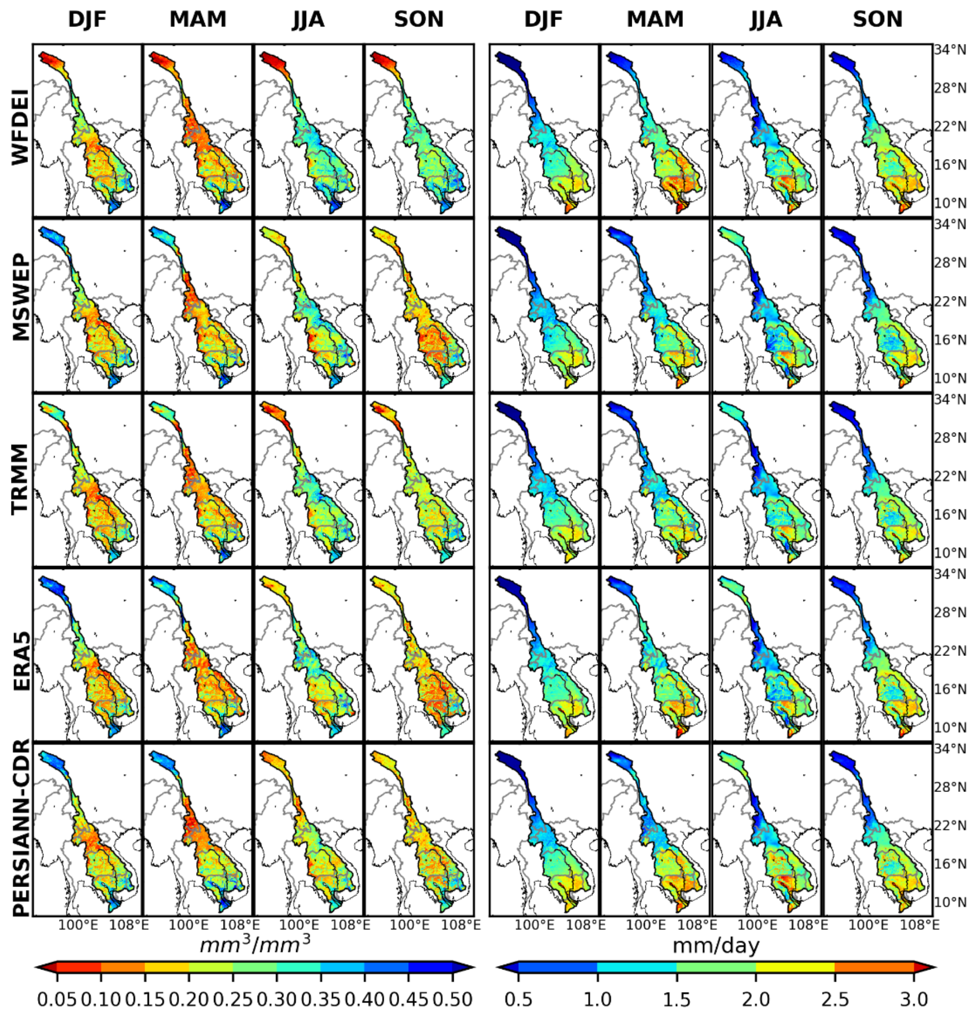

Figure 2-13. Spatial variability of the seasonal average of soil moisture (left) and ET (right) from five different simulations for the 1998-2016 period except for PERSIANN-CDR. Results for PERSIANN-CDR are shown for the 2000-2016 period. Soil moisture is shown for 10 cm depth of soil.

Results from the attributional analysis (Figure 2-14) suggest that runoff and soil moisture show the strongest response to precipitation uncertainties compared to other hydrologic variables such as TWS and ET (Figure 2-14c and Figure 2-14e). While these results provide some insights on the sensitivity of water balance components to precipitation input, further investigation is warranted to provide a more detailed and mechanistic understanding of the effect of precipitation uncertainty on the partitioning of precipitation into different water balance terms.

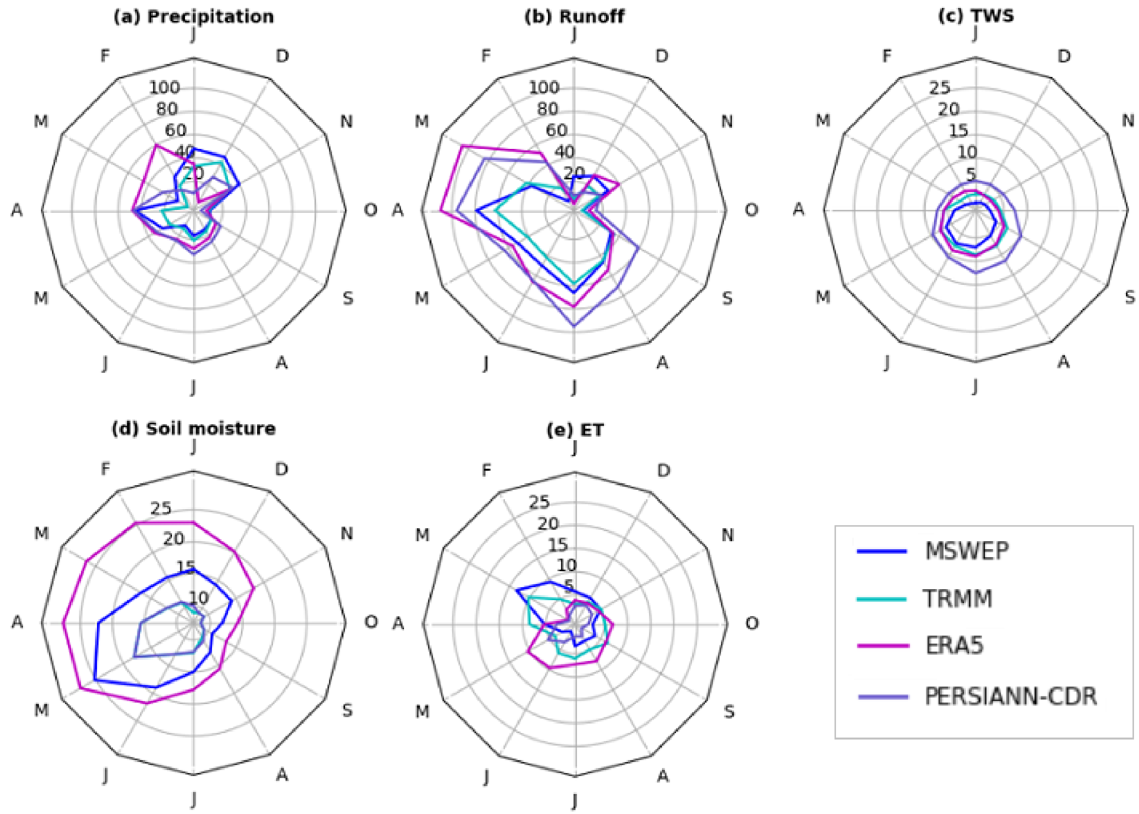

Figure 2-14. An attributional analysis of monthly runoff (b), TWS (c), soil moisture (d), and ET (e) in response to the differences in precipitation (a). Note that all changes are calculated taking WFDEI as the benchmark. The differences in precipitation and resulting differences in the runoff, TWS, soil moisture, and ET are shown as percentages in the radial axis. Note that the radial axes are different among plots. J to D in the angular axis represents the month from January to December.

2.4 Summary and Conclusions

This study examines the propagation of precipitation uncertainty into hydrological simulations over the MRB using CLM5 at a high spatial resolution of 0.05° (~5 km). A baseline simulation is first conducted using the WFDEI forcing. Then, four additional simulations are conducted by replacing precipitation data in the WFDEI forcing with precipitation from MSWEP, TRMM, ERA5, and PERSIANN-CDR. Results are validated with observed streamflow, TWS, and soil moisture. Results from simulations driven by five different precipitation datasets are then used to compare and evaluate various streamflow signatures and seasonal patterns of simulated TWS, soil moisture, and ET. To the authors' best knowledge, this is the first study to investigate precipitation uncertainty in hydrological simulations over the entire MRB using a fully process-based LSM.

We synthesize our key findings as follows: First, substantial differences are found between streamflow simulations driven by different precipitation datasets and the degree of such differences varies spatially across the MRB. Second, the effect of precipitation uncertainty is the largest on the peak flow and most simulations tend to overestimate flood peak. Simulated peak flow in wet and dry years is also subject to substantial uncertainties that undermine the model's ability to accurately reproduce the seasonal flood pulse, even though the contrast between dry and wet years in the streamflow climatology is well captured by most simulations. Third, results indicate that using high-resolution precipitation data would not necessarily improve model performance; simulations forced by WFDEI precipitation with relatively coarse resolution outperform those based on high-resolution datasets. Further, the performance of streamflow, TWS, and soil moisture simulations based on the MSWEP precipitation is comparable to that from WFDEI despite MSWEP being the highest resolution precipitation data used in this study. Fourth, there is no single precipitation data that could promisingly capture various streamflow signatures for different periods, suggesting that model parameters from calibration for a certain period using a particular climate forcing could not be used with different forcing data. For example, if flood pulse simulations are of interest, one could select a different precipitation dataset than if drought were to examine. Fifth, the propagation of precipitation uncertainty to streamflow simulations is non-linear and the uncertainty may even amplify. Sixth, substantial differences are also found in the simulation of TWS, soil moisture, and ET driven by different precipitation even though the broad seasonal variations agree well among different simulations. We note that because model parameters are kept constant across all simulations, the uncertainties discussed in this study are solely due to the differences in precipitation input.

The robustness of uncertainty analysis could have been improved if the model did not lack the representation of certain hydrological processes important in the MRB. For example, the MOSART routing scheme used in CLM5 does not simulate some of the floodplain processes that might have impacted the simulations in the LMRB. Further, CLM5 does not simulate the effects of dam and reservoir operation, reported to have detectable impacts on the Mekong flood pulse especially after 2010 (Shin et al., 2020). Improvements in topographic representation and input parameter scaling particularly for MOSART could also improve streamflow simulations. The vector-based routing scheme mizuRoute (Mizukami et al., 2021) showed promising performance in global streamflow simulations; such a scheme might improve regional simulations as well but is computationally intensive for high-resolution applications (Mizukami et al., 2021). Some of the parameters that are sensitive to streamflow and affect the partitioning of surface and subsurface runoff could be calibrated to address part of the uncertainty that may not be related to the choice of precipitation data. As the goal of this paper is to investigate precipitation uncertainty, addressing these caveats related to model process representation and parameter sensitivity form future research directions for our forthcoming publications.

Despite some limitations, this study provides major advances in simulating the hydrology of the MRB using a fully distributed LSM capable of simulating non-linear dynamics of hydrological processes on a full physical basis, providing a better understanding of the propagation of precipitation uncertainty into streamflow and other key hydrological variables including TWS, soil moisture, and ET.

Chapter 3. Climatic and Anthropogenic Controls on Groundwater Dynamics in the Mekong River Basin

Based on: Kabir, T., Felfelani, F., & Pokhrel, Y. (2022). Climatic and Anthropogenic Controls on Groundwater Dynamics in the Mekong River Basin, Journal of Hydrology. [Under Revision]

3.1 Introduction

Groundwater is a crucial component of the global water cycle (Condon et al., 2021; Cooper, 2010; Ferguson & Maxwell, 2010; Miguez-Macho & Fan, 2012a). It is the world's largest freshwater resource that supplies water to billions of people, forms an integral part of irrigated agriculture, and contributes to the health of many ecosystems (Stefan Siebert & Döll, 2010, Cuthbert et al., 2019; Gleeson et al., 2012). At least one-fourth of the world's population heavily relies on groundwater (Döll, 2009). The dependence will likely continue to grow in the future due to the increase in population and associated demands for water, especially agricultural (Siebert & Döll, 2010, Siebert et al., 2015). Agricultural irrigation—which accounts for over 70% of the total freshwater withdrawal and 90% of the consumptive water use (Gleick, 2018; Shiklomanov, 2000)—is reliant heavily on groundwater in many global regions, especially those with limited surface water (N. Hanasaki et al., 2013; Leng et al., 2014; Reinecke et al., 2021; Yoshihide Wada et al., 2013). This reliance is expected to rise sharply owing to increased irrigation needs in relatively dry agricultural regions (Ambika & Mishra, 2019; Crosbie et al., 2013; Scanlon et al., 2012; Yoshihide Wada et al., 2013) or even in relatively humid regions such as the Mekong River Basin (MRB) that are experiencing rapid agricultural intensification (Hoang et al., 2019; T. T. H. Nguyen et al., 2012; Sakamoto et al., 2009) or increased groundwater pumping as surface water availability continues to decline (Erban & Gorelick, 2016; Minderhoud et al., 2017). Therefore, there is a growing need, as well as an interest, to improve our understanding of groundwater processes, especially through process-based modeling; however, major challenges remain due to the complexity of groundwater system (Cuthbert et al., 2019; Y. Fan et al., 2019; Ying Fan et al., 2007; Gleeson et al., 2016).

Groundwater dynamics is modulated by a variety of regional to local hydrological processes that are intricately interconnected and governed by climatic drivers, topographic controls, and hydrogeological characteristics (Cuthbert et al., 2019). Thus, groundwater research poses unique challenges compared to the study of surface water and it is exceedingly difficult to assess and predict the changes in groundwater systems, especially over large scales (E Condon & Maxwell, 2015; Engdahl, 2017; Sophocleous, 2002). Observational data challenges make groundwater research even more daunting (Evans et al., 2020; Megdal et al., 2015), which is particularly true for modeling studies that require such data both to constrain and validate the models. Especially in data-limited regions, even selecting an appropriate model can be challenging (P. Kumar et al., 2021; Tegegne et al., 2017). Parsimonious models are often used in such regions because of their simplicity and limited data requirements (Pande et al., 2012; Quichimbo et al., 2021). However, while parsimonious models could realistically simulate certain hydrologic variables under constrained conditions, the models are not well suited to study process interactions and the complexities therein (e.g., land use change, vegetation processes, soil hydrology) (Fabrizio Fenicia et al., 2011; W. Wu et al., 2010), especially considering that a system response to changing climatic and human drivers can be non-linear (Mcguire & Mcdonnell, 2010; Sivapalan et al., 2002).

Conversely, process-based models (e.g., land surface models; LSMs), offer a more physically-based representation of surface and subsurface hydrological processes, including infiltration, soil moisture dynamics, and groundwater recharge, making these models more robust and reliable for application in different regions and climates, especially in data-limited basins such as the MRB (Koirala et al., 2014; Y. Pokhrel, Koirala, et al., 2014). Furthermore, LSMs offer promising avenues for future research on land-atmosphere coupling, enabling an improved understanding of the dynamic interactions between groundwater and the atmosphere, and more broadly within the entire Earth system (Clark et al., 2015b). As such, many large-scale groundwater modeling studies use LSMs account for groundwater in a relatively simple manner or with minimal groundwater parametrizations (Koirala et al., 2019; Yadu N. Pokhrel et al., 2016).

Despite the challenges in representing groundwater in LSMs due to data scarcity, among others, notable progress has been made toward improved groundwater parameterizations. Some of the noteworthy advances include the representation of linear groundwater reservoir (F. Fenicia et al., 2006), surface water-groundwater interactions (Y. Fan & Schaller, 2009; Kollet & Maxwell, 2008; Reed M. Maxwell & Kollet, 2008; Miguez-Macho & Fan, 2012a, 2012b), lateral groundwater flow (Barlage et al., 2021; Felfelani et al., 2021; Inge E.M. De Graaf & Stahl, 2022; Zeng et al., 2018), and groundwater pumping for irrigation (Felfelani et al., 2021; Inge E.M. de Graaf et al., 2019; Leng et al., 2014; Nie et al., 2018; Y. Pokhrel et al., 2012; Yadu N. Pokhrel et al., 2015; Yoshihide Wada et al., 2010). These efforts have led to groundwater representations with varying degree of complexity in different LSMs including the Variable Infiltration Capacity Model (VIC) (Liang et al., 2003), MATSIRO (Pokhrel et al., 2015), Community Land Model (CLM) (Kluzek, 2013; D. M. Lawrence, Fisher, Koven, Oleson, Zeng, et al., 2019b; Keith W. Oleson et al., 2013; Sean C. Swenson et al., 2019), and Noah-MP (Nie et al., 2018).

However, most of these model development studies have focused on data-rich regions such as the US aquifer systems where groundwater is depleting alarmingly due to rapidly increased pumping for irrigation (R. M. Maxwell et al., 2015; Nie et al., 2019, 2021, 2022; Doll et al., 2014; Y. N. Pokhrel et al., 2015), leaving major gaps that come with challenges, toward using the models in regions where groundwater issues are rapidly emerging, but data are scarce (Jayakumar & Lee, 2017). The MRB is a perfect example of such regions where upstream water management (Dang et al., 2016; Galelli et al., 2022; Hecht et al., 2019; Y. Pokhrel, Burbano, et al., 2018), climate change and variability (Mauricio E. Arias et al., 2012; Delgado et al., 2012; Thompson et al., 2013), and increased groundwater pumping for domestic and irrigation uses are rapidly transforming groundwater dynamics but basin-scale groundwater modeling studies are rare, if not non-existent (Dang et al., 2016; Johnston & Kummu, 2012; Y. Pokhrel, Burbano, et al., 2018) primarily because of the basin wide data limitations to constrain and validate the model (Erban et al., 2014; Erban & Gorelick, 2016). Very crucially, leaving the growing anthropogenic influence aside, even the natural dynamics of groundwater systems, especially over the entire MRB, is not adequately studied (Lacombe et al., 2017).

Further, growing number of observational studies have reported dramatic shifts in groundwater systems over the lower MRB (LMRB)—especially the Mekong Delta region—due to the influence of growing anthropogenic activates over the past decade (Duy et al., 2021; Haddeland et al., 2006; Kazama et al., 2007; Lee et al., 2017; Loc et al., 2021; Tatsumi & Yamashiki, 2015; Tu et al., 2022a). Few studies investigated the historical groundwater situation at the sub-catchment level of the MRB under the influence of climate change, irrigation, and groundwater extraction (Gunnink et al., 2021; Hoanh et al., 2012; S. Shrestha et al., 2016; Tatsumi & Yamashiki, 2015). Other studies underlined the critical issues, such as groundwater pollution, and saltwater intrusion in the Mekong Delta and contaminant transport, that is directly linked with groundwater flow and groundwater depletion (Minderhoud et al., 2017; Tran et al., 2022). However, no basin scale groundwater study exists and process-based models have been rarely used to simulate these changes, resolve the interactions among various governing processes, and identify the key drivers (Johnston & Kummu, 2012). Fundamentally, little advancement has been made in understanding the critical controls of climate, physiography, and anthropogenic drivers on the dynamics of groundwater over the MRB.

Such lack of basin-scale groundwater modeling considering climatic and anthropogenic drivers critically hinders the understanding of evolving groundwater systems over the MRB, with implications on reliable future projections of water resource availability and use under climate change and intensified anthropogenic activities (Jasechko et al., 2014). Some global modeling studies have examined water and energy balances over the MRB (e.g., Haddeland et al., 2006; Guillaume Lacombe et al., 2017; Tatsumi & Yamashiki, 2015; Felfelani et al., 2017). However, they have applied global models at a relatively coarse spatial resolution (e.g., 50-100km), not accounting for finer scale processes including lateral flow (e.g., Felfelani et al., 2021; Krakauer et al., 2014) that are crucial in governing groundwater dynamics in the MRB's landscapes with high climatic, topographic, and hydrogeologic gradients (Cooper, 2010; Hung et al., 2012; Y. Pokhrel, Burbano, et al., 2018). Lastly, while some sub-basin scale studies have provided insights on local-scale groundwater changes, basin-scale and long-term (e.g., decadal evolutions) changes and patterns of groundwater dynamics for the MRB are largely lacking.

Here, we address the gaps identified above by focusing on the following three scientific contributions, and to advance groundwater modeling over the MRB. First, we present a fully distributed and process based LSM for the MRB, which simulates key hydrological processes on a full physical basis, including improved parameterizations for inter-grid lateral groundwater flow and aquifer pumping. Second, we use the model for a mechanistic investigation of interactions among the processes governing surface water and groundwater flows, including groundwater recharge and discharge, considering basin scale climatic drivers and human activities, and encompassing fine scale process heterogeneities. Third, despite dearth of data to fully constrain the model, we present first-order quantification of the effects of increased irrigation and groundwater pumping on groundwater flow processes and storage dynamics over the LMRB.

We are aware of the challenges, and more so of the pressing need to improve our ability to simulate groundwater dynamics at the basin scale over the MRB. The primary goal is to capture the basin-scale patterns of groundwater dynamics and quantify the human-induced changes in groundwater systems; the underlying objective is to provide a foundational framework for basin wide groundwater studies in the MRB considering key governing processes and their response to the major climatic and human factors. Such a framework is expected to advance the current state of groundwater modeling in the MRB and open avenues for further research, including model enhancements. We address the following scientific questions: 1) How do climatic drivers, physiographic conditions, and topographic characteristics govern groundwater processes—specifically recharge, discharge, and lateral flow—across the MRB? 2) What role does groundwater dynamics across the MRB play in modulating surface water systems in the LMRB? 3) How are anthropogenic activities—specifically irrigation and groundwater pumping—impacting groundwater systems in the LMRB? The model we use is the Community Land Model version 5 (CLM5) with the latest updates on groundwater parameterizations (see section 2.2).

3.2 Study Area and Methods

3.2.1 Study Area

The MRB is shared by six countries in Southeast Asia: China, Myanmar, Lao PDR, Thailand, Cambodia, and Vietnam (MRC, 2005). The upper MRB (UMRB) is characterized by a steep narrow valley, with its geometry determined primarily by Himalayan orogeny (Carling, 2009). The LMRB can be divided into four regions: i) the northern Highlands, characterized by high elevation and dense vegetation, ii) the Khorat Plateau that includes much of the lowlands and a relatively flat landscape, iii) the Tonle Sap basin and iv) the Mekong Delta with an alluvial floodplain (Lacombe et al., 2017). The northern Highlands include the north of Thailand and Laos and extend into Vietnam. The Khorat Plateau covers most of northeast Thailand with its northern and eastern margin in central Laos and has a consistent basin elevation. Farther downstream, Tonle Sap Lake (TSL) covers the southern portion of Laos and most of Cambodia.

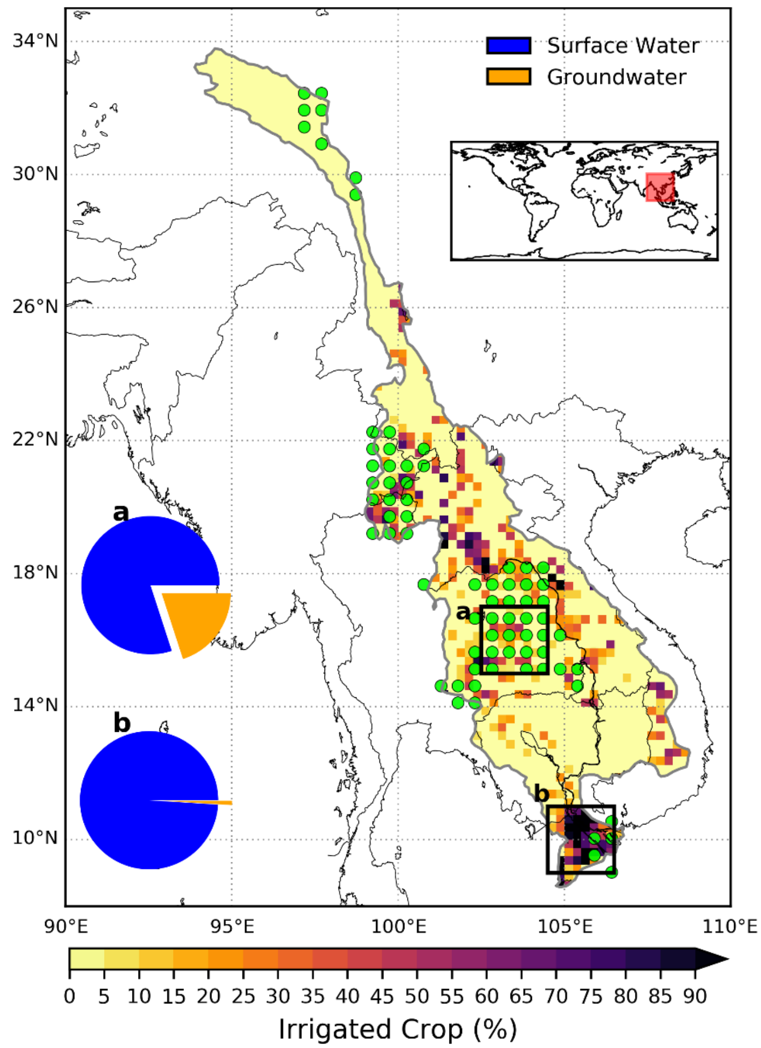

Figure 3-1. Fractional area of irrigated cropland in the MRB with areas marked by green circles indicating groundwater-irrigated regions. The pie charts depict the groundwater use fraction for two selected regions marked with black squares where groundwater withdrawal for irrigation is relatively high. Upper right inset shows the location of the MRB in the global map.

The climate across the MRB is tropical monsoonal. Precipitation patterns are seasonal, with the majority of annual totals occurring during the wet season between May and October (Kabir et al., 2022); the highest rainfall of over 2500 mm/yr occurs in the Highlands of Laos and the lowest of less than 1000 mm/yr over the Khorat Plateau in northeast Thailand. MRB is characterized by dense forest coverage towards the north and crop areas in the LMRB and

Mekong Delta towards the south (Figure 3-1). Surface water has historically been the dominant water resource for irrigation. However, over the past two decades, household wells and large-scale, deeper pumping for municipal and industrial purposes including irrigation have risen substantially (Hoanh et al., 2014). Currently, there are over one million wells in the Mekong Delta (Gunnink et al., 2021; Hoanh et al., 2014; Loc et al., 2021; Minderhoud et al., 2017) and the interest in further expanding the use of groundwater for agriculture is increasing (Tran et al., 2022).

3.2.2 Model

We use CLM5, which is the land component of the Community Earth System Model version 2 (CESM2) that resolves various surface and subsurface hydrological processes (e.g., soil and plant hydrology, snow physics, river routing, crop modeling) coupled with energy and biogeochemical (carbon and nitrogen) cycles on a complete physical basis (Danabasoglu et al., 2020). Although CLM5 and similar LSMs were traditionally designed to simulate surface water and energy fluxes within the Earth system model (ESM) frameworks, major advances have been made in recent years to represent sub-surface hydrological processes (Haddeland, Clark, Franssen, Ludwig, Voß, Arnell, Bertrand, Best, Folwell, Gerten, Gomes, Gosling, Hagemann, Hanasaki, Harding, Heinke, Kabat, Koirala, Oki, Polcher, Stacke, Viterbo, Weedon, & and Pat Yeh, 2011; Yadu N. Pokhrel et al., 2016). For example, CLM5 simulates key subsurface processes, including infiltration, plant hydraulics, soil moisture dynamics, and groundwater, that drive groundwater recharge on a full physical basis (Clark et al., 2015b; Kennedy et al., 2019; D. M. Lawrence, Fisher, Koven, Oleson, Swenson, et al., 2019; K W Oleson et al., 1978). Highly detailed groundwater models require extensive data and are exceedingly challenging to implement in the MRB, whereas simplistic process representation in parsimonious or lumped models can lead to uncertainties when hydrological processes are highly nonlinear or dynamic (Paniconi & Putti, 2015). Thus, we use CLM5, striking a balance between data requirements and process representation. The standard CLM5 includes a subsurface hydrology scheme with only a vertical exchange of water (D. M. Lawrence, Fisher, Koven, Oleson, Zeng, et al., 2019b; Sean C. Swenson et al., 2019). We use an advanced model version that includes the representation of lateral flow and aquifer pumping to account for the consumptive use of water for irrigation (Felfelani et al., 2021). The lateral groundwater flow is represented by Darcy's law following Fan et al. (2007), while the pumping scheme is based on HiGW-MAT model (Pokhrel et al., 2015).

The lateral flow is driven primarily by groundwater head difference—influenced by factors such as climate and topography (i.e., topographic slope in baseflow generation)—between two adjacent cells and computed based on Darcy's law (Y Fan & Li, 2013) as $\mathrm{Q}n = \mathrm{WT}(\frac{\mathrm{h}n-\mathrm{h}c}{l})$, where h$n$ and hc are the hydraulic head in n$^{\mathrm{th}}$ neighbor and center grid cells, respectively, T is the transmissivity, l is the distance between cells, and W=$\boldsymbol{\Delta}x\ \sqrt{}(0.5\tan\left(\frac{\pi}{8}\right))$ is the width of an imaginary octagon that replaces the square grid cell to provide an equal chance for all eight neighboring cells to interact with the center cell (Felfelani et al., 2021). When water table lies within the soil layer, the positive net lateral flow is added to soil layers in sequential order beginning from the soil layer right above the water table and the negative net lateral flow is removed from soil layers in sequential order beginning from the soil layer right below the water table (any residual is taken from the underlying aquifer layer) (Felfelani et al., 2021). When the water table is below the soil column, the net lateral flow is added (removed) to (from) the aquifer storage (Felfelani et al., 2021). Further details of the lateral flow and mass balance of each grid cell can be found in Felfelani et al., (2021). In CLM5 soil hydrologic processes are explicitly resolved up to 8.5m depth and water table depth can vary from 0 to 80 m (Felfelani et al., 2021).

The subsurface is depicted using a high vertical resolution and improved solution to the Richard's equation to resolve soil water movement across layers (Felfelani et al., 2021). When unconfined aquifer under the soil column is activated, drainage from the lowest soil layer (recharge; q_{rech}) is controlled by a head-based lower boundary condition (i.e., q_{rech}=q_i + $\partial \theta_{liqi} \frac{\partial q_i}{\partial \theta_{liqi}}$). Here, q_i is the water flux across the lowest interface and θq_{liqi} is the liquid volumetric soil moisture. When the water table is within the soil column, recharge rate is determined using Darcy's equation across the water table. In this configuration, subsurface runoff decays exponentially depending on the water table depth (z_{wt}), that is, $q_{sub} = \theta_{ice} q_{drai,max}$ exp ($-f_{drai} z_{wt}$), where, θ_{ice} is ice impedance factor, $q_{drai,max}$ is the maximum subsurface runoff when $z_{wt} = 0$ and is set to $q_{drai,max} = 10\sin(\beta)$; β is the mean grid cell topographic slope in radians and f_{drai} is the decay factor.

3.2.3 Subsurface Hydrologic Parameters

Hydraulic properties of the soil are weighted combinations of the mineral properties, determined based on sand and clay contents (Clapp & Hornberger, 1978; Cosby et al., 1984) and organic properties of the soil (D. M. Lawrence & Slater, 2008). Hydraulic conductivity is defined at the depth of the interface between two adjacent soil layers and is a function of saturated hydraulic conductivity, the liquid volumetric soil moisture of the two layers and an ice impedance factor Θ_{ice} (NCAR, 2019). Note that the lateral hydraulic conductivity (K_{lat}) is determined from the vertical hydraulic conductivity (K_{ver})—resolved in the vertical one-dimensional soil movement—and percent of clay in the soil layer represents the anisotropy factor (i.e., $C_{clay} = K_{lat}/K_{ver}$) as described in Fan et al., (2007) and Zeng et al., (2016).

The prognostic aquifer transmissivity (T) is estimated based on the water table depth and hydraulic conductivity (Fan et al., 2007). If water table depth lies within the soil column,

$T=T_1+T_2$, where T_1 is the transmissivity of the saturated portion of the soil column (i.e., from the water table to the bottom most layer) and T_2 is the transmissivity of the depth below the bottom most layer (Felfelani et al., 2021). Here, T_2 is estimated using hydraulic conductivity of the bottom most layer, exponentially decayed with depth. A more in-depth discussion on the aquifer transmissivity estimation can be found in Felfelani et al., (2021) and Fan et al., (2007).

3.2.4 Irrigation Parameterizations

Irrigation application is dynamically responsive to the simulated soil moisture conditions (Ozdogan et al., 2010). When irrigation is enabled, the crop areas of each grid cell are divided into irrigated and rainfed fractions based on a dataset of areas equipped for irrigation (Portmann et al., 2010). Irrigated and rainfed crops are placed on separate soil columns and irrigation is applied only to the irrigated portion. In irrigated croplands, a check is conducted once per day (in the first-time step after 6 AM local time) to determine whether irrigation is required on that day. Irrigation is triggered if crop leaf area index > 0, and the available soil moisture is below a specified threshold (Felfelani et al., 2018).

In the standard CLM5, irrigation water is applied to the soil column as an add-on to precipitation, withdrawing water from surface water (i.e., water in the main river channel) as a sole source of irrigation (NCAR, 2019). In the improved version of CLM5 used in this study, groundwater supplied fraction (provided in the model as input data) is extracted from the groundwater (from the aquifer or from the soil layers when water table is within soil column) and rest of the irrigation water requirement is withdrawn from the main channel (Felfelani et al., 2021). This model version is validated in continental US and found to adequately capture the subsurface dynamics as well as groundwater depletion (Felfelani et al., 2021), adding confidence on the use of the model in other basin such as the MRB.

3.2.5 Surface Water Routing

To simulate streamflow, we use Model for Scale Adaptive River Transport (MOSART), a process-based model that uses kinematic wave formulations to route runoff as described in Li et al., (2015). The model uses a hydrography dataset, available globally at a spatial resolution of 0.125°. Topographic parameters such as flow direction, channel length, and channel slope, were obtained using the Dominant River Tracking (DRT) algorithm (H. Y. Li et al., 2015); MOSART is the standard river routing scheme employed in CLM5.

3.3 Data

We use WATCH Forcing Data methodology applied to ERA-Interim reanalysis (WFDEI) global meteorological forcing data at 0.5° spatial resolution and 3-hour timely intervals (Weedon et al., 2014). WFDEI has been widely used in the LSM-based studies (Pinnington et al., 2018) and sensitivity analysis on the MRB by Kabir et al., (2022) suggests that WFDEI reproduce observed hydrological fluxes and states including streamflow, terrestrial water storage (TWS), and soil moisture in the MRB better than many other high-resolution climate forcing datasets. We utilize the International Geosphere-Biosphere Programme (IGBP) soil data to define soil characteristics at different soil layers.

We utilize the Global Map of Irrigated Areas version 5 (GMIAv5) (Siebert et al. 2015) for circa 2005, available at 0.083° spatial resolution (Figure 3-2) to specify the contribution of groundwater to total irrigation water withdrawals. In the MRB, fractional groundwater contribution varies substantially, ranging from 0-25% and with most groundwater irrigation areas found in northern Thailand (Figure 3-1 and Figure 3-2). Irrigation is predominantly surface water based in other parts of the basin. The equilibrium water table depth (i.e., climatologic mean that represents the long-term balance between the climate-driven recharge and the topography-driven lateral flow) (Fan et al., 2013), aggregated to 0.05° resolution, is used to initialize the water table depth in CLM5 to reduce the spin-up period (Zeng et al., 2018). We use observed streamflow data from the Mekong River Commission (MRC) to validate streamflow simulations at six gauging locations across the basin.

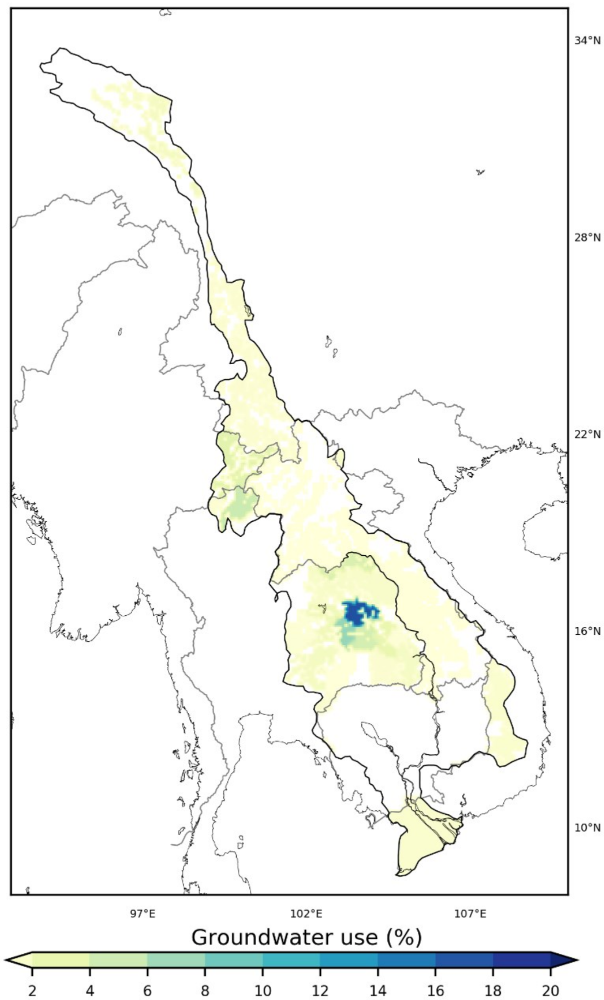

Figure 3-2. Groundwater contribution (in the percentage of each grid cell area) to the total irrigation water withdrawal based on the Global Map of Irrigated Areas Version 5 (GMIAv5) dataset (S. Siebert et al., 2015). The map shows the data for 2005.

To validate TWS, we use monthly Gravity Recovery and Climate Experiment (GRACE) data: two mass concentration (mascon) solutions from the Center for Space Research (CSR)

(Save et al., 2016) at the University of Texas at Austin and Jet Propulsion Laboratory (JPL) (Watkins et al., 2014) at California Institute of Technology are used. To validate soil moisture, we use the data from Soil Moisture Active Passive (SMAP) satellite mission (Entekhabi et al., 2015); ground-based soil moisture data are not available for the MRB. There are no basin scale data available to reasonably validate simulated groundwater table. Thus, we used the synthesized data by digitizing the data published in the previous literature (Tiwari et al. 2023).

3.4 Experimental Settings

We conduct four simulations with varied settings and time periods (Table 3-1) over the MRB at 0.05° spatial resolution (~5 km). First, a multi-decadal simulation is performed without considering irrigation and pumping (i.e., natural state), referred to as the control (CTRL) simulation. This simulation is used to investigate the MRB's natural groundwater dynamics and its climatic and physiographic controls.

Table 3-1: Experiments and model configurations.

Simulation	Irrigation	Pumping	Irrigation Water Source	Groundwater Use	Simulation Period
CTRL	No	No	No Irrigation	0	1979-2016
CTRL_SW	Yes	No	Surface Water	0	1979-2016
Sim_GWSW	Yes	Yes	Surface and Groundwater	GMIAv5	2000-2016
Sim_GW	Yes	Yes	Groundwater	100 %	2000-2016

Then, we conduct three additional simulations with varying irrigation water use scenarios to investigate the role of irrigation and groundwater pumping in perturbing groundwater dynamics. The CTRL simulation is first spun up for 100 years by using WFDEI forcing data repeatedly for the year 1979. (Rodell et al., 2005). The CTRL simulation is performed without activating irrigation and pumping. The CTRL_SW is based on CTRL but activating irrigation where full irrigation demand is met from surface water sources. Sim_GWSW is based on CTRL, with irrigation and groundwater pumping activated for conjunctive use from surface and groundwater. Sim_GW simulation represents a situation where the irrigation demand is met solely from groundwater. Since widespread irrigation in the MRB began in the 1990s, we conduct Sim_GWSW and Sim_GW simulations for a shorter period beginning in 2000. Head-based lower boundary condition and lateral flow are active in all simulations. The experiments are designed to capture the natural groundwater dynamics of the MRB and the potential consequences of anthropogenic impacts such as irrigation and groundwater pumping.

3.5 Results

3.5.1 Surface and Subsurface Water Variations

Comparison of the simulated monthly streamflow with observations at six gauging stations across the LMRB indicates that the model performs well in capturing the temporal dynamics of streamflow and its seasonality (correlation coefficient ranges between 0.8-0.99 and NSE ranges between 0.7 to 0.95 across various stations). Given minimal precipitation during the dry season in the MRB (Hung et al., 2012; Y. Pokhrel, Burbano, et al., 2018; Sun et al., 2021), groundwater discharge is arguably the primary contributor to streamflow, particularly during this period. Thus, and given that no extensive basin-wide data exist for a direct groundwater validation, we focus on the evaluation of low flow indicators that serve as a proxy of groundwater discharge (i.e., baseflow) simulations (Pat J.F. Yeh & Eltahir, 2005) along with a limited validation of simulated water table anomaly with observations. In general, flows having 85, 90, and 95 percent exceedance probability, i.e., Q85, Q90, and Q95, respectively, are simulated reasonably well across all stations (Figure 3-3a-f). The mean percent deviation (MPD) of simulated and observed Q95, Q90, and Q85 ranges between 4-8%, 1.5-10%, and 1.5-11%, respectively. These comparisons of annual and low flows as well as the temporal patterns suggest that the model reasonably simulates low flow, hence the underlying groundwater discharge or baseflow generation.

The temporal pattern of the simulated groundwater table anomaly represents a comparatively stable trend, unlike the observed water table changes in the MRB that depict a continuous decline from 2007 to 2016. Nevertheless, the model captures the declining trend of water table depletion, including some of the major water table decline in 2010 and 2014 despite certain discrepancies in the magnitude (Figure 3-3i-k). The model also captures some of the observed water table recoveries (Figure 3-3k). The findings indicate that the model can reasonably capture the observed groundwater anomaly, the seasonal and inter-annual dynamics of groundwater changes. We note that a direct comparison between the water table derived from a 5 km model grid and very limited point-scale observations is not fully compatible; thus, these evaluations should be interpreted with sufficient caution. Further, there could be added uncertainties due to climate forcing particularly precipitation (Kabir et al., 2022), subsurface parameterization and insufficient representation of the groundwater irrigation areas that can lead to underestimation of water table decline. Most importantly, the validation locations are predominantly located in the Mekong Delta, where groundwater can be influenced by sea water intrusion and tides, factors currently not accounted for in the model. However, due to high data paucity (e.g., lack of basin-wide, continuous monitoring of groundwater levels), this is the only viable evaluation of our simulations in addition to the validation of discharge and TWS (Figures 3-3 and 3-5). Given complex topographic features across the MRB, use of a global-scale LSM, and limited data to constrain process simulations, we consider these results to be satisfactory to study groundwater processes over the MRB.

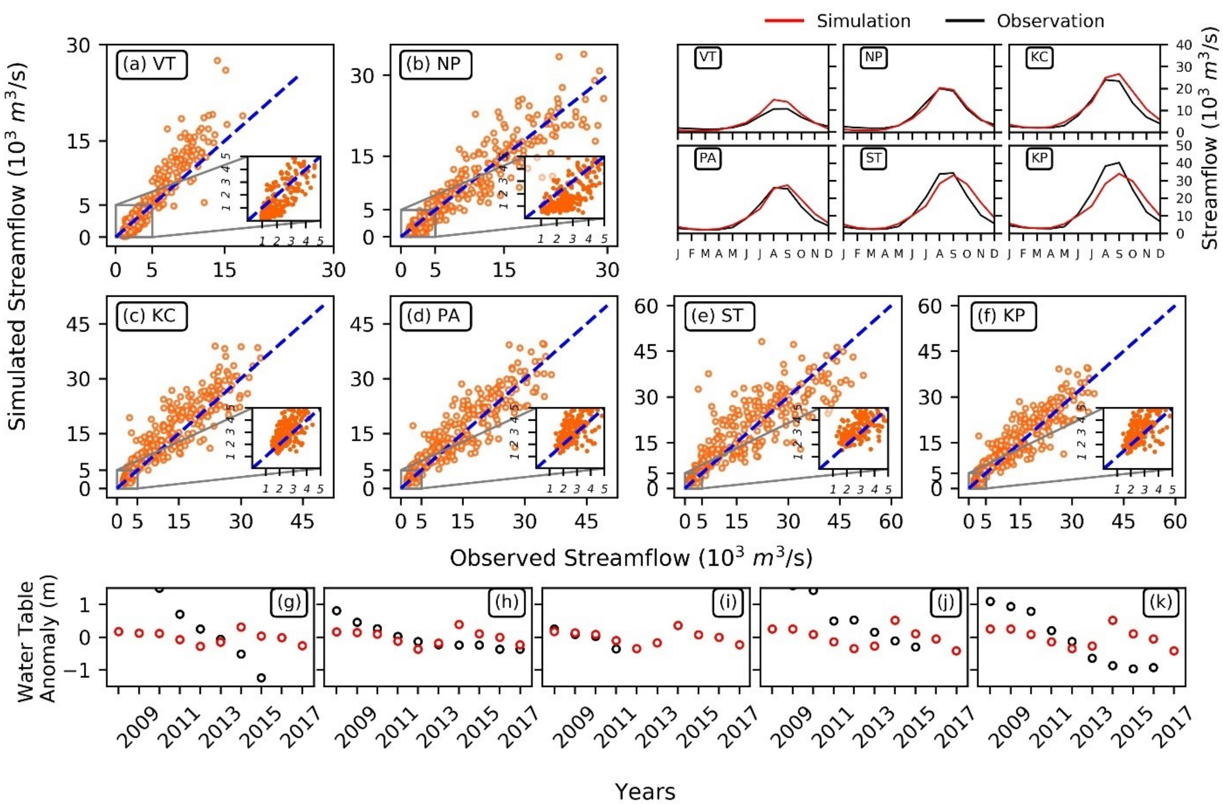

Figure 3-3. Evaluation of simulated monthly streamflow (1979-2016) at six mainstream gauging stations in the LMRB: VT (Vientien), NP (Nakhon Phenom), KC (Kong Chiam), PA (Pakse), ST (Stung Treng), KP (Kampong Cham). The station locations are shown in Figure 3-4. The zoomed boxes in panels a-f depict the low flows for each station. The six subplots in the upper right panels represent a comparison of seasonal cycle of observed (black) and simulated (red) streamflow. Results presented here are based on Sim_GWSW simulation (see Table 3-1). Panels (g-k) show the comparison of the simulated water table anomaly with the observation (red: simulation; black: observation). Note that the mean of all available well heads within a given grid cell is used for a relatively consistent comparison of point data and grid-based simulations.

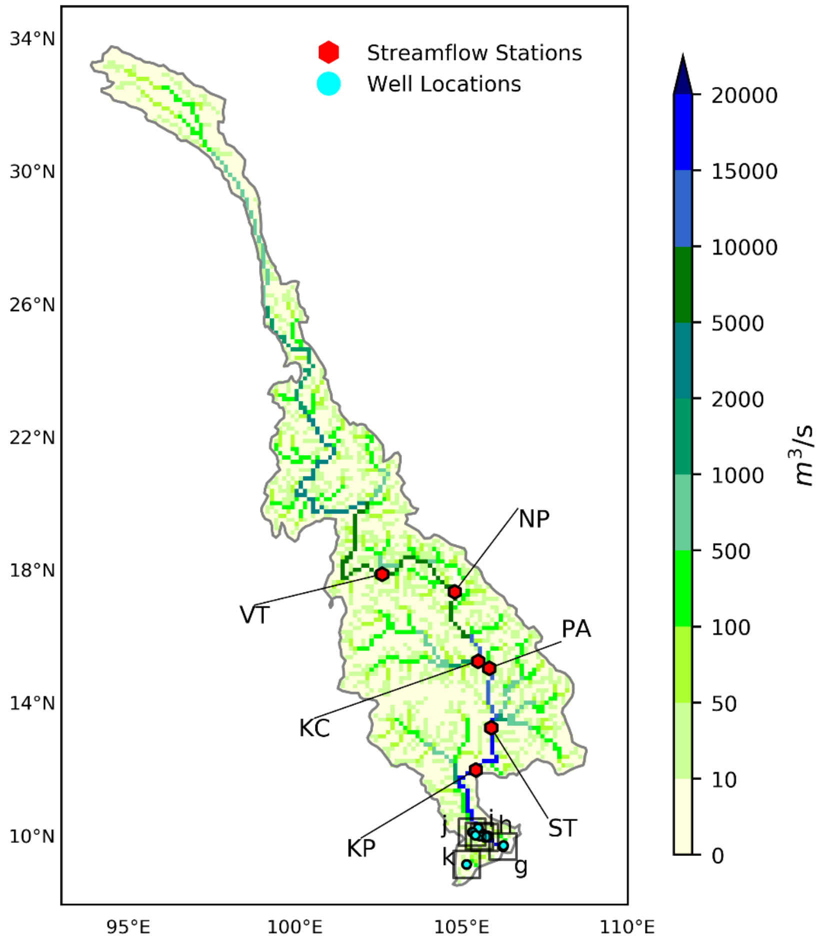

Figure 3-4. Mean annual streamflow across the MRB from Sim_GWSW simulation (Table 1 in the manuscript: simulation with irrigation water sourced from both surface and groundwater). Streamflow validation station locations are shown as red hexagons and observation well locations are shown as blue circle. Mean well head (wells that located in a single grid cell) is used for validation.

Similar to streamflow, CLM5 well simulates the temporal variations of basin averaged TWS anomaly (Figure 3-5). It is evident from Figure 3-5 that the temporal variability is accurately reproduced along with the historical dry-wet transitions compared to GRACE observations (i.e., shaded areas in Figure 3-5). The good agreement with GRACE is evident not only visually but also statistically as indicated by a high R^2 (0.96) and low root mean square error (RMSE) (21.2 mm). However, the model did miss some of the events, such as in 2002 and 2011—two notable flood years in the MRB (Chinh et al., 2016; Dushmanta et al., 2007), and the simulated peak is slightly underestimated. Some of these underestimations and discrepancies are likely caused by missing representations of floodplain storage, particularly in the LMRB (Y. Pokhrel et al., 2018).

We find that subsurface storage plays a critical role in modulating the total TWS variations and hence the hydrology of the MRB (Figure 3-5a-b). Notably, subsurface storage accounts for ~81% of TWS amplitude, while groundwater anomaly explains 65% of the TWS anomaly in the MRB (subtracting soil moisture anomaly from the TWS anomaly). About 15% of the seasonal TWS amplitude is explained by surface water storage (Figure 3-5, pie chart), in line with the findings of previous studies (Y. Pokhrel, Shin, et al., 2018b) that reported this contribution to be ~13% based on a global LSM HiGW-MAT that is similar to CLM5 in process representation. Because GRACE provides the vertically integrated total TWS, not individual components, groundwater and surface water contribution could not be individually validated, and there are no other similar modeling studies for the entire MRB to cross-compare these individual TWS components. The comparison of seasonal TWS anomaly with GRACE data reveals that the overall seasonal variation is simulated reasonably well (Figure 3-5c-j). Furthermore, the broad spatial pattern of the basin wide seasonal TWS anomaly is consistent with the GRACE data. However, some discrepancies are evident in the LMRB, likely due to uncertainty in precipitation (Kabir et al., 2022) in addition to model parameterizations. The ability to perform a more in-depth comparison with GRACE data is limited because of the inconsistency in spatial resolution between model and GRACE data.

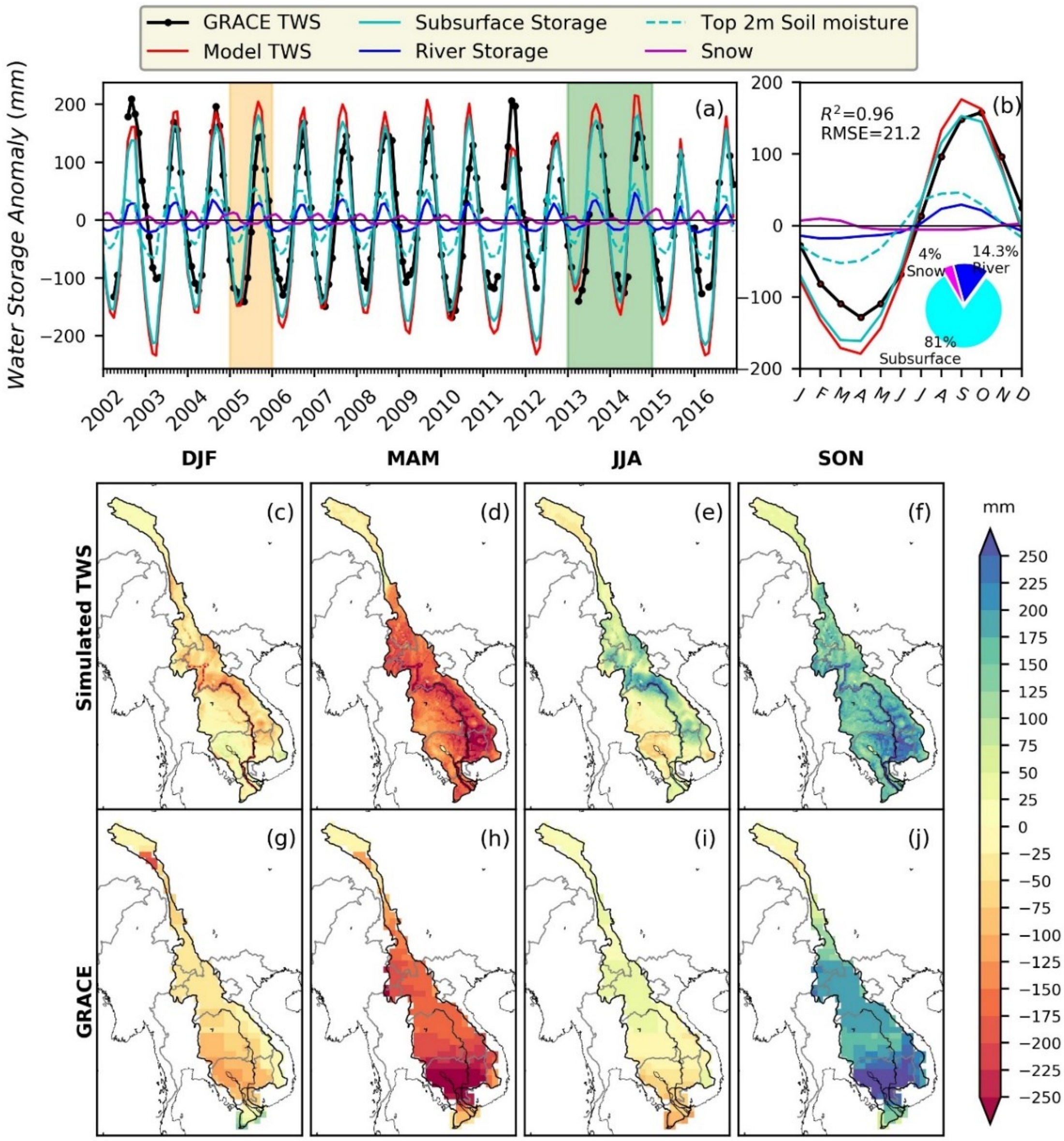

Figure 3-5. Comparison of simulated and GRACE-based monthly terrestrial water storage anomaly averaged over the MRB for the 2002–2016 period (a). Simulated surface (river storage and snow) and subsurface water storage and its components (top 2m soil moisture) are also shown. Individual components of surface water storage include water stored in rivers, small sub-grid scale water bodies, snow, and canopy. In contrast, subsurface water storage includes water stored in the soil column as soil moisture and groundwater. The right panel (b) shows the seasonal cycle. R^2 and RMSE are shown in the right panel. Yellow and green shades highlight dry-wet contrasts. Panels c-j present the spatial variability in the seasonal average of terrestrial water storage anomaly from simulation and GRACE data for the same period. Results presented here are based on the Sim_GWSW simulation.

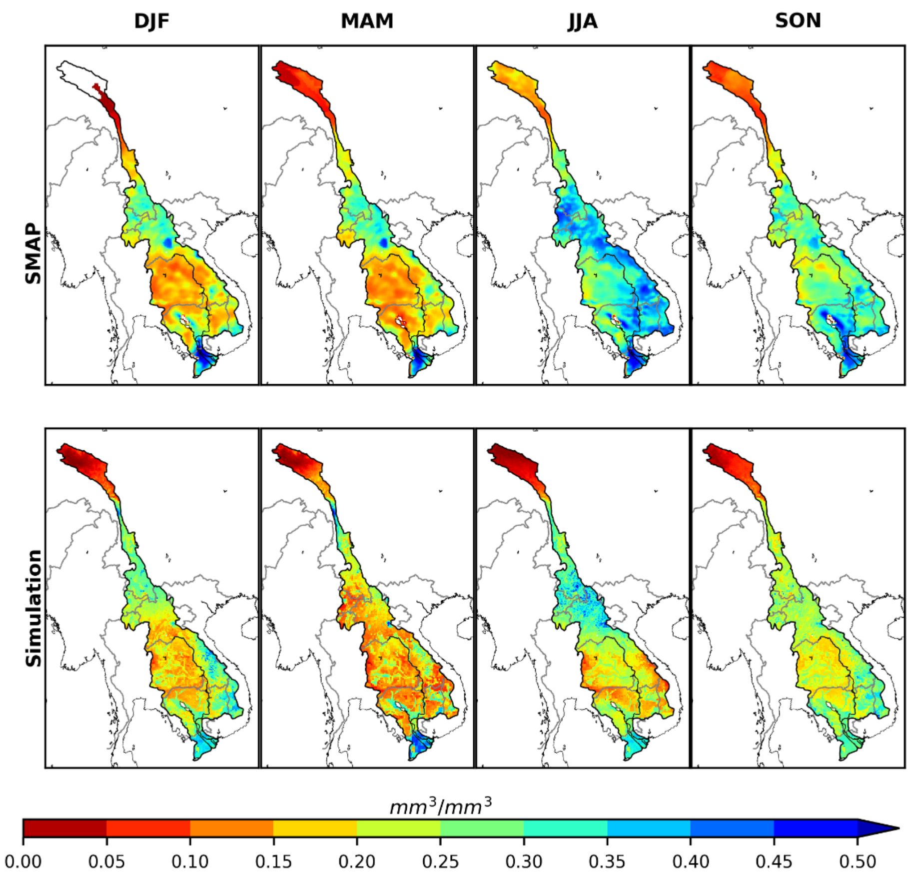

Figure 3-6. Comparison of simulated and SMAP based mean seasonal soil moisture (Entekhabi et al., 2015) on top 5 cm soil layer for year 2016.

We further compare simulated soil moisture with SMAP observations (Figure 3-6). Broad arid and humid contrasts of the soil moisture across the basin are reasonably reproduced in the simulation. There are, however, some disagreements in the wet season (September-November), likely due to precipitation uncertainty (Kabir et al., 2022) or uncertainties in SMAP data (e.g., vegetation cover affects SMAP signal) (Colliander et al., 2020; Ma et al., 2017). These evaluations of TWS and soil moisture indicate that CLM5 simulates the subsurface hydrodynamics of the MRB reasonably well and could be used to examine the mechanistic interactions of the groundwater processes. Additionally, dominance of subsurface storage variation on TWS anomaly indicates a strong control of groundwater in MRB's water cycle and hence highlight the importance of improving groundwater processes understanding.

3.5.2 Groundwater Flow Patterns and Drivers

Simulated annual average groundwater recharge in the MRB has distinct spatial variability, ranging from less than 100 mm/yr to over 1,000 mm/yr, with recharge rates generally decreasing from the UMRB to the LMRB (Figure 3-7a). High recharge rates are simulated in regions (deep blue color in Figure 3-7a) where precipitation rates are generally high. Laos and Vietnam are two such regions with high groundwater recharge and discharge rates. Some regions in the LMRB’s floodplains are evident with net negative groundwater recharge (capillary rise) likely under shallow groundwater conditions, i.e., groundwater responds to soil moisture stress and contributes to evapotranspiration (ET). As expected, groundwater discharge follows similar spatial patterns of recharge (Figure 3-7b). However, some areas with high recharge and low discharge rates are simulated (zoomed boxes in Figure 3-7a and 3-7b), suggesting that small-scale variations in soil characteristics and topographical factors govern regional groundwater flow and redistribute recharge spatially.

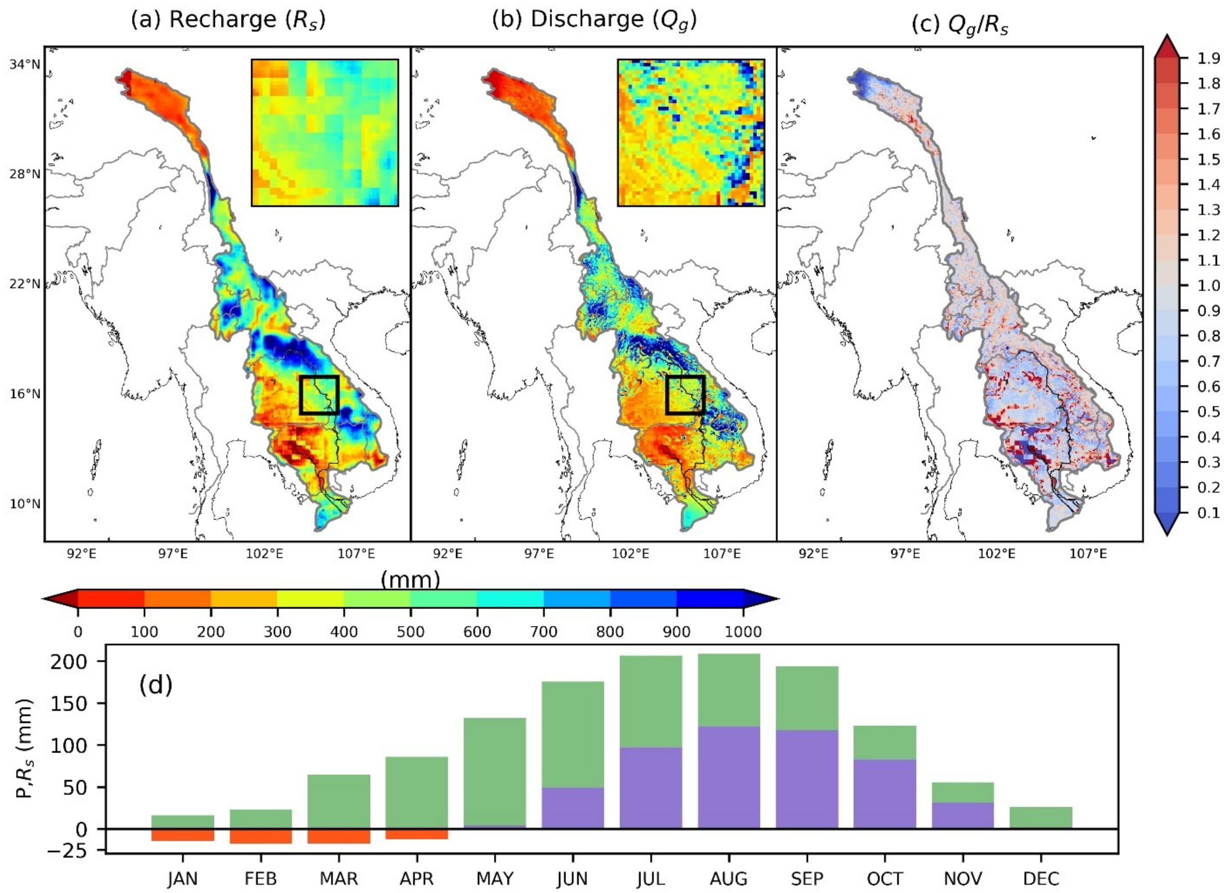

Figure 3-7. (a) Annual average groundwater recharge (R_s), (b) groundwater discharge (Q_g), and (c) groundwater discharge to recharge ratio (Q_g/ R_s) for the 1979 to 2016 period. Q_g/R_s <1 indicates groundwater contributor areas shown by different shades of blue, whereas Q_g/R_s >1 marks groundwater receiver parts of the basin in different shades of red. The bottom panel (d) shows recharge (R_s) and precipitation (P) climatology for the same period. The results presented here are based on CTRL simulation.

To provide further insights on relatively smaller scale processes and responses, we examine the basin-wide recharge to precipitation (R_s/P) ratio (Figure 3-8a) and surface and subsurface fluxes in different regions across the MRB (Figure 3-78-m) that represent diverse topography, climate, soil, and vegetation characteristics. High precipitation during the wet season (June - September) is observed in locations b, c, and e. Similarly, high recharge and groundwater discharge are evident in these regions, with similar magnitude and climatological patterns. These regions in the UMRB are dominated by dense natural vegetation (Figure 3-9) and sandy soil deposits (~60 % sand content) (Figure 3-10) that favor precipitation infiltrating and generating high groundwater recharge (Figures 3-7b-d). Thus, high R_s/P (i.e., R_s/P between 40-50%) is observed (Figures 8b-d). In addition to soil and vegetation characteristics, the high climatic and topographic gradient affects groundwater flow that drives discharge to the surrounding valley regions. However, there is no linear correlation between groundwater recharge and discharge with the topographic slope. Other possible factors, such as low water table gradient and relatively homogeneous soil texture (dominated mainly by sandy soil deposits) (Figure 3-10), affect direct recharge and discharge impeding regional groundwater flow.

In contrast, relatively downstream towards the LMRB (Figure 3-8f-g), R_s/P is rather high; however, relatively low discharge indicates possible control of local- to regional-scale groundwater flow. Topographic slope, soil characteristics, and water table gradient are likely to affect the divergence of groundwater discharge (Figure 3-8f-g). Furthermore, more heterogeneous soil composition is observed in these regions (Figure 3-10), which acts as the critical factor in controlling groundwater flow. For example, in the intermediate soil layers (Figure 3-10, layers 6-10), there is more heterogeneity in soil texture to impact groundwater flow paths. Relative control of regional flow owing to differences in topographic slope as well as heterogeneous medium (soil characteristics) is evident in the mountainous regions in the MRB (Figure 3-8e-g).

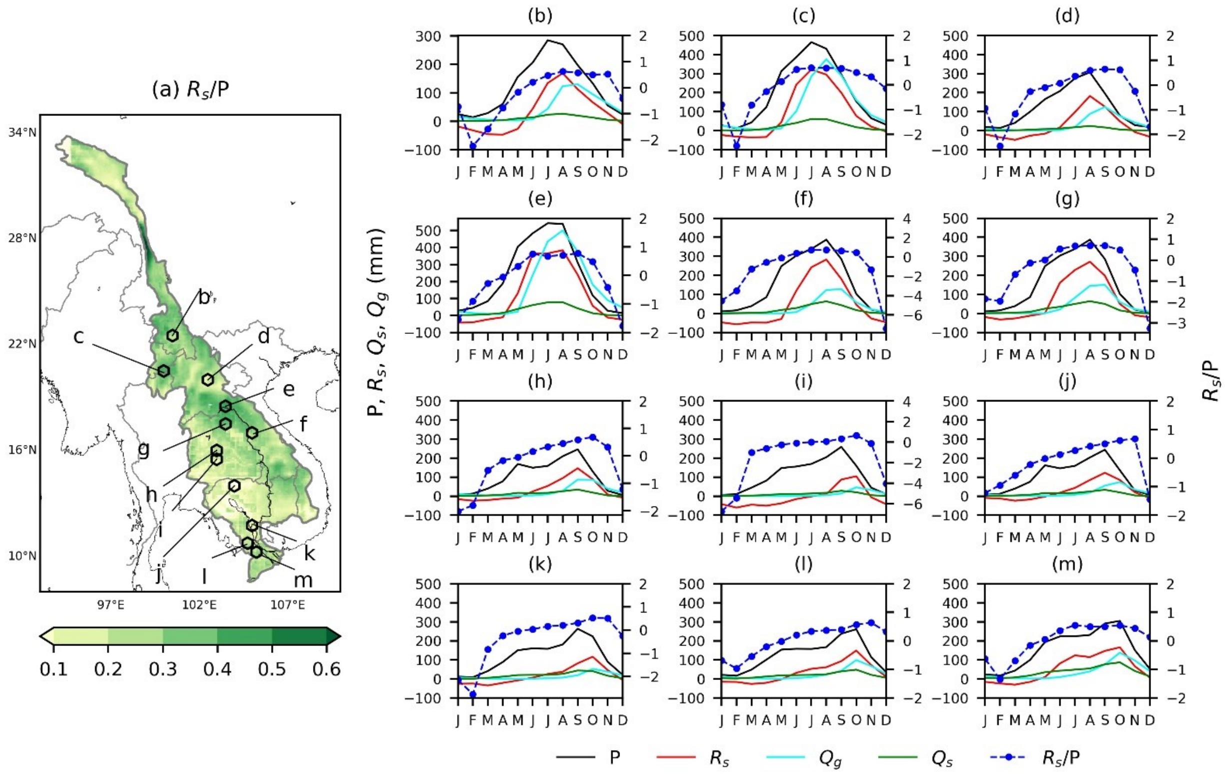

Figure 3-8. Spatial distribution of annual average recharge to precipitation ratio (R_s/P) (a), climatology of precipitation (P), groundwater recharge (R_s), surface runoff (Q_s), groundwater discharge (Q_g) and R_s/P for different locations across the basin are shown in panels b-m. Locations are indicated in panel a (black hexagon). The results presented here are based on CTRL simulation for the 1979-2016 period. Locations b, c, and d exemplify topographically complex regions (high variations in topographic slope) in the northern mountainous areas with moderate to high precipitation. Locations e, f, and g illustrate a high permeability zone with intense precipitation. Conversely, locations h, i, and j have low permeability in the flat floodplains in the MRB around the TSL region. Lastly, locations k, l, and m represent the Mekong Delta.

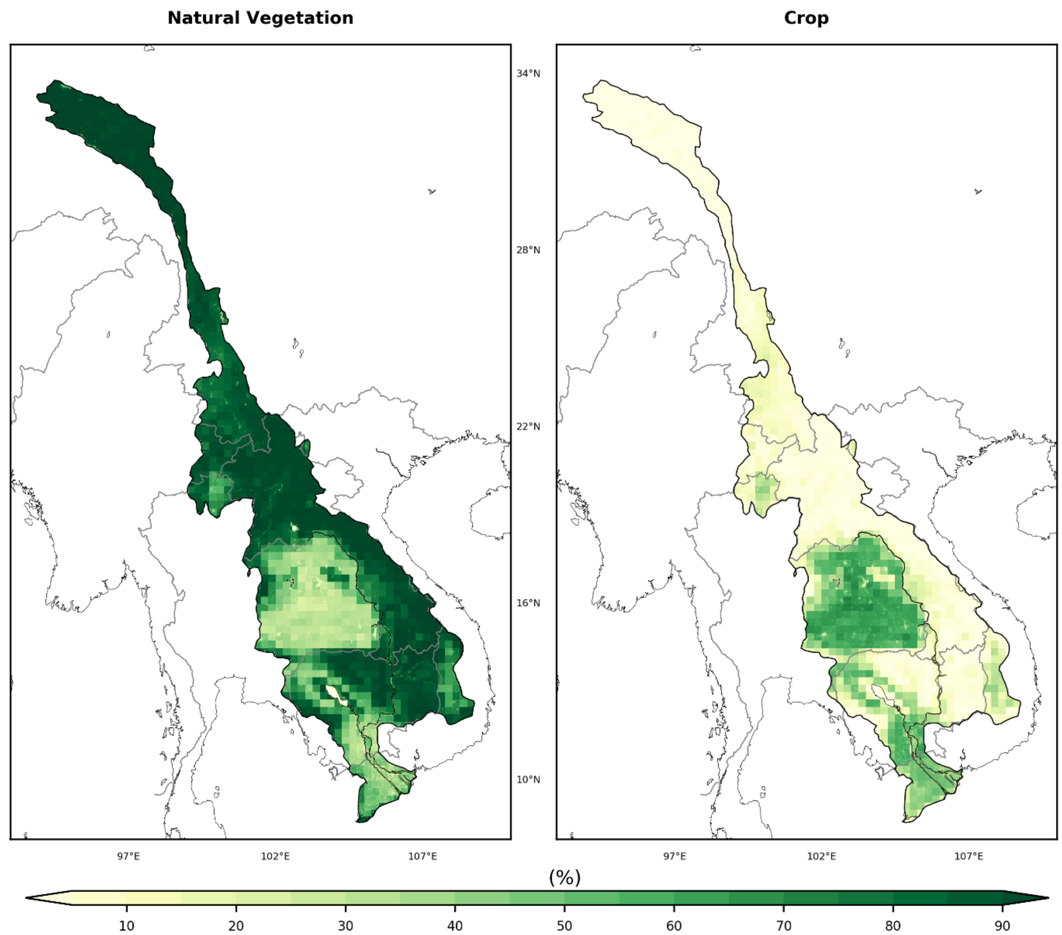

Figure 3-9. Two dominant land cover types (natural vegetation and crop shown are as percentage of each grid cell area. Data are taken from the Land Use Model Intercomparison Project (LUMIP) (D. M. Lawrence et al., 2016).

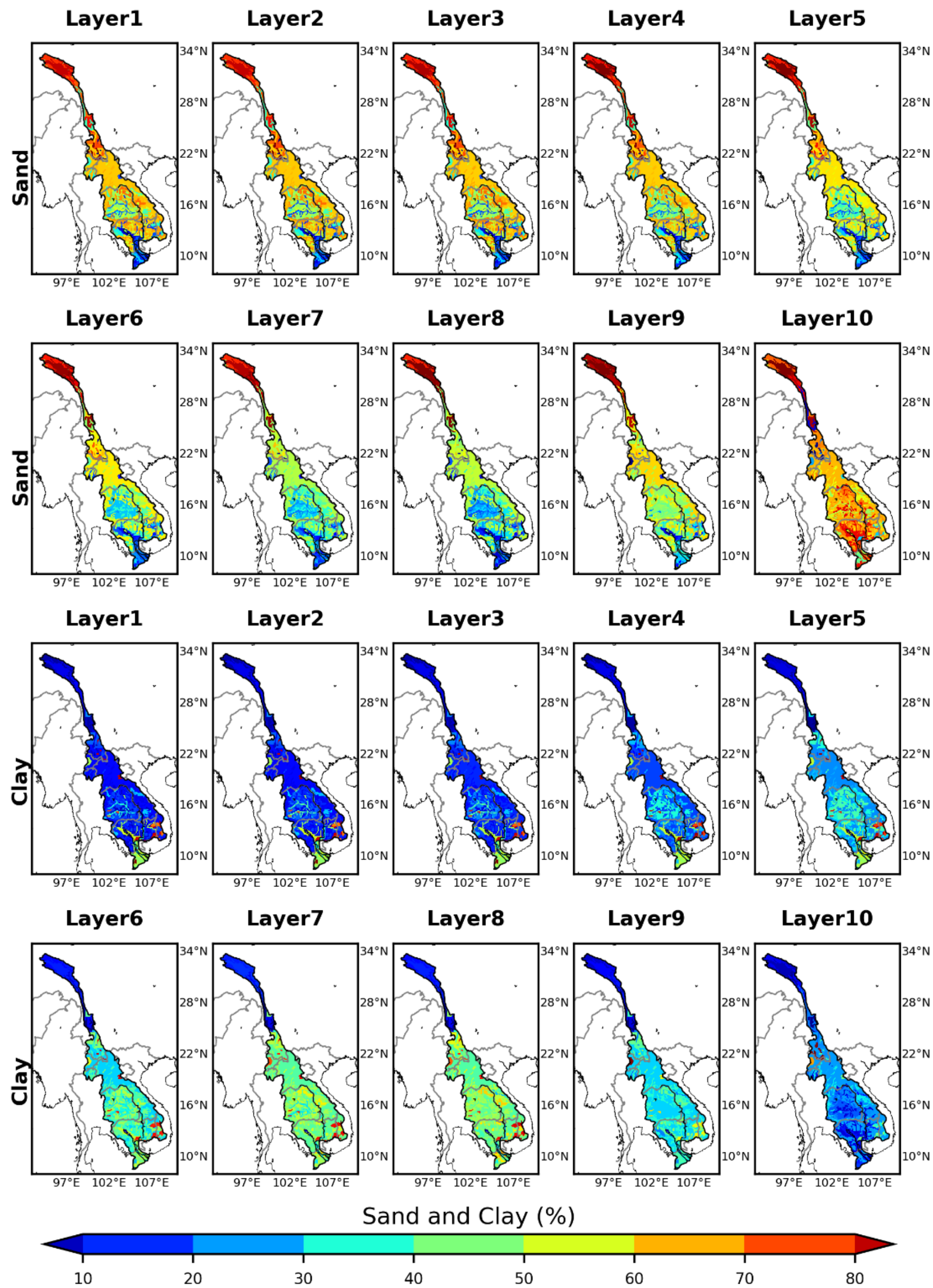

Figure 3-10. Sand and clay content of 10 soil layers. First two rows represent sand content and next two rows represent clay content of the soil. Dataset is based on the International Geosphere-Biosphere Program (IGBP) Task GSD (2014).

Farther downstream in the LMRB floodplains (Figure 3-8h-j), R_s/P is relatively low, in the order of ~10%, likely because the soil composition (alluvial clay is ~60% of the soil composition) inhibits quick percolation and recharge. Precipitation intensity is moderate in the

LMRB floodplains. Also, in the wet season, relatively high soil moisture in the LMRB (Figure 3-6) can create soil saturation near the surface that virtually makes the soil impermeable and cause less recharge than in other regions (Figure 3-8b-g). In addition, there is consistently high ET that leads to low groundwater recharge in comparison to the amount of water that infiltrates into the soil (Figure 3-11). Therefore, despite the high or moderate precipitation rate, a relatively low recharge rate is evident. Thus, soil characteristics has a critical control over the groundwater flow in the LMRB floodplains. Besides, the low gradient in the water table influenced by flat topography in the LMRB floodplains controls the groundwater flow in this region. R_s/P varies in the Mekong Delta ranging from 0.2 to 0.4. Like the floodplain in the LMRB, high clay content in the soil inhibits groundwater recharge in the Mekong Delta. One primary reason for low recharge could be the presence of shallow clay layers (Figure 3-10), which act as a confining layer limiting recharge. Similar findings in the Mekong Delta have also been reported by (Tu et al., 2022). Overall, climatic, and physiographic conditions, along with soil characteristics, play a crucial role in governing recharge and discharge. We note that we do not simulate the effects of dams and reservoirs that could influence groundwater recharge in the areas with substantial water impoundment.

The ratio of basin-wide discharge to recharge (Q_g/R_s) provides further insight into the groundwater flow pathways and the impacts of the basin-wide water budget. A vast majority of the basin area (indicated as different shades of blue color in Figure 3-7c) is a groundwater receiver, suggesting that groundwater a dominant component of the basin-wide water budget in the LMRB. Overall, groundwater recharge and discharge zones follow the MRB's north-to-south and east-to-west topographic and climatic gradients.

3.5.3 Climatic Control of Groundwater Flow

High recharge and discharge zones are generally located in areas with high annual precipitation and are strongly influenced by precipitation climatology. Basin averaged recharge rate peaks above 100 mm in August, the middle of the wet season in the MRB (Figure 3-7d and Figure 3-11). In contrast, recharge drops below 40 mm during the onset of the dry season in November. About 73% of annual recharge occurs between July and September, during which 40% of annual precipitation occurs (Figure 3-7e). Precipitation and recharge in the basin are highly correlated (R^2=0.71), suggesting a strong climate control on groundwater variations. Across the basin, the average recharge-to-rainfall ratio is 34% annually and substantially higher during the wet season (~52%) than during the dry season (~6%), indicating that rainfall seasonality plays a crucial role in governing annual groundwater recharge. Therefore, wet-season rainfall substantially contributes to groundwater replenishment and can potentially buffer subsurface storage during drought. This is well studied and known in the Amazon River basin (Miguez-Macho & Fan, 2012a, 2012b; Yadu N. Pokhrel et al., 2013; Yadu N. Pokhrel, Fan, et al., 2014) but remains largely unexamined in the MRB.

3.5.4 Role of Groundwater in Surface Water Dynamics and Governing Drivers

Groundwater discharge over the MRB is simulated to be ~401 mm/yr, accounting for over 50% of annual river discharge (Figure 3-8). Groundwater recharge and discharge peaks occur during the wet season with a 1-2 month delayed and dampened response to precipitation (Figure 3-8b-h and Figure 3-11). A shorter time lag between precipitation and infiltration is observed in the UMRB, which is characterized by sandy soil deposits that enhance rapid infiltration particularly during heavy rain events. Generally, we observe longer response time and high spatial variability toward the LMRB alluvial floodplains (Figure 3-11). Groundwater recharge and discharge have a 2-3 month delayed response to infiltration and precipitation in the LMRB, allowing groundwater recharge to carry over to the subsequent season and acts as a critical source of baseflow to rivers to maintain dry season flow. Also, comparable magnitude of basin-scale groundwater discharge and total runoff over the entire dry period (November-May) further underscores that groundwater supports the bulk of the total streamflow and its seasonal variation essentially governs surface water fluxes (Figure 3-11). Further, a substantially higher negative R_s/P during the dry season (Figures 3-8f and 3-8i) suggests that groundwater storage significantly contributes to augmenting soil moisture and ET. Particularly in the LMRB, some regions are evident where a negative R_s/P ratio is observed for consecutive 3-4 months after the offset of the wet season in September (Figure 3-8e-g), suggesting that groundwater responds to soil moisture deficit for a considerable period when precipitation is low. Basin-wide negative recharge during December to May further indicates that groundwater acts as a basin-wide soil moisture buffer to support dry season soil moisture and ET (Figure 3-11) implying that groundwater dynamics has a far-reaching influence on the water and energy cycle in the MRB.

Overall, the interaction between groundwater and surface water in the MRB is regulated by a complex set of drivers, including seasonal variations in precipitation, soil properties and topography. The impacts of human activities, such as irrigation and groundwater pumping, are discussed in the later section. Notably, the results are simulation-based and depend on a variety of model parameterizations such as soil layer configurations, subsurface parameterizations, and input datasets used all of which are subject to certain degree of uncertainty, which all can affect simulation outcomes. However, our results provide detailed insights on the different groundwater processes from surface (infiltration) to the subsurface (groundwater discharge), leading to a mechanistic understanding on the dynamic interactions among the tightly coupled surface water-groundwater processes across the MRB.

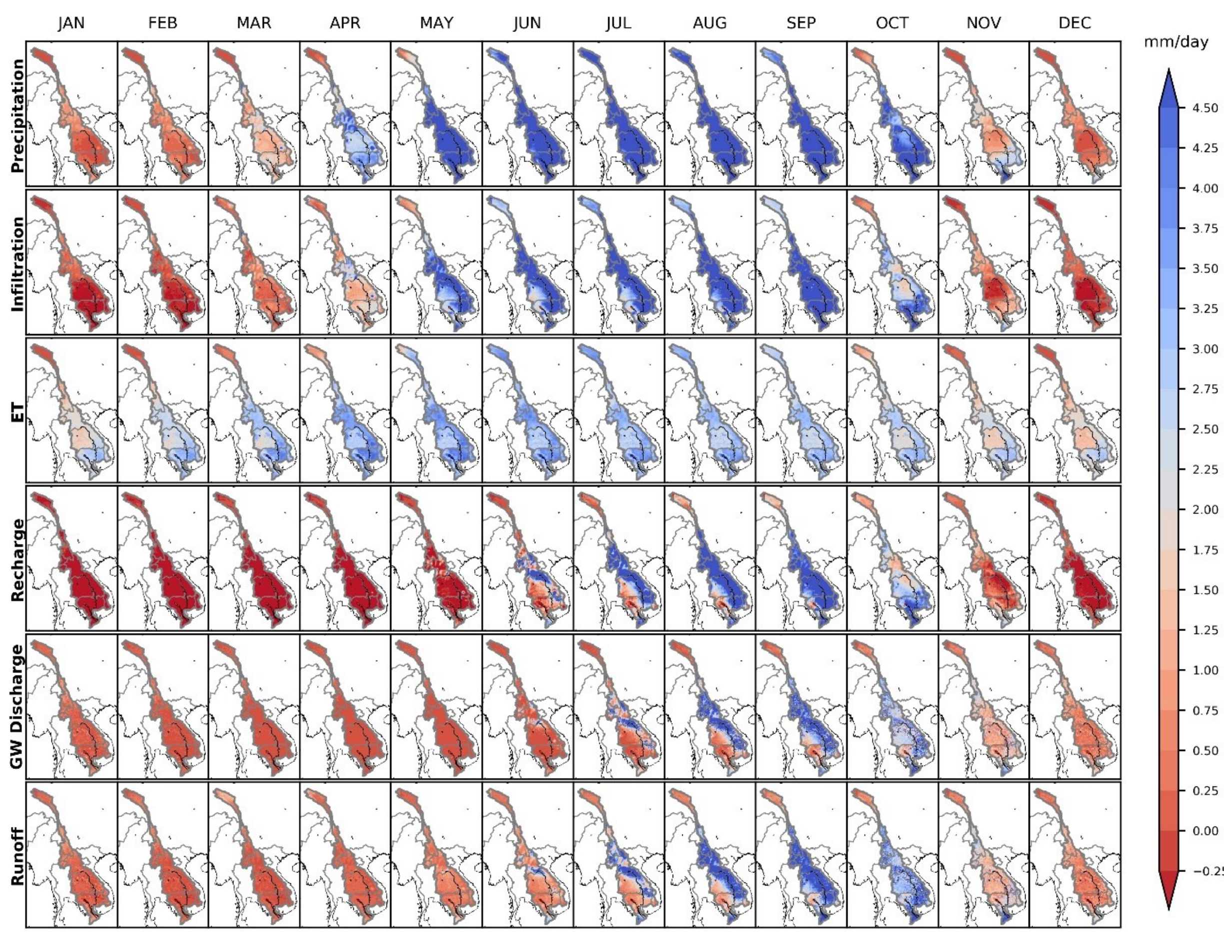

Figure 3-11. Spatial variability of the monthly mean precipitation (P), Infiltration (I_f), ET, groundwater recharge (R_s), groundwater discharge (Q_g) and total runoff (Q_T) rates for the 1979-2016 period. The vertical panels represent different months.

3.5.5 Groundwater Flow Impacted by Aquifer Pumping

Finally, we examine how increased groundwater pumping for irrigation impacts groundwater systems in the MRB. We specifically quantify the changes in groundwater flow and water table depth caused by increased aquifer pumping for dry season irrigation. We focus on the Mekong Delta region that accounts for the majority of irrigated crops and where widespread irrigation is increasing in recent years; in other parts of the MRB, agricultural systems are mostly rainfed. The simulated annual irrigation demand in the MRB varies from ~25 to over 250 mm (Figure 3-12a). In some portions of the Mekong Delta, irrigation demand is relatively high, for example, up to 200 mm/yr (Figure 3-12a), and these results are consistent with previous estimates reported in global scale studies for year 2010 (Wada et al., 2016).

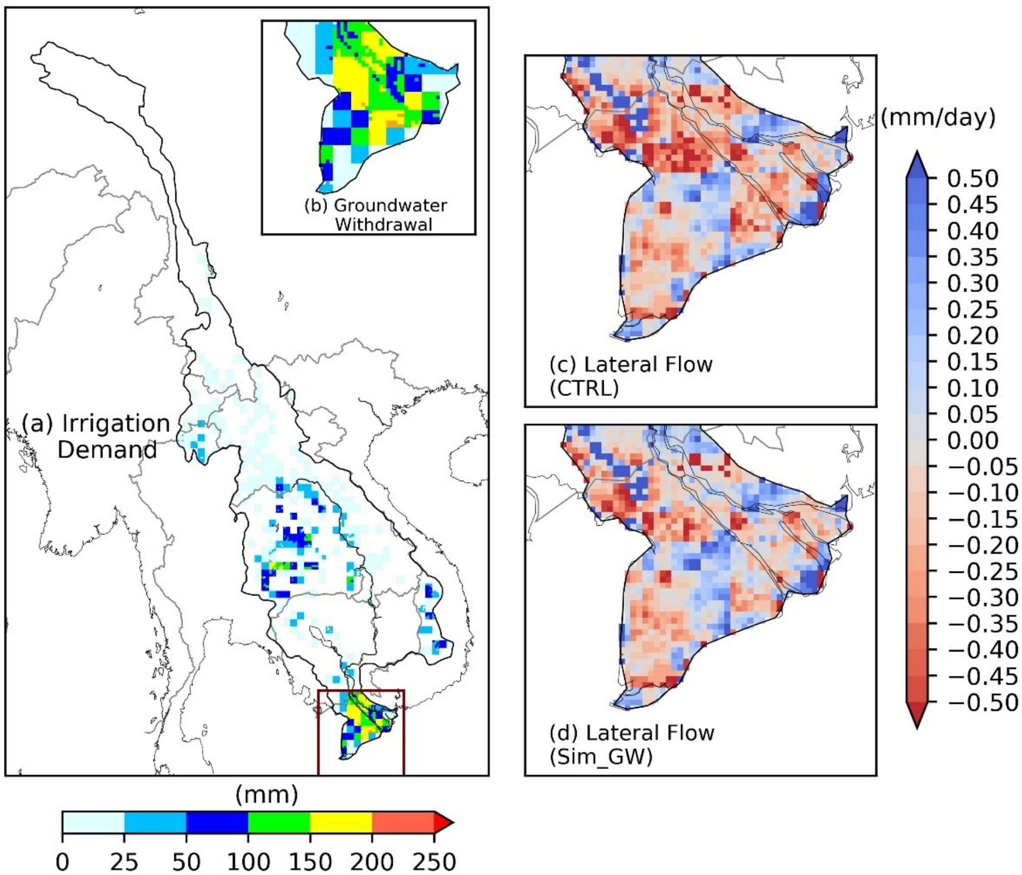

Figure 3-12. Mean annual irrigation demand simulated for the 2000-2016 period (a). Groundwater withdrawal for irrigation (b) (red box in panel (a)), and lateral groundwater flow from CTRL (c) and Sim_GW (d) simulations over the Mekong Delta. Panel (c) and (d) share the same color bar. Units are indicated next to the color bars. Note that the groundwater supplied fraction of irrigation water demand is used around the year 2005 and made consistent throughout the simulation period of 2000-2016.

Irrigation validation could be further enhanced by using satellite-based datasets (i.e., Brocca et al., (2018); Koch et al., (2020)). However, our results should be interpreted with caution because of possible uncertainties arising from the uncertainty in climate forcing and irrigation datasets used. Further, there could be under-representation of the recent irrigation development that is likely to cause an underestimated groundwater withdrawal. A more in-depth evaluation is not possible because of the lack of spatially explicit datasets on irrigation withdrawals in the MRB.

Irrigation-pumping imposes a water table gradient, causing up to half a meter of water table decline in the Mekong Delta (Figure 3-13a). In general, when averaged over a long period, the simulated effect of groundwater pumping is not substantial even in the Mekong Delta, especially in comparison to that in other major agricultural regions worldwide. This is so even when irrigation demand is met from the groundwater resource (i.e., Sim_GW simulation). Since irrigation development in the MRB is relatively recent (i.e., it started a few decades ago), long-term climate variability balances the pumping effects. However, widespread storage depletion is simulated in the Mekong Delta during the selected dry years (i.e., 2005 and 2015). The depletion is more than double in pumping cells in 2005 and 2015 compared to the long-term average water level decline and substantially large area of depletion is readily discernible (Figure 3-13b-c). Depletion reaches ~1m at the center of the Mekong Delta and ~0.5 m at the borders during 2005 under the increased influence of groundwater pumping (Sim_GW simulation). These results are consistent with previous estimates reported by regional scale studies on the Mekong Delta, although the simulated absolute depletion may be underestimated because the information on the recent increase in groundwater pumping for irrigation (Minderhoud et al., 2017, 2020) is not accounted for in our model.

Water table gradient induces a shift in groundwater flow in the Mekong Delta (Figure 3-13b-c), notably during dry years. The decline in water table (Figure 3-13b) drives large flow towards the pumping cells from the surrounding, resulting in an increase in groundwater discharge in the neighboring cells (in Sim_GW simulation) (positive difference) compared to the CTRL simulation (Figure 3-13e-f). Such pumping-induced alterations of groundwater dynamics, particularly during dry years, imply that groundwater depletion in the Mekong Delta could be exacerbated if prolonged droughts were to occur in the future.

The change in lateral groundwater flow (based on signs) further signifies the growing influence of irrigation and pumping on the region's groundwater systems (Figure 3-12c-d). For instance, red cells in Figure 3-12c (lateral outflow) turn blue (lateral inflow) due to the pumping-induced head gradient that triggers a substantial lateral flow towards the cone of depression (red blob, Figure 3-13b). Overall, the lateral flow is not substantial compared to the individual cell's water budget at the spatial resolution at which all the simulations are conducted (0.05°). In general, groundwater withdrawals are likely to be unsustainable in the Mekong Delta if irrigation and pumping continue to expand in the future. Notably, the model shows promising potential to simulate irrigation and its influence on groundwater, and in identifying depletion hotspots. However, it is important to note that local scale phenomena such as cone of depression resulting from pumping-induced water table gradient may not have been captured adequately at the current spatial resolution (i.e., 5 km).

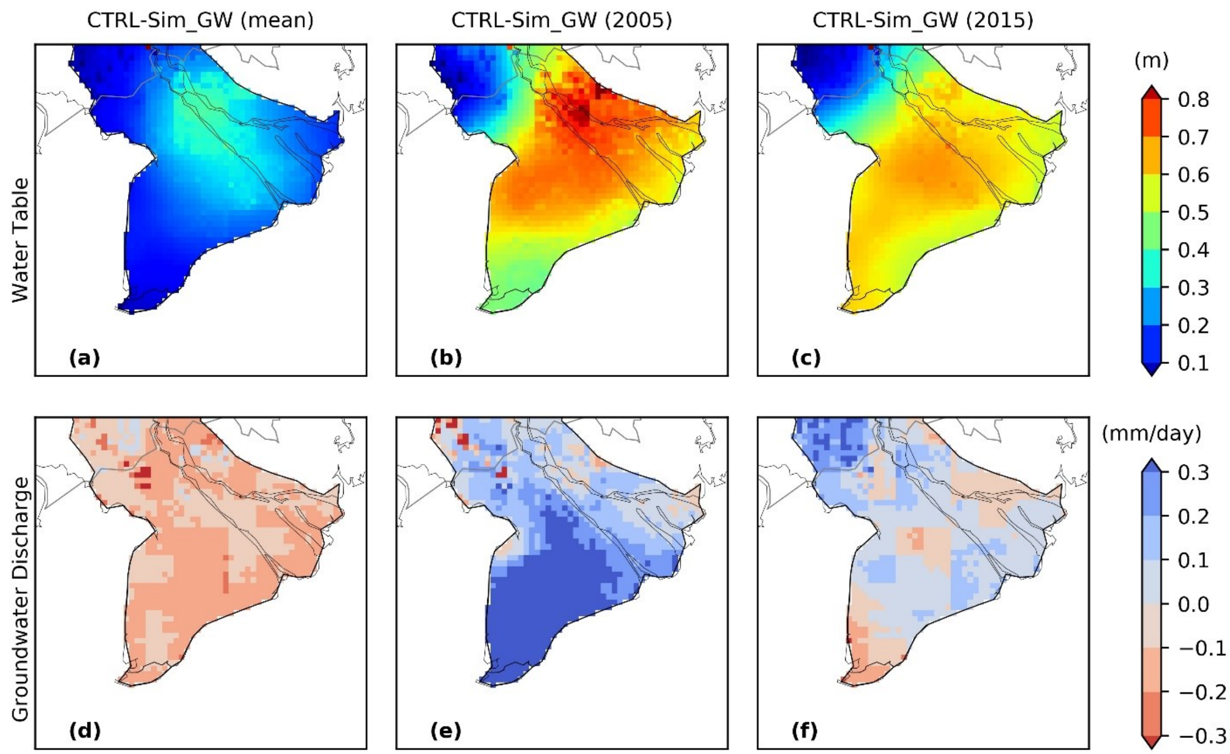

Figure 3-13. Differences in water table depth and groundwater discharge between CTRL and Sim_GW simulations (see Table 3-1) for three different time windows (i.e., differences in long-term mean and two dry years of 2005 and 2015). Note that the mean represents the 2000-2016 period. Top row shows differences in water table depth (a, b and c) and bottom row shows differences in groundwater discharge (d, e and f). The color bars differ among top and bottom panels. Top color bar represents change in water table depth with larger positive values indicating a deeper water table (i.e., a decline) in Sim_GW simulation. Bottom color bar represents change in groundwater discharge (positive values indicate an increase in Sim_GW simulation).

3.6 Conclusion

This study examines groundwater mechanisms, governing processes, and the interactions between groundwater and surface water under natural conditions and anthropogenic influences over the MRB using a fully process-based LSM with improved groundwater representation that accounts for lateral groundwater flow and aquifer pumping. Results are first validated with observed streamflow, water table, GRACE-based TWS, and SMAP-based soil moisture data, then used to examine groundwater flow processes across the MRB, the governing mechanism, and the effects of increasing irrigation activities on groundwater systems in the LMRB. The following summarizes the key findings of the study.

First, groundwater flow in the MRB exhibits high spatially heterogeneities, driven by a combination of factors including regional topography, climate, and local or regional scale subsurface characteristics. The climate (precipitation intensity and seasonality) has a first-order control on recharge and discharge variations across the basin. Further, regional subsurface characteristics dominantly control the recharge dynamics, especially in the LMRB. Second, in the LMRB, groundwater is the dominant source of streamflow, and its spatial variation and seasonality strongly modulate surface water dynamics; in some regions, groundwater perennially feeds streamflow. This mechanism is highlighted using an in-depth analysis over selected regions across the MRB with varying climatic, hydrologic, and geologic characteristics. Third, groundwater storage acts as a hydrological buffer and contributes substantially to soil moisture and ET for a considerable period of the year. These findings suggest a strong control of groundwater dynamics on the MRB's surface water and energy balances, with potential implications of perturbing the natural groundwater dynamics on surface water and energy fluxes. Fourth, groundwater use for irrigation has not had notable impact on groundwater dynamics over the long term, but the model simulates a region-wide storage depletion in the Mekong Delta during dry years, resulting in a shift in groundwater dynamics, also altering the magnitude and direction of groundwater discharge and lateral flow.

We note that our results are based on model simulations and may include uncertainties arising, for example, from forcing data, model resolution and imperfect groundwater parameterizations. Thus, the results should be interpreted with caution particularly for local scale implications of groundwater depletion hotspots and cone of depression. Further, the irrigation and groundwater data we used are from global databases, which may not include the most recent developments in groundwater irrigation, potentially underestimating the irrigation-induced changes in groundwater in the Mekong Delta. Our study offers a detailed discussion on the natural groundwater dynamics in the MRB as well as the potential impacts of irrigation development and groundwater withdrawal. A more comprehensive understanding of the groundwater dynamics in the MRB could require consideration of dams and reservoir operation and inclusion of local scale irrigation practices in the simulation, which forms a potential avenue for future research. Future studies could address these limitations by further refining model parameterizations, improving process representation, and using any new datasets. Despite certain limitations, this study provides the first results on groundwater modeling for the entire MRB and by using a process-based LSM that includes a prognostic groundwater scheme and aquifer pumping for irrigation. Our study also advances groundwater modeling capabilities in data-limited regions such as the MRB.

Chapter 4. Analysis of Drought Recovery under the Influence of Climate Change and Human Impacts

Based on: Kabir, T & Pokhrel, Y. (2023). Drought recovery under climate change and human impacts, Geophysical Research Letter. [Under Preparation]

4.1 Introduction

Drought recovery—a complex and multi-faceted process—influenced by a range of hydrological, ecological, and socio-economic factors (Jiao et al., 2021; Yang Li et al., 2023; L. Liu et al., 2019; Schwalm et al., 2017). Drought recovery refers to the time it takes for a system to bounce back to pre-drought conditions after a drought event (Guy Davidesko1,2, Amir Sagy1, 2014; J. Wu et al., 2019, 2020). Understanding of the drought recovery can be extremely complex as recovery time can vary greatly depending on a range of factors such as soil moisture (Samaniego et al., 2013; Sheffield et al., 2004; Sheffield & Wood, 2008), precipitation patterns (A F Van Loon et al., 2014), vegetation dynamics and plant phenology (Yang Li et al., 2023), catchment characteristics (Anne F. Van Loon et al., 2016) and water management practices (J. Wu et al., 2018). Thus, it is difficult to accurately understand drought recovery time, particularly under changing climatic conditions and anthropogenic disturbances and study on drought recovery is largely limited. Alternately, increasing attention is given to the conventional assessment of droughts frequency, intensity, duration, and the likelihood of occurrence under varying climate change scenarios using a range of approaches, including remote sensing (Aghakouchak et al., 2015; Anne F. Van Loon et al., 2016; J. Wu et al., 2019), hydrological modeling (Elkouk et al., 2021; Y. Pokhrel et al., 2021), and data analytics (Jiang & Zhou, 2023; Mondal et al., 2023; Yin et al., 2023) and machine learning . These studies have advanced our understanding of the global risk of drought and demonstrate varying potential to enhance drought preparedness and response efforts. Drought recovery, however, remains largely underexplored hindering our ability to adequately quantify drought risk across global regions (Peterson et al., 2021; Sheffield et al., 2012; Wen Wang et al., 2016).

The present understanding of drought is extremely limited and has generally focused on water deficits such as precipitation (Singh et al., 2021), terrestrial water storage deficit (Geruo et al., 2017; Long et al., 2013), and drought propagation (J. Wu et al., 2020) as opposed to the ability of the hydrological system to attain the pre-drought condition such as restoring groundwater recharge and runoff and surface water flow, etc. Drought characteristics have large variability that is unique in terms of severity, duration, and spatial extent, and traits of recovery are very likely to be different in different geographical and climatic settings (Yuting et al., 2017). Very few studies investigated recovery of record-breaking drought such as the California drought in 2014 (Alam et al., 2021; Yuting et al., 2017), and the millennium drought in southern Australia during 1997-2001. These studies suggest drought recovery time as a crucial indicator of drought risk assessment and provided in-depth insight into how drought risk can be exacerbated considering drought recovery time (Hao & AghaKouchak, 2013; Anne F. Van Loon, 2015). However, such studies over the large domain or global scale are largely lacking, hindering our ability to fully understand global drought risk across different regions with varying climatic and geographic settings.

Further, understanding of global drought recovery patterns are limited to vegetation restoration (Yang Li et al., 2023), gross primary production, and phenology development, a complex function of the terrestrial water cycle recovery and its components such as precipitation and soil moisture recovery. Studies that particularly investigated hydrological drought recovery linked precipitation recovery and ecosystem restoration time from the conventional belief that watersheds always recover from drought when precipitation is recovered. However, divergent response of drought to precipitation recovery exists and evidence suggests that drought recovery is not simply a function of precipitation recovery. The watershed in southern Australia is the best example of one such region that didn't recover fully and many parts of the watersheds didn't show any sign of recovery even though precipitation is recovered (Peterson et al., 2021). Other studies suggested that there are time lags in recovery of the terrestrial water cycle components; for instance, in comparison, the recovery of baseflow exhibits a longer time lag than the recovery of streamflow.

Also, understanding recovery can largely vary upon the scale of analysis, and it is crucial to understand at which scale recovery is locally relevant. Some studies acknowledged the necessity of studying drought recovery, providing a framework for drought recovery study. Yet no notable studies examined historical trajectories of drought recovery and the likelihood of different climate zones and biodiversity hotspot recovering from historical droughts. This knowledge gap is particularly challenging given the expected increase in frequency and intensity of droughts due to climate change. Studies suggested that many regions have experienced prolonged drought and more short-term drought before approaching to recovery state. Without a thorough understanding of the recovery process, we risk underestimating the long-term effects of droughts and developing inadequate response measures.

In addition, the increase in global temperature and the probability of multiple extremes such as drought and heatwaves are likely to occur substantially, and the cumulative effect in drought recovery is a crucial indicator of drought risk. Despite its significant impact, limited studies have focused on drought recovery and underlying mechanisms and drivers. Therefore, there is a need of comprehensive assessments of drought recovery mechanisms and their interactions with other factors, such as climate change and global warming, land use change, and biodiversity loss, to systematically examine the global drought risk. Further, a substantial body of literature exists on the multi-model ensemble-based study of drought assessment, the spatiotemporal pattern of drought severity under current and future climate, and human impact scenarios using different drought indices. However, opportunities and challenges remain in further understanding drought and examining the resilience of hydrological systems to recover from repetitive drought events even before fully recovering from a short-term drought.

Here we present a global assessment of drought recovery. To quantify drought recovery, we estimate drought recovery time in different climate zones globally over a historical timescale. By examining the global pattern of drought recovery, we identify regions of greater sensitivity to drought non-recovery and the areas that may have finite resilience to climate change and human impacts that lead to the persistence of longer drought duration and slow recovery. We provide a mechanistic understanding of the drivers that leads to longer recovery time. Here we quantify the post-drought recovery time of runoff (streamflow) at grid (0.5° spatial resolution) using a multi-model ensemble study for historical periods. We focus on runoff as its sensitivity to drought is well documented, and its spatiotemporal patterns can be estimated in several ways. Simulations are conducted under the framework of the Inter-Sectoral Impact Model Intercomparison Project, phase 3a (ISIMIP3a; https://www.isimip.org/). We use the multi-model weighted mean of runoff indices, calculated by weighting the ensemble members on the basis of their continent-level skill scores of simulations of hydrological fluxes and storages. We address the following science question through this study: (1) How is drought recovery time affected by climate variability and human impacts on different global regions? (2) What is the impact of prolonged drought recovery time on ecosystem sustainability in various climate zones and biodiversity hotspots?

4.2 Methods

4.2.1 Model Simulation setting and Forcing Data

We use simulated monthly discharge (0.5◦×0.5◦spatial resolution) for the period 1901–2019 from five global hydrological models (GHMs): CWatM, H08, WaterGAP2-2e, HydroPy, and Jules-w2. All simulations are carried out under the modeling framework of phase 3a of the Inter-Sectoral Impact Model Inter-comparison Project (ISIMIP3a:www.isimip.org/protocol/#isimip3a). All models simulate the key terrestrial hydrological processes, including soil vegetation and river processes. GSWP3 meteorological forcing data is used to simulate the models participating in the ISIMIP3 protocols. The climate variables included in the forcing data are precipitation, air temperature, solar radiation (short and long wave), wind speed, specific humidity, and surface pressure, which are bias-adjusted and downscaled to 0.5° × 0.5° spatial resolution of the hydrology models. A comprehensive description of bias adjustment and downscaling can be found in the previous literature. An overview of the model characteristics of each of the GHMs, and the methods used to parameterize hydrological processes and human impact, can be found in table 4-1.

Table 4-1. The main characteristics of the GHMs based on ISIMIP 3a used in the study. Abbreviations for five water use sectors that are represented in the model: Do (domestic), Li (livestock), In (industry), Ir (irrigation), Ma (manufacturing).

Type	Name	Land use change	Water use	Water regulations
GHM	H08	Annual	Do, In and Ir	Dams and reservoirs
	WaterGap2-2e	Static land use	Do, In, Ir, Li, and Ma	Dams and reservoirs
	HydroPy	Annual crop fraction	Ir	No dams and reservoirs
	CWatM	Annual	Ir	No dams and reservoirs
	Jules-w2	Annual		No dams and reservoirs

4.2.2 Identification of Drought Events and Drought Recovery

Hydrological drought events are identified based on standardized runoff index (SRI). SRI is calculated as follows: SRI $= \frac{Runoff - mean\ runoff}{Standard\ deviation}$. SRI < -2 indicates extreme drought condition. First, SRI is calculated at timescale of 1,6,9,12 months. Finally, 12-month SRI (SRI12) is used in the analysis for capturing long-term droughts disregarding short term fluctuations in runoff. SRI12 is smoothened by a 3-month forward moving window to smooth out short-term fluctuation and highlights the longer-term trends in drought severity. Drought recovery is defined as the duration (months) starting from the month from the SRI12 < -2 to the months when SRI bounce back to long term mean or SRI12 = 0 after drought events. A drought event and recovery that is fully contained between 1901-2019 is analyzed in calculating mean drought recovery time. For example, drought that started in 2016 and ends after 2019 is not considering in calculating mean drought recovery time. This may lead to possible underestimation of drought events. However, given that we are analyzing for a long historical timescale from 1901-2019, mean drought event and recovery time will not be substantially impacted. Finally, drought recovery time, recovery pattern and drivers are analyzed on various spatial scales. IPCC-SREX climate zones are identified to analyze drought over broad spatial scale. Alternately, some watershed and country scale analysis are performed to differentiate how drought recovery can vary over different spatial domains.

4.3 Results and Discussions

4.3.1 Validation of Streamflow

Figure 4-1 presents the combined assessment of streamflow simulation by various members of the GHMs ensemble at river stations chosen from eight hydrobelts across the globe. The ensemble member's simulation performance varies across different hydrobelts, demonstrating better agreement with observations in BOR, EQT, NDR, NML, and NST, with high correlation and low RMSE. However, relatively weak agreement is observed in SDR and SST. Although the simulations perform well in general in the BOR hydrobelt, some inconsistencies are detected in Lena and Yenisei watersheds. Moreover, none of the simulations can accurately replicate the observed magnitude and timing of the streamflow peak in the Brahmaputra basin. Additionally, the simulations fail to capture the magnitude and timing of flow in the Colorado basin, possibly because they do not account for dams and reservoirs, which can impact the ensemble mean's performance. Nonetheless, all ensemble members perform well in the Amazon and Mekong basins, which are wet basins with significant rainfall throughout the year. Generally, a wide range of variability among ensemble members is observed in highly managed basins such as Mackenzie, Missouri, Colorado, and St. Lawrence, primarily due to varying water use and regulations parameterizations in the ensemble models.

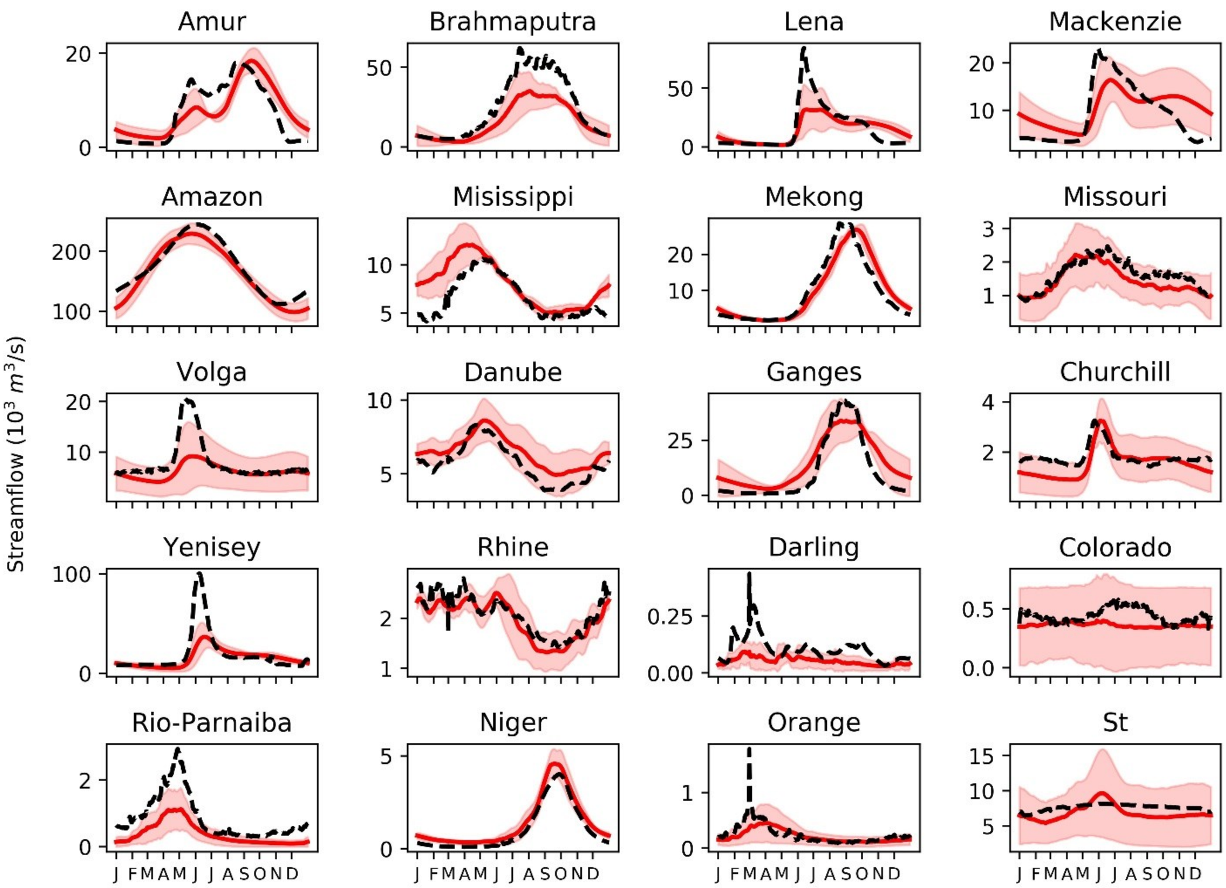

Figure 4-1. Comparison of seasonal cycle of simulated and observed streamflow. The red line indicated the average simulated streamflow climatology, and the shaded region shows the distribution across all ensemble members. Black like indicates the observed streamflow obtained from the global runoff data centre (GRDC). Validation stations are chosen across eight hydrobelts. Hydrobelts are named: BOR= boreal, NML = northern mid-latitude, NDR= northern dry, NST = northern subtropical, EQT = equatorial, SML=southern mid-latitude, SDR = southern dry and SST = southern subtropical.

4.3.2 Validation of TWS

To verify the models' ability to simulate storage variations in conjunction with hydrological flux such as streamflow, the TWS anomaly is compared to GRACE observations. The TWS validation includes all major watersheds. In general, all ensemble members perform well in replicating the seasonal dynamics and amplitude variations of TWS anomaly, with less variability observed in simulated TWS between ensemble members compared to streamflow simulations. However, there are certain disparities in some river basins, such as Amur, Churchill, and Indus, which may be due to differences among ensemble members in their representation of water use and regulations and soil layer classification, leading to significant discrepancies compared to GRACE observations.

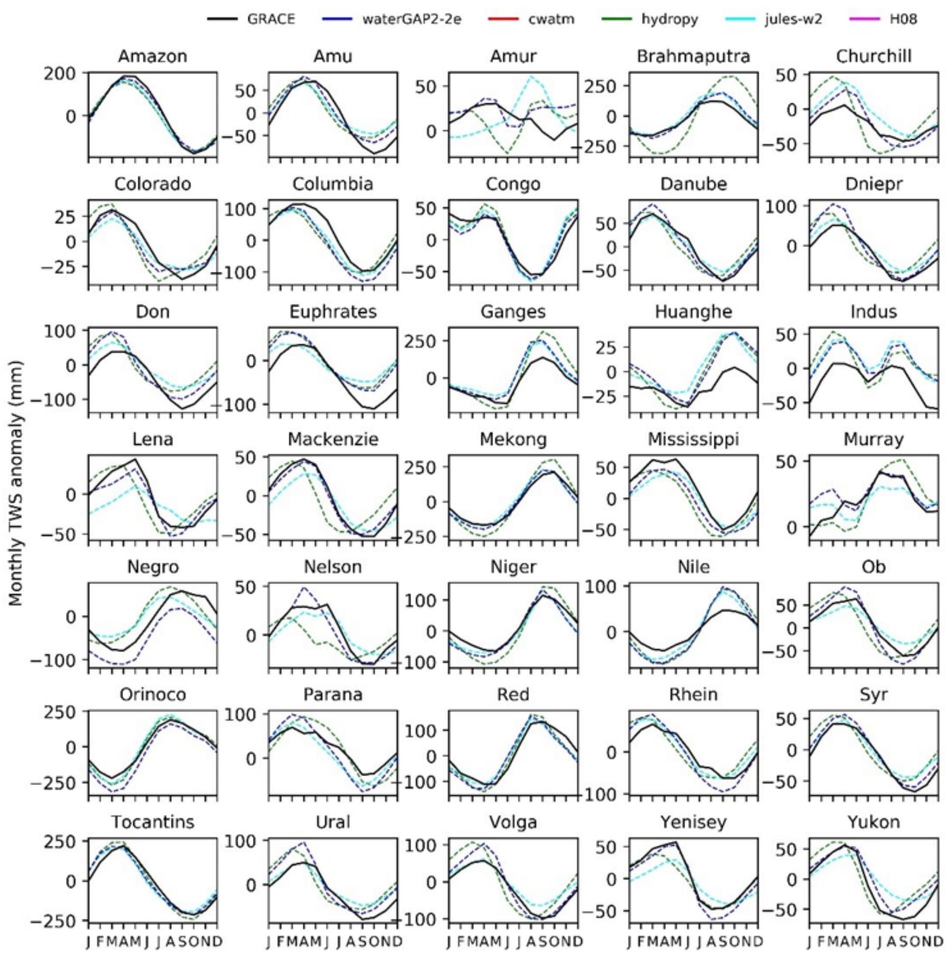

Figure 4-2. Seasonal cycle of simulated and GRACE TWS anomaly for the selected river basins. The thick black line represents the mean of GRACE products from CSR and JPL mascon.

4.3.3 Variations of Simulated Fluxes and Storages

The results show notable disparities in the simulated fluxes and storages across ensemble members (Figure 4-3, 4-4 and 4-5), which are attributable to differing model parameterizations and water management practices. Specifically, there are significant differences between CWatM and the other models in terms of runoff, with CWatM producing higher runoff than the other models. Additionally, there are considerable discrepancies in the simulated ET, with CWatM exhibiting higher ET compared to all other models. This discrepancy in ET is likely due to the wet bias present in CWatM, which affects both soil moisture and ET simulation.

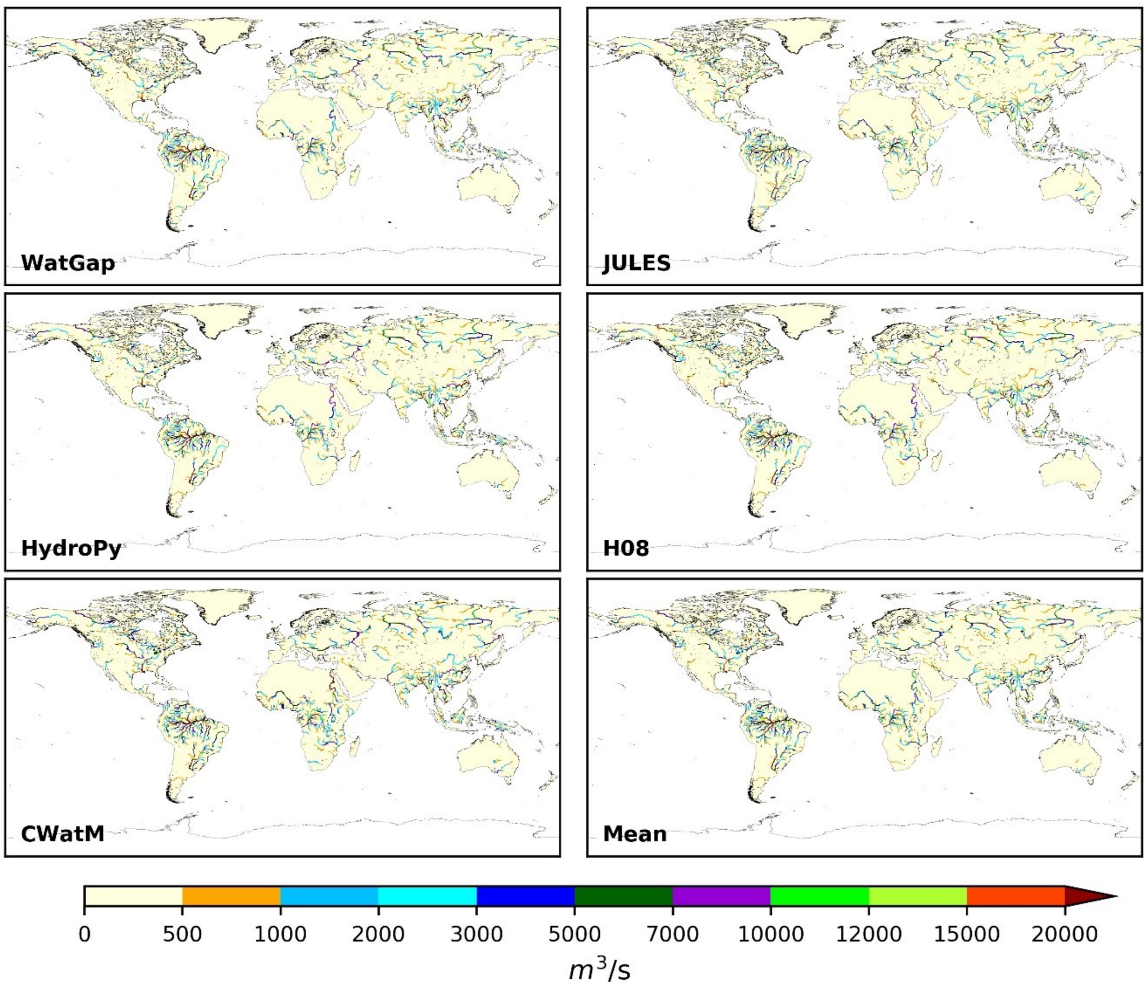

Figure 4-3. Simulated streamflow from all ensemble model members.

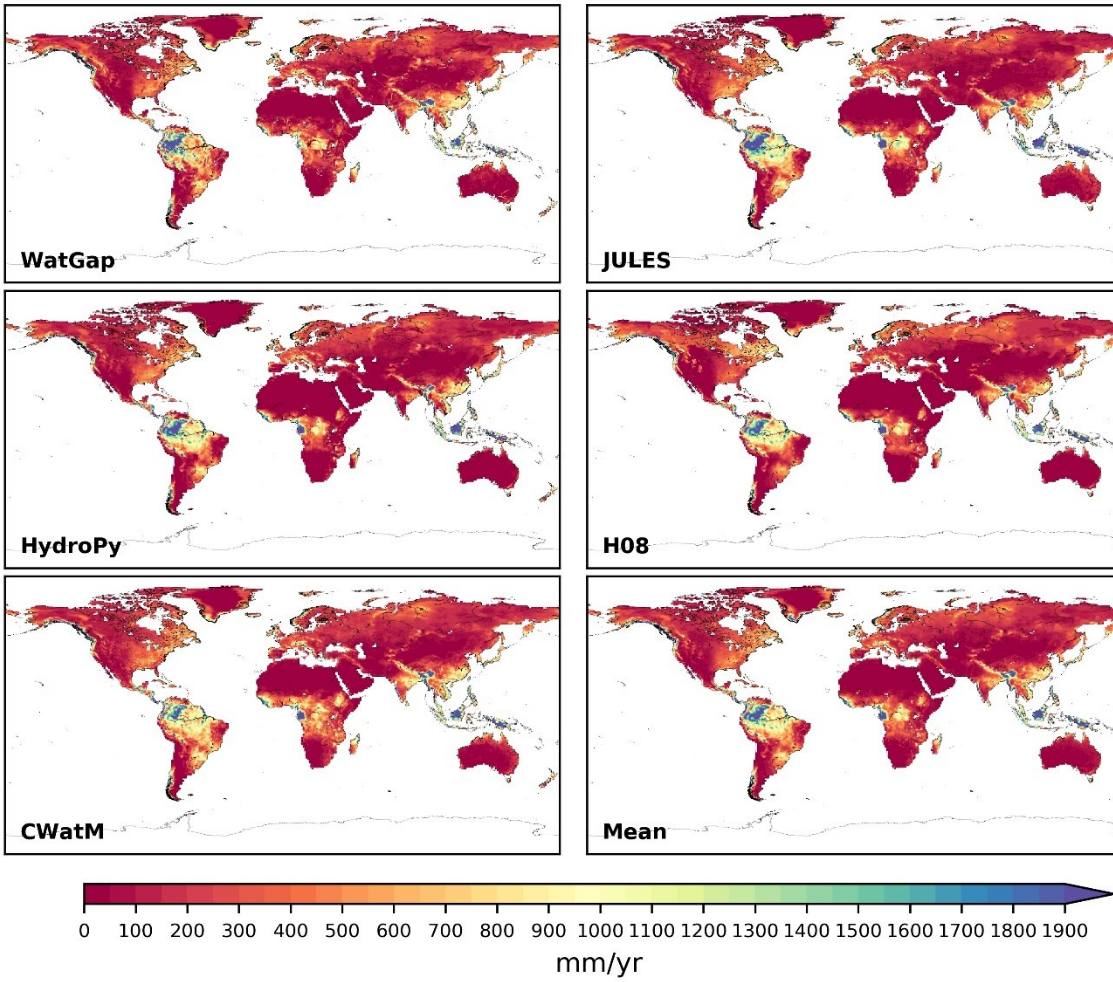

Figure 4-4. Simulated runoff from all model members.

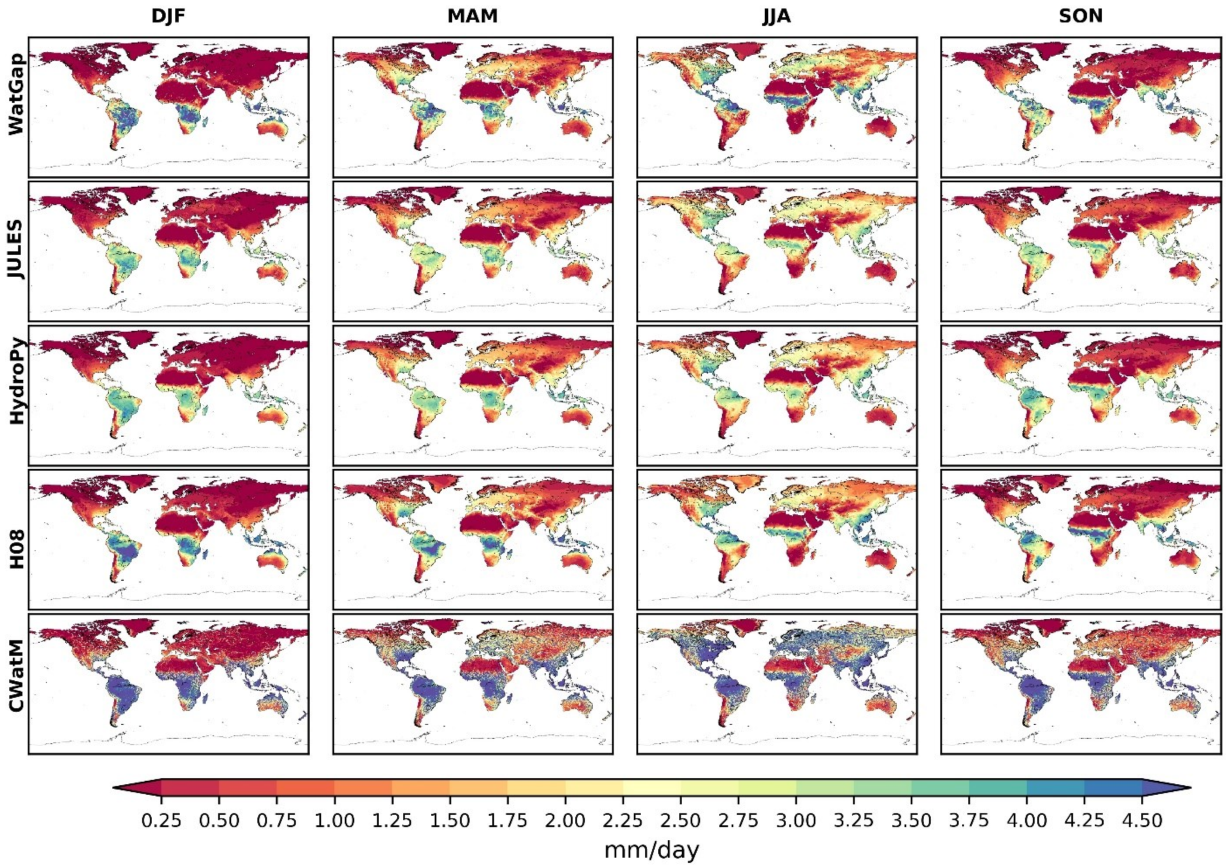

Figure 4-5. Seasonal ET variations from different ensemble model members.

4.3.4 Drought Events and Spatial Pattern of Hydrological Drought Recovery Time

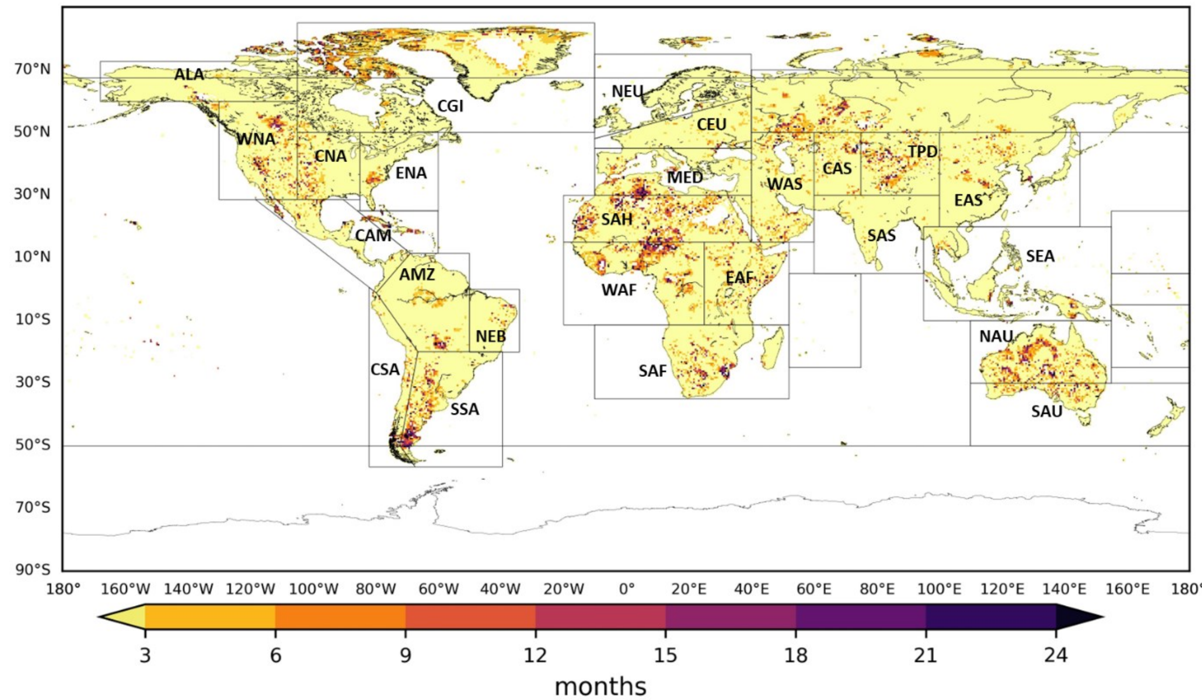

Figure 4-6. Spatial pattern of drought recovery time. The figure shows the ensemble's mean recovery time of selected models used in this study. Different SREX climate zones are shown in the map. 12-month SRI applied in recovery calculation to account for relatively long-term drought (see Methods – different time integration applied).

Figure 4-6 depicts a prominent spatial pattern of drought recovery time across different regions. The recovery time tends to be longer in several zones, including SSA, CNA, WNA, CGI, SAH, TIB, and NAU. The northern high latitude, particularly the Russian far east and Alaska, experiences the longest recovery times. The Sahel region in the SAH zone and the NAU and SAU regions also exhibit longer recovery times over a large spatial extent. In very dry systems, recovery times increase with decreasing precipitation, while arid and semi-arid regions show the longest recovery times. This reflects a trend where regions with more precipitation experience a quicker recovery after drought events. Some regions exist having longer drought development time than recovery time.

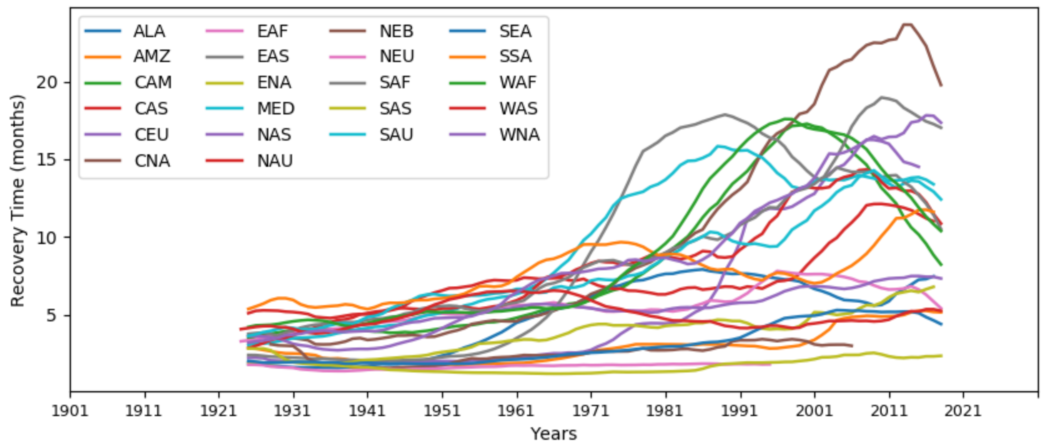

Figure 4-7. Drought recovery time of different decades. A Thirty months moving forward window average method is applied to capture the long-term trajectories of drought recovery time.

Overall, there is a substantial increase in drought recovery time across most of the climate zones including NEB, CEU, WNA. The increase in recovery time is particularly prominent post-1980, possibly due to the effects of climate change-induced alterations in precipitation patterns and surface temperature. Thus, climate change significantly affect the land's water budget, leading to a prolonged recovery time of drought events because of reduction in global runoff and streamflow.

4.4 Conclusion

This chapter employs a multi-model ensemble approach to investigate the drought recovery time across different climate zones and its drivers using five global hydrological models (H08, WaterGAP2-2e, CWatM, HydroPy, and Jules-W2) output within the modeling framework of phase 3a of the Inter-Sectoral Impact Model Intercomparison Project (ISIMIP3a). The chapter heighlights that recovery time is longest in water-limited regions and has exhibited an upward trend across all climate zones in recent decades. Results underscore the significant influence of climate as a key driver of drought recovery time, and highlight the critical need for a comprehensive understanding of climate change and water availability across diverse global regions.

Chapter 5. Summary and Conclusion

Despite significant progress in hydrological modeling, uncertainty remains regarding the ability of the models to capture the intricate behavior of various surface and subsurface hydrologic processes, and the impacts of land-water management practices when applied across varying spatial domain.

In Chapter 2, the propagation of precipitation uncertainty into hydrological simulations over the Mekong River basin (MRB) is investigated using the Community Land Model version 5 (CLM5) at a relatively high spatial resolution of 0.05° (~5 km). Simulations conducted using different precipitation datasets (reanalysis and satellite) are compared to investigate the discrepancies in streamflow, terrestrial water storage (TWS), and evapotranspiration (ET) caused by precipitation uncertainty. Results indicate that precipitation is a key factor impacting the accuracy of simulated streamflow in the MRB; the peak flow is particularly sensitive to precipitation input. Notable differences are also observed among TWS, soil moisture, and ET simulated using different precipitation products. Further, precipitation data with a higher spatial resolution did not improve the simulations, contrary to the common perception that using meteorological forcing with higher spatial resolution would improve hydrological simulations. The chapter provides crucial insights on precipitation-induced uncertainties in process-based hydrological modeling and uncovers these uncertainties in the MRB.

In Chapter 3, CLM5 with an improved groundwater and irrigation parameterizations and with a better representation of irrigation areas is used to investigate the groundwater dynamics of the MRB. The chapter provides an in-depth understanding of various groundwater mechanisms in the MRB, focusing on groundwater flow processes that are modulated by climate variability and physiographic features, and primary drivers of groundwater-surface water interactions as well as the influence of anthropogenic activities on groundwater dynamics. Overall results indicate high spatial heterogeneity in groundwater recharge and discharge across the basin governed by climate and subsurface characteristics. A pronounced seasonality is found in groundwater recharge due to precipitation, with substantial carryover to the consecutive dry season that modules soil moisture. Importantly, groundwater discharge is a dominant source of streamflow all year round, which suggests a strong surface water-groundwater coupling in the MRB. Finally, our results indicate that irrigation pumping is directly altering groundwater flows and storages; climate variability smoothens pumping effects over long times, but the model simulates region-wide groundwater depletion in the Mekong Delta during dry years. This chapter provides key insights on the evolving groundwater systems in the MRB, and also advancing process-based groundwater modeling capabilities.

In Chapter 4, the drought recovery and its potential drivers are investigated using a multi-model ensemble approach. Five global hydrological models (i.e., H08, WaterGAP2-2e, CWatM, HydroPy, and Jules-W2) under historical climate for the period 1901–2019 are used for the analysis. All simulations are carried out under the modeling framework of phase 3a of the Inter-Sectoral Impact Model Intercomparison Project (ISIMIP3a). Hydrological drought recovery time (based on standardized runoff index) is investigated for different climate regions. Results indicate that drought recovery time is the longest in the water-limited regions and there has been a sharp upward trend in recovery time across all climate zones over the past several decades. The climate is a dominant driver that significantly affects drought recovery time. This chapter provides key insights on the drought recovery across global regions and highlights the importance of understanding climate change and water availability across different global regions.

REFERENCES

Aghakouchak, A., Farahmand, A., Melton, F. S., Teixeira, J., Anderson, M. C., Wardlow, B. D., & Hain, C. R. (2015). Reviews of geophysics remote sensing of drought: Progress, challenges. *Reviews of Geophysics*, *53*, 1–29. https://doi.org/10.1002/2014RG000456.

Alam, S., Gebremichael, M., Ban, Z., Scanlon, B. R., Senay, G., & Lettenmaier, D. P. (2021). Post-Drought Groundwater Storage Recovery in California's Central Valley. *Water Resources Research*, *57*(10), 1–21. https://doi.org/10.1029/2021WR030352

Ambika, A. K., & Mishra, V. (2019). Substantial decline in atmospheric aridity due to irrigation in India. *Environmental Research Letters*, *15*(12). https://doi.org/10.1088/1748-9326/abc8bc

Arias, M. E., Piman, T., Lauri, H., Cochrane, T. A., & Kummu, M. (2014). Dams on Mekong tributaries as significant contributors of hydrological alterations to the Tonle Sap Floodplain in Cambodia. *Hydrology and Earth System Sciences*, *18*(12), 5303–5315. https://doi.org/10.5194/hess-18-5303-2014

Arias, Mauricio E., Cochrane, T. A., Piman, T., Kummu, M., Caruso, B. S., & Killeen, T. J. (2012). Quantifying changes in flooding and habitats in the Tonle Sap Lake (Cambodia) caused by water infrastructure development and climate change in the Mekong Basin. *Journal of Environmental Management*, *112*, 53–66. https://doi.org/10.1016/j.jenvman.2012.07.003

Arias, Mauricio E., Cochrane, T. A., Norton, D., Killeen, T. J., & Khon, P. (2013). The flood pulse as the underlying driver of vegetation in the largest wetland and fishery of the mekong basin. *Ambio*, *42*(7), 864–876. https://doi.org/10.1007/s13280-013-0424-4

Bárdossy, A., & Das, T. (2008). *Hydrology and Earth System Sciences Influence of rainfall observation network on model calibration and application*. *Hydrol. Earth Syst. Sci* (Vol. 12). Retrieved from www.hydrol-earth-syst-sci.net/12/77/2008/

Barlage, M., Chen, F., Rasmussen, R., Zhang, Z., & Miguez-Macho, G. (2021). The Importance of Scale-Dependent Groundwater Processes in Land-Atmosphere Interactions Over the Central United States. *Geophysical Research Letters*, *48*(5), 1–10. https://doi.org/10.1029/2020GL092171

Beck, H. E., Van Dijk, A. I. J. M., De Roo, A., Dutra, E., Fink, G., Orth, R., & Schellekens, J. (2017). Global evaluation of runoff from 10 state-of-the-art hydrological models. *Hydrology and Earth System Sciences*, *21*(6), 2881–2903. https://doi.org/10.5194/hess-21-2881-2017

Beck, H. E., Van Dijk, A. I. J. M., Levizzani, V., Schellekens, J., Miralles, D. G., Martens, B., & De Roo, A. (2017). MSWEP: 3-hourly 0.25° global gridded precipitation (1979-2015) by merging gauge, satellite, and reanalysis data. *Hydrology and Earth System Sciences*, *21*(1), 589–615. https://doi.org/10.5194/hess-21-589-2017

Beven, K. J., & Kirkby, M. J. (1979). A physically based, variable contributing area model of basin hydrology. *Hydrological Sciences Bulletin*, *24*(1), 43–69. https://doi.org/10.1080/02626667909491834

Beven, Keith J., & Cloke, H. L. (2012). Comment on "hyperresolution global land surface modeling: Meeting a grand challenge for monitoring Earth's terrestrial water" by Eric F. Wood et al. *Water Resources Research*, *48*(1), 1–10. https://doi.org/10.1029/2010WR010090

Biemans, H., Hutjes, R. W. A., Kabat, P., Strengers, B. J., Gerten, D., & Rost, S. (2009). Effects of precipitation uncertainty on discharge calculations for main river basins. *Journal of Hydrometeorology*, *10*(4), 1011–1025. https://doi.org/10.1175/2008JHM1067.1

Bierkens, M. F. P., & van den Hurk, B. J. J. M. (2007). Groundwater convergence as a possible mechanism for multi-year persistence in rainfall. *Geophysical Research Letters*, *34*(2), 1–5. https://doi.org/10.1029/2006GL028396

Bierkens, M. F. P., Bell, V. A., Burek, P., Chaney, N., Condon, L. E., David, C. H., et al. (2015). Hyper-resolution global hydrological modelling: What is next?: "Everywhere and locally relevant" M. F. P. Bierkens et al. Invited Commentary. *Hydrological Processes*, *29*(2), 310–320. https://doi.org/10.1002/hyp.10391

Bisht, G., Riley, W. J., Hammond, G. E., & Lorenzetti, D. M. (2018). Development and evaluation of a variably saturated flow model in the global E3SM Land Model (ELM) version 1.0. *Geoscientific Model Development*, *11*(10), 4085–4102. https://doi.org/10.5194/gmd-11-4085-2018

Bonan, G. B., Lawrence, P. J., Oleson, K. W., Levis, S., Jung, M., Reichstein, M., et al. (2011). Improving canopy processes in the Community Land Model version 4 (CLM4) using global flux fields empirically inferred from FLUXNET data. *Journal of Geophysical Research*, *116*(G2), 1–22. https://doi.org/10.1029/2010jg001593

Brocca, L., Tarpanelli, A., Filippucci, P., Dorigo, W., Zaussinger, F., Gruber, A., & Fernández-Prieto, D. (2018). How much water is used for irrigation? A new approach exploiting coarse resolution satellite soil moisture products. *International Journal of Applied Earth Observation and Geoinformation*, *73*(August), 752–766. https://doi.org/10.1016/j.jag.2018.08.023

Carling, P. A. (2009). *The Geology of the Lower Mekong River*. *The Mekong: Biophysical Environment of an International River Basin* (1st ed.). Elsevier Inc. https://doi.org/10.1016/B978-0-12-374026-7.00002-4

Chaudhari, S., Pokhrel, Y., Moran, E., & Miguez-Macho, G. (2019). Multi-decadal hydrologic change and variability in the Amazon River basin: Understanding terrestrial water storage variations and drought characteristics. *Hydrology and Earth System Sciences*, *23*(7), 2841–2862. https://doi.org/10.5194/hess-23-2841-2019

Chen, A., Chen, D., & Azorin-Molina, C. (2018). Assessing reliability of precipitation data over the Mekong River Basin: A comparison of ground-based, satellite, and reanalysis datasets.

International Journal of Climatology, *38*(11), 4314–4334. https://doi.org/10.1002/joc.5670

Chinh, D. T., Bubeck, P., Dung, N. V., & Kreibich, H. (2016). The 2011 flood event in the Mekong Delta: preparedness, response, damage and recovery of private households and small businesses. *Disasters*, *40*(4), 753–778. https://doi.org/10.1111/disa.12171

Clapp, R. B. A., & Hornberger, G. M. (1978). Empirical Equations for Some Soil Hydraulic Properties, *14*(4).

Clark, M. P., Fan, Y., Lawrence, D. M., Adam, J. C., Bolster, D., Gochis, D. J., et al. (2015a). Hydrological partitioning in the critical zone: Recent advances and opportunities for developing transferable understanding of water cycle dynamics. *Water Resources Research*, 1–28. https://doi.org/10.1002/2015WR017096.Received

Clark, M. P., Fan, Y., Lawrence, D. M., Adam, J. C., Bolster, D., Gochis, D. J., et al. (2015b). Improving the representation of hydrologic processes in Earth SystemModels, 5929–5956. https://doi.org/10.1002/2015WR017096.Received

Colliander, A., Cosh, M. H., Kelly, V. R., Kraatz, S., Bourgeau-Chavez, L., Siqueira, P., et al. (2020). SMAP Detects Soil Moisture Under Temperate Forest Canopies. *Geophysical Research Letters*, *47*(19), 1–10. https://doi.org/10.1029/2020GL089697

Condon, L. E., & Maxwell, R. M. (2015). Evaluating the relationship between topography and groundwater using outputs from a continental-scale integrated hydrology model. *Water Resources Research*, *51*(8), 6602–6621. https://doi.org/10.1002/2014WR016774

Condon, L. E., Atchley, A. L., & Maxwell, R. M. (2020). Evapotranspiration depletes groundwater under warming over the contiguous United States. *Nature Communications*, *11*(1). https://doi.org/10.1038/s41467-020-14688-0

Condon, L. E., Kollet, S., Bierkens, M. F. P., Fogg, G. E., Maxwell, R. M., Hill, M. C., et al. (2021). Global Groundwater Modeling and Monitoring: Opportunities and Challenges. *Water Resources Research*, *57*(12), 1–27. https://doi.org/10.1029/2020WR029500

Cooper, M. (2010). Advanced Bash-Scripting Guide An in-depth exploration of the art of shell scripting Table of Contents. *Okt 2005 Abrufbar Uber Httpwww Tldp OrgLDPabsabsguide Pdf Zugriff 1112 2005*, *2274*(November 2008), 2267–2274. https://doi.org/10.1002/hyp

Cosby, B. J., Hornberger, G. M., Clapp, R. B., & Ginn, T. R. (1984). Exploration of the Relationships of Soil Moisture Characteristics to the Physical Properties of Soils, *20*(6), 682–690.

Crosbie, R. S., Scanlon, B. R., Mpelasoka, F. S., Reedy, R. C., Gates, J. B., & Zhang, L. (2013). Potential climate change effects on groundwater recharge in the High Plains Aquifer, USA. *Water Resources Research*, *49*(7), 3936–3951. https://doi.org/10.1002/wrcr.20292

Cuthbert, M. O., Gleeson, T., Moosdorf, N., Befus, K. M., Schneider, A., Hartmann, J., & Lehner, B. (2019). Global patterns and dynamics of climate–groundwater interactions.

Nature Climate Change, *9*(2), 137–141. https://doi.org/10.1038/s41558-018-0386-4

Danabasoglu, G., Lamarque, J. F., Bacmeister, J., Bailey, D. A., DuVivier, A. K., Edwards, J., et al. (2020). The Community Earth System Model Version 2 (CESM2). *Journal of Advances in Modeling Earth Systems*, *12*(2), 1–35. https://doi.org/10.1029/2019MS001916

Dang, T. D., Cochrane, T. A., Arias, M. E., Van, P. D. T., & de Vries, T. T. (2016). Hydrological alterations from water infrastructure development in the Mekong floodplains. *Hydrological Processes*, *30*(21), 3824–3838. https://doi.org/10.1002/hyp.10894

Dang, T. D., Chowdhury, A. F. M. K., & Galelli, S. (2020). On the representation of water reservoir storage and operations in large-scale hydrological models: Implications on model parameterization and climate change impact assessments. *Hydrology and Earth System Sciences*, *24*(1), 397–416. https://doi.org/10.5194/hess-24-397-2020

Delgado, J. M., Merz, B., & Apel, H. (2012). A climate-flood link for the lower Mekong River. *Hydrology and Earth System Sciences*, *16*(5), 1533–1541. https://doi.org/10.5194/hess-16-1533-2012

Di, L., Longuevergne, L., & Bridget, R. S. (2014). Uncertainty in evapotranspiration from land surface modeling, remote sensing, and GRACE satellites, (Vic), 5375–5377. https://doi.org/10.1002/2013WR014979.Reply

Dinh, K. D., Anh, T. N., Nguyen, N. Y., Bui, D. D., & Srinivasan, R. (2020). Evaluation of grid-based rainfall products and water balances over the Mekong river Basin. *Remote Sensing*, *12*(11). https://doi.org/10.3390/rs12111858

Döll, P. (2009). Vulnerability to the impact of climate change on renewable groundwater resources: A global-scale assessment. *Environmental Research Letters*, *4*(3). https://doi.org/10.1088/1748-9326/4/3/035006

Döll, P., Douville, H., Güntner, A., Müller Schmied, H., & Wada, Y. (2016). Modelling Freshwater Resources at the Global Scale: Challenges and Prospects. *Surveys in Geophysics*, *37*(2), 195–221. https://doi.org/10.1007/s10712-015-9343-1

Drewry, D. T., Kumar, P., Long, S., Bernacchi, C., Liang, X. Z., & Sivapalan, M. (2010). Ecohydrological responses of dense canopies to environmental variability: 1. Interplay between vertical structure and photosynthetic pathway. *Journal of Geophysical Research: Biogeosciences*, *115*(4), 1–25. https://doi.org/10.1029/2010JG001340

Dushmanta, D., Jahangir, A., Kazuo, U., Masayoshi, H., & Sadayuki, H. (2007). A two-dimensional hydrodynamic model for flood inundation simulation: a case study in the lower Mekong river basin. *HYDROLOGICAL PROCESSES*, *2274*(November 2008), 2267–2274. https://doi.org/10.1002/hyp

Duy, N. Le, Nguyen, T. V. K., Nguyen, D. V., Tran, A. T., Nguyen, H. T., Heidbüchel, I., et al. (2021). Groundwater dynamics in the Vietnamese Mekong Delta: Trends, memory effects, and response times. *Journal of Hydrology: Regional Studies*, *33*(May 2020), 100746.

https://doi.org/10.1016/j.ejrh.2020.100746

E Condon, L., & Maxwell, R. M. (2015). Evaluating the relationship between topography and groundwater using outputs from a continental-scale integrated hydrology model Laura. *Journal of the American Water Resources Association*, *5*(3), 2–2. https://doi.org/10.1002/2014WR016774

Elkouk, A., El Morjani, Z. E. A., Pokhrel, Y., Chehbouni, A., Sifeddine, A., Thober, S., & Bouchaou, L. (2021). Multi-model ensemble projections of soil moisture drought over North Africa and the Sahel region under 1.5, 2, and 3 °C global warming. *Climatic Change*, *167*(3–4), 1–18. https://doi.org/10.1007/s10584-021-03202-0

Engdahl, N. B. (2017). Transient effects on confined groundwater age distributions: Considering the necessity of time-dependent simulations. *Water Resources Research*, *53*(8), 7332–7348. https://doi.org/10.1002/2016WR019916

Entekhabi, B. D., Njoku, E. G., Neill, P. E. O., Kellogg, K. H., Crow, W. T., Edelstein, W. N., et al. (2015). (SMAP) Mission, *98*(5).

Erban, L. E., & Gorelick, S. M. (2016). Closing the irrigation deficit in Cambodia: Implications for transboundary impacts on groundwater and Mekong River flow. *Journal of Hydrology*, *535*, 85–92. https://doi.org/10.1016/j.jhydrol.2016.01.072

Erban, L. E., Gorelick, S. M., & Zebker, H. A. (2014). Groundwater extraction, land subsidence, and sea-level rise in the Mekong Delta, Vietnam. *Environmental Research Letters*, *9*(8). https://doi.org/10.1088/1748-9326/9/8/084010

Evans, T. B., White, S. M., & Wilson, A. M. (2020). Coastal Groundwater Flow at the Nearshore and Embayment Scales: A Field and Modeling Study. *Water Resources Research*, *56*(10), 1–15. https://doi.org/10.1029/2019WR026445

Fan, H., & He, D. (2015). Temperature and precipitation variability and its effects on streamflow in the upstream regions of the Lancang-Mekong and Nu-Salween Rivers. *Journal of Hydrometeorology*, *16*(5), 2248–2263. https://doi.org/10.1175/JHM-D-14-0238.1

Fan, X., & Luo, X. (2019). Precipitation and flow variations in the Lancang-Mekong River Basin and the implications of monsoon fluctuation and regional topography. *Water (Switzerland)*, *11*(10). https://doi.org/10.3390/w11102086

Fan, Y., & Schaller, M. F. (2009). River basins as groundwater exporters and importers: Implications for water cycle and climate modeling. *Journal of Geophysical Research Atmospheres*, *114*(4). https://doi.org/10.1029/2008JD010636

Fan, Y., Clark, M., Lawrence, D. M., Swenson, S., Band, L. E., Brantley, S. L., et al. (2019). Hillslope Hydrology in Global Change Research and Earth System Modeling. *Water Resources Research*, 1737–1772. https://doi.org/10.1029/2018WR023903

Fan, Y, & Li, H. (2013). Global Patterns of Groundwater, *13626*(February), 940–944.

Fan, Ying, Miguez-Macho, G., Weaver, C. P., Walko, R., & Robock, A. (2007). Incorporating water table dynamics in climate modeling: 1. Water table observations and equilibrium water table simulations. *Journal of Geophysical Research Atmospheres*, *112*(10), 1–17. https://doi.org/10.1029/2006JD008111

Faridzad, M., Yang, T., Hsu, K., Sorooshian, S., & Xiao, C. (2018). Rainfall frequency analysis for ungauged regions using remotely sensed precipitation information. *Journal of Hydrology*, *563*(January), 123–142. https://doi.org/10.1016/j.jhydrol.2018.05.071

Fekete, B. M., Vörösmarty, C. J., Roads, J. O., & Willmott, C. J. (2004). Uncertainties in precipitation and their impacts on runoff estimates. *Journal of Climate*, *17*(2), 294–304. https://doi.org/10.1175/1520-0442(2004)017<0294:UIPATI>2.0.CO;2

Felfelani, F., Wada, Y., Longuevergne, L., & Pokhrel, Y. N. (2017a). Natural and human-induced terrestrial water storage change: A global analysis using hydrological models and GRACE. *Journal of Hydrology*, *553*, 105–118. https://doi.org/10.1016/j.jhydrol.2017.07.048

Felfelani, F., Wada, Y., Longuevergne, L., & Pokhrel, Y. N. (2017b). Natural and human-induced terrestrial water storage change: A global analysis using hydrological models and GRACE. *Journal of Hydrology*, *553*, 105–118. https://doi.org/10.1016/j.jhydrol.2017.07.048

Felfelani, F., Pokhrel, Y., Guan, K., & Lawrence, D. M. (2018). Utilizing SMAP Soil Moisture Data to Constrain Irrigation in the Community Land Model. *Geophysical Research Letters*, *45*(23), 12,892-12,902. https://doi.org/10.1029/2018GL080870

Felfelani, F., Lawrence, D. M., & Pokhrel, Y. (2021). Representing Intercell Lateral Groundwater Flow and Aquifer Pumping in the Community Land Model. *Water Resources Research*, *57*(1), 1–24. https://doi.org/10.1029/2020WR027531

Fenicia, F., Savenije, H. H. G., Matgen, P., & Pfister, L. (2006). Is the groundwater reservoir linear? Learning from data in hydrological modelling. *Hydrology and Earth System Sciences*, *10*(1), 139–150. https://doi.org/10.5194/hess-10-139-2006

Fenicia, Fabrizio, Kavetski, D., & Savenije, H. H. G. (2011). Elements of a flexible approach for conceptual hydrological modeling : 1 . Motivation and theoretical development, *47*, 1–13. https://doi.org/10.1029/2010WR010174

Ferguson, I. M., & Maxwell, R. M. (2010). Role of groundwater in watershed response and land surface feedbacks under climate change. *Water Resources Research*, *46*(8), 1–15. https://doi.org/10.1029/2009WR008616

Fisher, R. A., & Koven, C. D. (2020). Perspectives on the Future of Land Surface Models and the Challenges of Representing Complex Terrestrial Systems. *Journal of Advances in Modeling Earth Systems*, *12*(4). https://doi.org/10.1029/2018MS001453

Galelli, S., Dang, T. D., Ng, J. Y., Chowdhury, A. F. M. K., & Arias, M. E. (2022).

Opportunities to curb hydrological alterations via dam re-operation in the Mekong. *Nature Sustainability*. https://doi.org/10.1038/s41893-022-00971-z

Geruo, A., Velicogna, I., Kimball, J. S., Du, J., Kim, Y., Colliander, A., & Njoku, E. (2017). Satellite-observed changes in vegetation sensitivities to surface soil moisture and total water storage variations since the 2011 Texas drought. *Environmental Research Letters*, *12*(5). https://doi.org/10.1088/1748-9326/aa6965

Gleeson, T., Wada, Y., Bierkens, M. F. P., & Van Beek, L. P. H. (2012). Water balance of global aquifers revealed by groundwater footprint. *Nature*, *488*(7410), 197–200. https://doi.org/10.1038/nature11295

Gleeson, T., Befus, K. M., Jasechko, S., Luijendijk, E., & Cardenas, M. B. (2016). The global volume and distribution of modern groundwater. *Nature Geoscience*, *9*(2), 161–164. https://doi.org/10.1038/ngeo2590

Gleick, P. H. (2018). *The World's Water Volume 9 - The report on freshwater resources*.

De Graaf, I. E.M., van Beek, L. P. H., Wada, Y., & Bierkens, M. F. P. (2014). Dynamic attribution of global water demand to surface water and groundwater resources: Effects of abstractions and return flows on river discharges. *Advances in Water Resources*, *64*, 21–33. https://doi.org/10.1016/j.advwatres.2013.12.002

De Graaf, I. E.M., Sutanudjaja, E. H., Van Beek, L. P. H., & Bierkens, M. F. P. (2015). A high-resolution global-scale groundwater model. *Hydrology and Earth System Sciences*, *19*(2), 823–837. https://doi.org/10.5194/hess-19-823-2015

de Graaf, Inge E.M., van Beek, R. L. P. H., Gleeson, T., Moosdorf, N., Schmitz, O., Sutanudjaja, E. H., & Bierkens, M. F. P. (2017). A global-scale two-layer transient groundwater model: Development and application to groundwater depletion. *Advances in Water Resources*, *102*, 53–67. https://doi.org/10.1016/j.advwatres.2017.01.011

de Graaf, Inge E.M., Gleeson, T., (Rens) van Beek, L. P. H., Sutanudjaja, E. H., & Bierkens, M. F. P. (2019). Environmental flow limits to global groundwater pumping. *Nature*, *574*(7776), 90–94. https://doi.org/10.1038/s41586-019-1594-4

De Graaf, Inge E.M., & Stahl, K. (2022). A model comparison assessing the importance of lateral groundwater flows at the global scale. *Environmental Research Letters*, *17*(4). https://doi.org/10.1088/1748-9326/ac50d2

Gunnink, J., Pham, H. Van, Oude Essink, G., & Bierkens, M. (2021). The 3D groundwater salinity distribution and fresh groundwater volumes in the Mekong Delta, Vietnam, inferred from geostatistical analyses. *Earth System Science Data Discussions*, *4441776*, 1–31. https://doi.org/10.5194/essd-2021-15

Gupta, H. V., Kling, H., Yilmaz, K. K., & Martinez, G. F. (2009). Decomposition of the mean squared error and NSE performance criteria: Implications for improving hydrological modelling. *Journal of Hydrology*, *377*(1–2), 80–91.

https://doi.org/10.1016/j.jhydrol.2009.08.003

Guy Davidesko1,2, Amir Sagy1, and Y. H. H. (2014). Geophysical Research Letters. *Geophysical Prospecting*, (April), 6298–6305. https://doi.org/10.1002/2014GL059323.Received

Haddeland, I., Lettenmaier, D. P., & Skaugen, T. (2006). Effects of irrigation on the water and energy balances of the Colorado and Mekong river basins. *Journal of Hydrology*, *324*(1–4), 210–223. https://doi.org/10.1016/j.jhydrol.2005.09.028

Haddeland, I., Clark, D. B., Franssen, W., Ludwig, F., Voß, F., Arnell, N. W., Bertrand, N., Best, M., Folwell, S., Gerten, D., Gomes, S., Gosling, S. N., Hagemann, S., Hanasaki, N., Harding, R., Heinke, J., Kabat, P., Koirala, S., Oki, T., Polcher, J., Stacke, T., Viterbo, P., Weedon, G. P., & and Pat Yeh. (2011). Multimodel Estimate of the Global Terrestrial Water Balance : Setup and First Results, 869–884. https://doi.org/10.1175/2011JHM1324.1

Haddeland, I., Clark, D. B., Franssen, W., Ludwig, F., Voß, F., Arnell, N. W., Bertrand, N., Best, M., Folwell, S., Gerten, D., Gomes, S., Gosling, S. N., Hagemann, S., Hanasaki, N., Harding, R., Heinke, J., Kabat, P., Koirala, S., Oki, T., Polcher, J., Stacke, T., Viterbo, P., Weedon, G. P., & Yeh, P. (2011). Multimodel estimate of the global terrestrial water balance: Setup and first results. *Journal of Hydrometeorology*, *12*(5), 869–884. https://doi.org/10.1175/2011JHM1324.1

Hamza, A., Anjum, M. N., Jehanzeb, M., Cheema, M., Chen, X., Afzal, A., et al. (2020). Precipitation Products over the Hindu Kush, (4).

Han, Zhiming, Huang, S., Huang, Q., Bai, Q., Leng, G., Wang, H., et al. (2020). Effects of vegetation restoration on groundwater drought in the Loess Plateau, China. *Journal of Hydrology*, *591*(July), 125566. https://doi.org/10.1016/j.jhydrol.2020.125566

Han, Zhongying, Long, D., Fang, Y., Hou, A., & Hong, Y. (2019a). Impacts of climate change and human activities on the fl ow regime of the dammed Lancang River in Southwest China. *Journal of Hydrology*, *570*(January), 96–105. https://doi.org/10.1016/j.jhydrol.2018.12.048

Han, Zhongying, Long, D., Fang, Y., Hou, A., & Hong, Y. (2019b). Impacts of climate change and human activities on the flow regime of the dammed Lancang River in Southwest China. *Journal of Hydrology*, *570*(December 2018), 96–105. https://doi.org/10.1016/j.jhydrol.2018.12.048

Hanasaki, N., Fujimori, S., Yamamoto, T., Yoshikawa, S., Masaki, Y., Hijioka, Y., et al. (2013). A global water scarcity assessment under Shared Socio-economic Pathways - Part 1: Water use. *Hydrology and Earth System Sciences*, *17*(7), 2375–2391. https://doi.org/10.5194/hess-17-2375-2013

Hanasaki, Naota, Yoshikawa, S., Pokhrel, Y., & Kanae, S. (2017). A global hydrological simulation to specify the sources of water used by humans. *Hydrology and Earth System Sciences Discussions*, *08*, 1–53. https://doi.org/10.5194/hess-2017-280

Hao, Z., & AghaKouchak, A. (2013). Multivariate Standardized Drought Index: A parametric multi-index model. *Advances in Water Resources*, *57*, 12–18. https://doi.org/10.1016/j.advwatres.2013.03.009

Hecht, J. S., Lacombe, G., Arias, M. E., Dang, T. D., & Piman, T. (2019). Hydropower dams of the Mekong River basin: A review of their hydrological impacts. *Journal of Hydrology*, *568*(October 2018), 285–300. https://doi.org/10.1016/j.jhydrol.2018.10.045

Hoang, L. P., van Vliet, M. T. H., Kummu, M., Lauri, H., Koponen, J., Supit, I., et al. (2019). The Mekong's future flows under multiple drivers: How climate change, hydropower developments and irrigation expansions drive hydrological changes. *Science of the Total Environment*, *649*, 601–609. https://doi.org/10.1016/j.scitotenv.2018.08.160

Hoanh, C. T., Facon, T., Thuon, T., Bastakoti, R. C., Molle, F., & Phengphaengsy, F. (2012). Irrigation in the lower mekong basin countries: The beginning of a new era? *Contested Waterscapes in the Mekong Region: Hydropower, Livelihoods and Governance*, *9781849770*, 143–172. https://doi.org/10.4324/9781849770866

Hoanh, C. T., Suhardiman, D., & Anh, L. T. (2014). Irrigation development in the Vietnamese Mekong Delta: Towards polycentric water governance? *International Journal of Water Governance*, *2*(2), 61–82. https://doi.org/10.7564/14-ijwg59

Huang, S., Kumar, R., Flörke, M., Yang, T., Hundecha, Y., Kraft, P., et al. (2017). Evaluation of an ensemble of regional hydrological models in 12 large-scale river basins worldwide, 381–397. https://doi.org/10.1007/s10584-016-1841-8

Hung, N. N., Delgado, J. M., Tri, V. K., Hung, L. M., Merz, B., Bárdossy, A., & Apel, H. (2012). Floodplain hydrology of the mekong delta, Vietnam. *Hydrological Processes*, *26*(5), 674–686. https://doi.org/10.1002/hyp.8183

Iui, I., & Yang, L. (1991). Intercomparison of Land-surface Parameterization Schemes s °, 1335–1350.

Jasechko, S., Jean, B. S., Gleeson, T., Wada, Y., Fawcett, P. J., Sharp, 1, Z. D., et al. (2014). The pronounced seasonality of global groundwater recharge, 5375–5377. https://doi.org/10.1002/2013WR014979.Reply

Jayakumar, R., & Lee, E. (2017). Climate change and groundwater conditions in the Mekong Region-A review. *Journal of Groundwater Science and Engineering*, *5*(1), 14–30.

Jiang, J., & Zhou, T. (2023). Agricultural drought over water-scarce Central Asia aggravated by internal climate variability. *Nature Geoscience*, *16*(February). https://doi.org/10.1038/s41561-022-01111-0

Jiao, T., Williams, C. A., De Kauwe, M. G., Schwalm, C. R., & Medlyn, B. E. (2021). Patterns of post-drought recovery are strongly influenced by drought duration, frequency, post-drought wetness, and bioclimatic setting. *Global Change Biology*, *27*(19), 4630–4643. https://doi.org/10.1111/gcb.15788

Johnston, R., & Kummu, M. (2012). Water Resource Models in the Mekong Basin: A Review. *Water Resources Management*, *26*(2), 429–455. https://doi.org/10.1007/s11269-011-9925-8

Júnior, J. L. S., Tomasella, J., & Rodriguez, D. A. (2015). Impacts of future climatic and land cover changes on the hydrological regime of the Madeira River basin. *Climatic Change*, *129*(1–2), 117–129. https://doi.org/10.1007/s10584-015-1338-x

Kabir, T., Pokhrel, Y., & Felfelani, F. (2022). On the Precipitation-Induced Uncertainties in Process-Based Hydrological Modeling in the Mekong River Basin. *Water Resources Research*, *58*(2). https://doi.org/10.1029/2021WR030828

Kazama, S., Hagiwara, T., Ranjan, P., & Sawamoto, M. (2007). Evaluation of groundwater resources in wide inundation areas of the Mekong River basin. *Journal of Hydrology*, *340*(3–4), 233–243. https://doi.org/10.1016/j.jhydrol.2007.04.017

Kennedy, D., Swenson, S., Oleson, K. W., Lawrence, D. M., Fisher, R., Carlos, A., & Gentine, P. (2019). Implementing Plant Hydraulics in the Community Land Model , Version 5 Journal of Advances in Modeling Earth Systems. https://doi.org/10.1029/2018MS001500

Kite, G. (2001). Modelling the mekong: Hydrological simulation for environmental impact studies. *Journal of Hydrology*, *253*(1–4), 1–13. https://doi.org/10.1016/S0022-1694(01)00396-1

Kling, H., Fuchs, M., & Paulin, M. (2012). Runoff conditions in the upper Danube basin under an ensemble of climate change scenarios. *Journal of Hydrology*, *424–425*, 264–277. https://doi.org/10.1016/j.jhydrol.2012.01.011

Kluzek, E. (2013). CESM Research Tools : CLM4 in Documentation.

Knoben, W. J. M., Freer, J. E., & Woods, R. A. (2019). Technical note: Inherent benchmark or not? Comparing Nash-Sutcliffe and Kling-Gupta efficiency scores. *Hydrology and Earth System Sciences*, *23*(10), 4323–4331. https://doi.org/10.5194/hess-23-4323-2019

Koch, J., Zhang, W., Martinsen, G., He, X., & Stisen, S. (2020). Estimating Net Irrigation Across the North China Plain Through Dual Modeling of Evapotranspiration. *Water Resources Research*, *56*(12). https://doi.org/10.1029/2020WR027413

Koirala, S., Yeh, P. J. F., Hirabayashi, Y., Kanae, S., & Oki, T. (2014). Global-scale land surface hydrologic modeling with the representation of water table dynamics. *Journal of Geophysical Research*, *119*(1), 75–89. https://doi.org/10.1002/2013JD020398

Koirala, S., Kim, H., Hirabayashi, Y., Kanae, S., & Oki, T. (2019). Sensitivity of Global Hydrological Simulations to Groundwater Capillary Flux Parameterizations. *Water Resources Research*, *55*(1), 402–425. https://doi.org/10.1029/2018WR023434

Kollet, S. J., & Maxwell, R. M. (2008). Capturing the influence of groundwater dynamics on land surface processes using an integrated, distributed watershed model. *Water Resources Research*, *44*(2), 1–18. https://doi.org/10.1029/2007WR006004

Krakauer, N. Y., Li, H., & Fan, Y. (2014). Groundwater flow across spatial scales: Importance for climate modeling. *Environmental Research Letters*, *9*(3). https://doi.org/10.1088/1748-9326/9/3/034003

Kumar, P., Zhang, Y., Ma, N., Mishra, A., & Panigrahy, N. (2021). Selecting hydrological models for developing countries : Perspective of global , continental , and country scale models over catchment scale models. *Journal of Hydrology*, *600*(April), 126561. https://doi.org/10.1016/j.jhydrol.2021.126561

Kumar, S. V., Peters-Lidard, C. D., Tian, Y., Houser, P. R., Geiger, J., Olden, S., et al. (2006). Land information system: An interoperable framework for high resolution land surface modeling. *Environmental Modelling and Software*, *21*(10), 1402–1415. https://doi.org/10.1016/j.envsoft.2005.07.004

Kumarasamy, K., & Belmont, P. (2018). Calibration parameter selection and watershed hydrology model evaluation in time and frequency domains. *Water (Switzerland)*, *10*(6). https://doi.org/10.3390/w10060710

Kummu, M., & Sarkkula, J. (2008). Impact of the Mekong River flow alteration on the Tonle Sap flood pulse. *Ambio*, *37*(3), 185–192. https://doi.org/10.1579/0044-7447(2008)37[185:IOTMRF]2.0.CO;2

Kuppel, S., Tetzlaff, D., Maneta, M. P., & Soulsby, C. (2018). What can we learn from multi-data calibration of a process-based ecohydrological model? *Environmental Modelling and Software*, *101*, 301–316. https://doi.org/10.1016/j.envsoft.2018.01.001

Lacombe, G., Douangsavanh, S., Baker, J., Hoanh, C. T., Bartlett, R., Jeuland, M., & Phongpachith, C. (2014). Are hydropower and irrigation development complements or substitutes? The example of the Nam Ngum River in the Mekong Basin. *Water International*, *39*(5), 649–670. https://doi.org/10.1080/02508060.2014.956205

Lacombe, Guillaume, Douangsavanh, S., Vongphachanh, S., & Pavelic, P. (2017). Regional assessment of groundwater recharge in the lower mekong basin. *Hydrology*, *4*(4), 1–18. https://doi.org/10.3390/hydrology4040060

Landerer, F. W., & Swenson, S. C. (2012). Accuracy of scaled GRACE terrestrial water storage estimates. *Water Resources Research*, *48*(4), 1–11. https://doi.org/10.1029/2011WR011453

Lauri, H., De Moel, H., Ward, P. J., Räsänen, T. A., Keskinen, M., & Kummu, M. (2012). Hydrology and Earth System Sciences Future changes in Mekong River hydrology: impact of climate change and reservoir operation on discharge. *Hydrol. Earth Syst. Sci*, *16*, 4603–4619. https://doi.org/10.5194/hess-16-4603-2012

Lauri, H., Räsänen, T. A., & Kummu, M. (2014). Using Reanalysis and Remotely Sensed Temperature and Precipitation Data for Hydrological Modeling in Monsoon Climate: Mekong River Case Study. *Journal of Hydrometeorology*, *15*(4), 1532–1545. https://doi.org/10.1175/jhm-d-13-084.1

Lawrence, D. M., & Slater, Æ. A. G. (2008). Incorporating organic soil into a global climate model, (May 2007), 145–160. https://doi.org/10.1007/s00382-007-0278-1

Lawrence, D. M., Oleson, K. W., Flanner, M. G., Thornton, P. E., Swenson, S. C., Lawrence, P. J., et al. (2011). Parameterization improvements and functional and structural advances in Version 4 of the Community Land Model. *Journal of Advances in Modeling Earth Systems*, *3*(3), 1–27. https://doi.org/10.1029/2011ms000045

Lawrence, D. M., Hurtt, G. C., Arneth, A., Brovkin, V., Calvin, K. V., Jones, A. D., et al. (2016). The Land Use Model Intercomparison Project (LUMIP) contribution to CMIP6: Rationale and experimental design. *Geoscientific Model Development*, *9*(9), 2973–2998. https://doi.org/10.5194/gmd-9-2973-2016

Lawrence, D. M., Fisher, R. A., Koven, C. D., Oleson, K. W., Swenson, S. C., Bonan, G., et al. (2019). The Community Land Model Version 5 : Description of New Features , Benchmarking , and Impact of Forcing Uncertainty Journal of Advances in Modeling Earth Systems, *5*, 4245–4287. https://doi.org/10.1029/2018MS001583

Lawrence, D. M., Fisher, R. A., Koven, C. D., Oleson, K. W., Swenson, S. C., Bonan, G., et al. (2019a). The Community Land Model Version 5: Description of New Features, Benchmarking, and Impact of Forcing Uncertainty. *Journal of Advances in Modeling Earth Systems*, *11*(12), 4245–4287. https://doi.org/10.1029/2018MS001583

Lawrence, D. M., Fisher, R. A., Koven, C. D., Oleson, K. W., Swenson, S. C., Bonan, G., et al. (2019b). The Community Land Model Version 5: Description of New Features, Benchmarking, and Impact of Forcing Uncertainty. *Journal of Advances in Modeling Earth Systems*, *11*(12), 4245–4287. https://doi.org/10.1029/2018MS001583

Lawrence, P. J., Feddema, J. J., Bonan, G. B., Meehl, G. A., O'Neill, B. C., Oleson, K. W., et al. (2012). Simulating the biogeochemical and biogeophysical impacts of transient land cover change and wood harvest in the Community Climate System Model (CCSM4) from 1850 to 2100. *Journal of Climate*, *25*(9), 3071–3095. https://doi.org/10.1175/JCLI-D-11-00256.1

Lee, E., Ha, K., Thi Minh Ngoc, N., Surinkum, A., Jayakumar, R., Kim, Y., & Bin Hassan, K. (2017). Groundwater status and associated issues in the Mekong-Lancang River Basin: International collaborations to achieve sustainable groundwater resources. *Journal of Groundwater Science and Engineering*, *5*(1), 1–13.

Leng, G., Huang, M., Tang, Q., Sacks, W. J., Lei, H., & Leung, L. R. (2013). Modeling the effects of irrigation on land surface fluxes and states over the conterminous United States: Sensitivity to input data and model parameters. *Journal of Geophysical Research Atmospheres*, *118*(17), 9789–9803. https://doi.org/10.1002/jgrd.50792

Leng, G., Huang, M., Tang, Q., Gao, H., & Leung, L. R. (2014). Modeling the effects of groundwater-fed irrigation on terrestrial hydrology over the conterminous United States. *Journal of Hydrometeorology*, *15*(3), 957–972. https://doi.org/10.1175/JHM-D-13-049.1

Li, D., Long, D., Zhao, J., Lu, H., & Hong, Y. (2017). Observed changes in flow regimes in the

Mekong River basin. *Journal of Hydrology*, *551*, 217–232. https://doi.org/10.1016/j.jhydrol.2017.05.061

Li, H. Y., Leung, L. R., Getirana, A., Huang, M., Wu, H., Xu, Y., et al. (2015). Evaluating global streamflow simulations by a physically based routing model coupled with the community land model. *Journal of Hydrometeorology*, *16*(2), 948–971. https://doi.org/10.1175/JHM-D-14-0079.1

Li, Yang, Zhang, W., Schwalm, C. R., Gentine, P., Smith, W. K., Ciais, P., et al. (2023). Widespread spring phenology effects on drought recovery of Northern Hemisphere ecosystems. *Nature Climate Change*, *13*(February). https://doi.org/10.1038/s41558-022-01584-2

Li, Yishan, Wang, W., Lu, H., Khem, S., Yang, K., & Huang, X. (2019). Evaluation of three satellite-based precipitation products over the lower mekong river basin using rain gauge observations and hydrological modeling. *IEEE Journal of Selected Topics in Applied Earth Observations and Remote Sensing*, *12*(7), 2357–2373. https://doi.org/10.1109/JSTARS.2019.2915840

Liang, X., Xie, Z., & Huang, M. (2003). A new parameterization for surface and groundwater interactions and its impact on water budgets with the variable infiltration capacity (VIC) land surface model. *Journal of Geophysical Research: Atmospheres*, *108*(16). https://doi.org/10.1029/2002jd003090

Liu, L., Gudmundsson, L., Hauser, M., Qin, D., Li, S., & Seneviratne, S. I. (2019). Revisiting assessments of ecosystem drought recovery. *Environmental Research Letters*, *14*(11). https://doi.org/10.1088/1748-9326/ab4c61

Liu, Y., Hejazi, M., Kyle, P., Kim, S. H., Davies, E., Miralles, D. G., et al. (2016). Global and regional evaluation of energy for water. *Environmental Science and Technology*, *50*(17), 9736–9745. https://doi.org/10.1021/acs.est.6b01065

Loc, H. H., Van Binh, D., Park, E., Shrestha, S., Dung, T. D., Son, V. H., et al. (2021). Intensifying saline water intrusion and drought in the Mekong Delta: From physical evidence to policy outlooks. *Science of the Total Environment*, *757*, 143919. https://doi.org/10.1016/j.scitotenv.2020.143919

Long, D., Scanlon, B. R., Longuevergne, L., Sun, A. Y., Fernando, D. N., & Save, H. (2013). GRACE satellite monitoring of large depletion in water storage in response to the 2011 drought in Texas. *Geophysical Research Letters*, *40*(13), 3395–3401. https://doi.org/10.1002/grl.50655

Van Loon, A F, Tijdeman, E., Wanders, N., Lanen, H. A. J. Van, Teuling, A. J., & Uijlenhoet, R. (2014). How climate seasonality modifies drought duration and deficit. *Journal of Geophysical Research*, *175*(4449), 238. https://doi.org/10.1038/175238c0

Van Loon, Anne F. (2015). Hydrological drought explained. *Wiley Interdisciplinary Reviews: Water*, *2*(4), 359–392. https://doi.org/10.1002/WAT2.1085

Van Loon, Anne F., Gleeson, T., Clark, J., Van Dijk, A. I. J. M., Stahl, K., Hannaford, J., et al. (2016). Drought in the Anthropocene. *Nature Geoscience*, *9*(2), 89–91. https://doi.org/10.1038/ngeo2646

Luo, Q., Wen, J., Hu, Z., Lu, Y., & Yang, X. (2020). Parameter Sensitivities of the Community Land Model at Two Alpine Sites in the Three-River Source Region. *Journal of Meteorological Research*, *34*(4), 851–864. https://doi.org/10.1007/s13351-020-9205-8

Luo, X., Wu, W., He, D., Li, Y., & Ji, X. (2019). Hydrological Simulation Using TRMM and CHIRPS Precipitation Estimates in the Lower Lancang-Mekong River Basin. *Chinese Geographical Science*, *29*(1), 13–25. https://doi.org/10.1007/s11769-019-1014-6

Ma, C., Li, X., Wei, L., & Wang, W. (2017). Multi-scale validation of SMAP soil moisture products over cold and arid regions in Northwestern China using distributed ground observation data. *Remote Sensing*, *9*(4). https://doi.org/10.3390/rs9040327

Maxwell, R. M., Condon, L. E., & Kollet, S. J. (2015). A high-resolution simulation of groundwater and surface water over most of the continental US with the integrated hydrologic model ParFlow v3. *Geoscientific Model Development*, *8*(3), 923–937. https://doi.org/10.5194/gmd-8-923-2015

Maxwell, Reed M., & Kollet, S. J. (2008). Interdependence of groundwater dynamics and land-energy feedbacks under climate change. *Nature Geoscience*, *1*(10), 665–669. https://doi.org/10.1038/ngeo315

Mcguire, K. J., & Mcdonnell, J. J. (2010). Hydrological connectivity of hillslopes and streams : Characteristic time scales and nonlinearities, *46*, 1–17. https://doi.org/10.1029/2010WR009341

Megdal, S. B., Gerlak, A. K., Varady, R. G., & Huang, L. Y. (2015). Groundwater Governance in the United States: Common Priorities and Challenges. *Groundwater*, *53*(5), 677–684. https://doi.org/10.1111/gwat.12294

Merz, R., Parajka, J., & Blöschl, G. (2009). Scale effects in conceptual hydrological modeling. *Water Resources Research*, *45*(9), 1–15. https://doi.org/10.1029/2009WR007872

Miguez-Macho, G., & Fan, Y. (2012a). The role of groundwater in the Amazon water cycle: 1. Influence on seasonal streamflow, flooding and wetlands. *Journal of Geophysical Research Atmospheres*, *117*(15), 1–30. https://doi.org/10.1029/2012JD017539

Miguez-Macho, G., & Fan, Y. (2012b). The role of groundwater in the Amazon water cycle: 2. Influence on seasonal soil moisture and evapotranspiration. *Journal of Geophysical Research Atmospheres*, *117*(15). https://doi.org/10.1029/2012JD017540

Minderhoud, P. S. J., Erkens, G., Pham, V. H., Bui, V. T., Erban, L., Kooi, H., & Stouthamer, E. (2017). Impacts of 25 years of groundwater extraction on subsidence in the Mekong delta, Vietnam. *Environmental Research Letters*, *12*(6). https://doi.org/10.1088/1748-9326/aa7146

Mizukami, N., Clark, M. P., Gharari, S., Kluzek, E., Pan, M., Lin, P., et al. (2021). A Vector-Based River Routing Model for Earth System Models: Parallelization and Global Applications. *Journal of Advances in Modeling Earth Systems*, *13*(6), 1–20. https://doi.org/10.1029/2020MS002434

Mondal, S., K. Mishra, A., Leung, R., & Cook, B. (2023). Global droughts connected by linkages between drought hubs. *Nature Communications*, *14*(1), 1–13. https://doi.org/10.1038/s41467-022-35531-8

Monteiro, J. A. F., Strauch, M., Srinivasan, R., Abbaspour, K., & Gücker, B. (2016). Accuracy of grid precipitation data for Brazil: Application in river discharge modelling of the Tocantins catchment. *Hydrological Processes*, *30*(9), 1419–1430. https://doi.org/10.1002/hyp.10708

Mousa, B. G., & Shu, H. (2020). Spatial Evaluation and Assimilation of SMAP, SMOS, and ASCAT Satellite Soil Moisture Products Over Africa Using Statistical Techniques. *Earth and Space Science*, *7*(1), 1–16. https://doi.org/10.1029/2019EA000841

MRC. (2005). Hydrology of the Mekong Basin, Mekong River Commission, Vientiane. *Mrc*, (November).

NCAR. (2019). CLM5 Documentation Release, 337.

Nguyen, D. C. H., Ascough, J. C., Maier, H. R., Dandy, G. C., & Andales, A. A. (2017). Optimization of irrigation scheduling using ant colony algorithms and an advanced cropping system model. *Environmental Modelling and Software*, *97*, 32–45. https://doi.org/10.1016/j.envsoft.2017.07.002

Nguyen, T. T. H., de Bie, C. A. J. M., Ali, A., Smaling, E. M. A., & Chu, T. H. (2012). Mapping the irrigated rice cropping patterns of the Mekong delta, Vietnam, through hyper-temporal spot NDVI image analysis. *International Journal of Remote Sensing*, *33*(2), 415–434. https://doi.org/10.1080/01431161.2010.532826

Nie, W., Zaitchik, B. F., Rodell, M., Kumar, S. V., Anderson, M. C., & Hain, C. (2018). Groundwater Withdrawals Under Drought: Reconciling GRACE and Land Surface Models in the United States High Plains Aquifer. *Water Resources Research*, *54*(8), 5282–5299. https://doi.org/10.1029/2017WR022178

Nie, W., Zaitchik, B. F., Rodell, M., Kumar, S. V., Arsenault, K. R., Li, B., & Getirana, A. (2019). Assimilating GRACE Into a Land Surface Model in the Presence of an Irrigation-Induced Groundwater Trend. *Water Resources Research*, *55*(12), 11274–11294. https://doi.org/10.1029/2019WR025363

Nie, W., Zaitchik, B. F., Rodell, M., Kumar, S. V., Arsenault, K. R., & Badr, H. S. (2021). Irrigation Water Demand Sensitivity to Climate Variability Across the Contiguous United States. *Water Resources Research*, *57*(3), 1–16. https://doi.org/10.1029/2020WR027738

Nie, W., Kumar, S. V., Arsenault, K. R., Peters-Lidard, C. D., Mladenova, I. E., Bergaoui, K., et al. (2022). Towards effective drought monitoring in the Middle East and North Africa (MENA) region: implications from assimilating leaf area index and soil moisture into the Noah-MP land surface model for Morocco. *Hydrology and Earth System Sciences*, *26*(9), 2365–2386. https://doi.org/10.5194/hess-26-2365-2022

Nilsson, C., Reidy, C. A., Dynesius, M., & Revenga, C. (2005). Fragmentation and flow regulation of the world's large river systems. *Science*, *308*(5720), 405–408. https://doi.org/10.1126/science.1107887

Niu, G. Y., Yang, Z. L., Dickinson, R. E., & Gulden, L. E. (2005). A simple TOPMODEL-based runoff parameterization (SIMTOP) for use in global climate models. *Journal of Geophysical Research Atmospheres*, *110*(21), 1–15. https://doi.org/10.1029/2005JD006111

Oleson, K., & Lawrence, D. (2013). NCAR / TN-503 + STR NCAR Technical Note July 2013 Technical Description of version 4 . 5 of the Community Land Model (CLM), (March 2014).

Oleson, K W, Niu, G., Yang, Z., Lawrence, D. M., Thornton, P. E., Lawrence, P. J., et al. (1978). Improvements to the Community Land Model and their impact on the hydrological cycle, *14*(4). https://doi.org/10.1029/2007JG000563

Oleson, Keith W., Lawrence, D. M., Bonan, G. B., Drewniak, B., Huang, M., Koven, C. D., et al. (2013). Technical Description of version 4.5 of the Community Land Model (CLM), (July), NCAR/TN-503+STR. Retrieved from http://www.cesm.ucar.edu/models/cesm1.2/clm/CLM45_Tech_Note.pdf

Ozdogan, Multu, Rodell, M., Beaudoing, H. K., & Toll, D. L. (2010). Simulating the Effects of Irrigation over the United States in a Land Surface Model Based on Satellite-Derived Agricultural Data, 171–184. https://doi.org/10.1175/2009JHM1116.1

Ozdogan, Mutlu, Yang, Y., Allez, G., & Cervantes, C. (2010). Remote sensing of irrigated agriculture: Opportunities and challenges. *Remote Sensing*, *2*(9), 2274–2304. https://doi.org/10.3390/rs2092274

Ozdogan, Mutlu, Rodell, M., Beaudoing, H. K., & Toll, D. L. (2010). Simulating the effects of irrigation over the united states in a land surface model based on satellite-derived agricultural data. *Journal of Hydrometeorology*, *11*(1), 171–184. https://doi.org/10.1175/2009JHM1116.1

Pande, S., Savenije, H. H. G., Bastidas, L. A., & Gosain, A. K. (2012). A Parsimonious Hydrological Model for a Data Scarce Dryland Region, 909–926. https://doi.org/10.1007/s11269-011-9816-z

Paniconi, & Putti, M. (2015). Physically based modeling in catchment hydrology at 50: Survey and outlook. *Journal of the American Water Resources Association*, (51). https://doi.org/doi:10.1002/ 2015WR017780

Pelletier, J. D., Dipankar, A., Stevens, B., Heinze, R., Moseley, C., Zängl, G., et al. (2016).

Journal of Advances in Modeling Earth Systems. *Journal of Advances in Modeling Earth Systems*, *6*, 963–986. https://doi.org/10.1002/2015MS000526.Received

Peterson, T. J., Saft, M., Peel, M. C., & John, A. (2021). Watersheds may not recover from drought. *Science*, *372*(6543), 745–749. https://doi.org/10.1126/science.abd5085

Petra, D., Schmied Hannes M€uller, S. C., T., P. F., & 2, E. A. (2014). Water Resources Research, 5375–5377. https://doi.org/10.1002/2013WR014979.Reply

Phi Hoang, L., Lauri, H., Kummu, M., Koponen, J., Vliet, M. T. H. V., Supit, I., et al. (2016). Mekong River flow and hydrological extremes under climate change. *Hydrology and Earth System Sciences*, *20*(7), 3027–3041. https://doi.org/10.5194/hess-20-3027-2016

Piman, T., Lennaerts, T., & Southalack, P. (2013). Assessment of hydrological changes in the lower mekong basin from basin-wide development scenarios. *Hydrological Processes*, *27*(15), 2115–2125. https://doi.org/10.1002/hyp.9764

Pinnington, E., Quaife, T., & Black, E. (2018). Impact of remotely sensed soil moisture and precipitation on soil moisture prediction in a data assimilation system with the JULES land surface model. *Hydrology and Earth System Sciences*, *22*(4), 2575–2588. https://doi.org/10.5194/hess-22-2575-2018

Pokhrel, Y., Hanasaki, N., Koirala, S., Cho, J., Yeh, P. J. F., Kim, H., et al. (2012). Incorporating anthropogenic water regulation modules into a land surface model. *Journal of Hydrometeorology*, *13*(1), 255–269. https://doi.org/10.1175/JHM-D-11-013.1

Pokhrel, Y., Koirala, S., Yeh, P. J.-F., Hanasaki, N., Longuevergne, L., Kanae, S., & Oki, T. (2014). Incorporation of groundwater pumping in a global Land Surface Model with the representation of human impacts, 5375–5377. https://doi.org/10.1002/2013WR014979.Reply

Pokhrel, Y., Burbano, M., Roush, J., Kang, H., Sridhar, V., & Hyndman, D. W. (2018). A review of the integrated effects of changing climate, land use, and dams on Mekong river hydrology. *Water (Switzerland)*, *10*(3), 1–25. https://doi.org/10.3390/w10030266

Pokhrel, Y., Shin, S., Lin, Z., Yamazaki, D., & Qi, J. (2018a). Potential Disruption of Flood Dynamics in the Lower Mekong River Basin Due to Upstream Flow Regulation. *Scientific Reports*, *8*(1), 1–13. https://doi.org/10.1038/s41598-018-35823-4

Pokhrel, Y., Shin, S., Lin, Z., Yamazaki, D., & Qi, J. (2018b). Potential Disruption of Flood Dynamics in the Lower Mekong River Basin Due to Upstream Flow Regulation. *Scientific Reports*, *8*(1), 1–13. https://doi.org/10.1038/s41598-018-35823-4

Pokhrel, Y., Felfelani, F., Satoh, Y., Boulange, J., Burek, P., Gädeke, A., et al. (2021). Global terrestrial water storage and drought severity under climate change. *Nature Climate Change*, *11*(3), 226–233. https://doi.org/10.1038/s41558-020-00972-w

Pokhrel, Y. N., Koirala, S., Yeh, P. J.-F., Hanasaki, N., Longuevergne, L., Kanae, S., & Oki, T.

(2014). Water Resources Research, 5375–5377. https://doi.org/10.1002/2013WR014979.Reply

Pokhrel, Yadu N., Fan, Y., Miguez-Macho, G., Yeh, P. J. F., & Han, S. C. (2013). The role of groundwater in the Amazon water cycle: 3. Influence on terrestrial water storage computations and comparison with GRACE. *Journal of Geophysical Research Atmospheres*, *118*(8), 3233–3244. https://doi.org/10.1002/jgrd.50335

Pokhrel, Yadu N., Fan, Y., & Miguez-Macho, G. (2014). Potential hydrologic changes in the Amazon by the end of the 21st century and the groundwater buffer. *Environmental Research Letters*, *9*(8). https://doi.org/10.1088/1748-9326/9/8/084004

Pokhrel, Yadu N., Koirala, S., Yeh, P. J.-F., Hanasaki, N., Longuevergne, L., Kanae, S., & Oki, T. (2014). Water Resources Research, 5375–5377. https://doi.org/10.1002/2013WR014979.Reply

Pokhrel, Yadu N., Koirala, S., Yeh, P. J. F., Hanasaki, N., Longuevergne, L., Kanae, S., & Oki, T. (2015). Incorporation of groundwater pumping in a global Land Surface Model with the representation of human impacts. *Water Resources Research*, *51*(1), 78–96. https://doi.org/10.1002/2014WR015602

Pokhrel, Yadu N., Hanasaki, N., Wada, Y., & Kim, H. (2016). Recent progresses in incorporating human land–water management into global land surface models toward their integration into Earth system models. *Wiley Interdisciplinary Reviews: Water*, *3*(4), 548–574. https://doi.org/10.1002/wat2.1150

Portmann, F. T., Siebert, S., & Döll, P. (2010). MIRCA2000-Global monthly irrigated and rainfed crop areas around the year 2000: A new high-resolution data set for agricultural and hydrological modeling. *Global Biogeochemical Cycles*, *24*(1), n/a-n/a. https://doi.org/10.1029/2008gb003435

Quichimbo, E. A., Singer, M. B., Michaelides, K., Hobley, D. E. J., & Rosolem, R. (2021). DRYP 1 . 0 : a parsimonious hydrological model of DRYland Partitioning of the water balance, 6893–6917.

Raimonet, M., Oudin, L., Thieu, V., Silvestre, M., Vautard, R., Rabouille, C., & Le Moigne, P. (2017). Evaluation of gridded meteorological datasets for hydrological modeling. *Journal of Hydrometeorology*, *18*(11), 3027–3041. https://doi.org/10.1175/JHM-D-17-0018.1

Räsänen, T. A., Koponen, J., Lauri, H., & Kummu, M. (2012). Downstream Hydrological Impacts of Hydropower Development in the Upper Mekong Basin. *Water Resources Management*, *26*(12), 3495–3513. https://doi.org/10.1007/s11269-012-0087-0

Räsänen, T. A., Someth, P., Lauri, H., Koponen, J., Sarkkula, J., & Kummu, M. (2017). Observed river discharge changes due to hydropower operations in the Upper Mekong Basin. *Journal of Hydrology*, *545*, 28–41. https://doi.org/10.1016/j.jhydrol.2016.12.023

Reinecke, R., Müller Schmied, H., Trautmann, T., Seaby Andersen, L., Burek, P., Flörke, M., et al. (2021). Uncertainty of simulated groundwater recharge at different global warming levels: A global-scale multi-model ensemble study. *Hydrology and Earth System Sciences*, *25*(2), 787–810. https://doi.org/10.5194/hess-25-787-2021

Rodell, M., Houser, P. R., Berg, A. A., & Famiglietti, J. S. (2005). Evaluation of 10 methods for initializing a land surface model. *Journal of Hydrometeorology*, *6*(2), 146–155. https://doi.org/10.1175/JHM414.1

Sakamoto, T., Van Phung, C., Kotera, A., Nguyen, K. D., & Yokozawa, M. (2009). Analysis of rapid expansion of inland aquaculture and triple rice-cropping areas in a coastal area of the Vietnamese Mekong Delta using MODIS time-series imagery. *Landscape and Urban Planning*, *92*(1), 34–46. https://doi.org/10.1016/j.landurbplan.2009.02.002

Samaniego, L., Kumar, R., & Zink, M. (2013). Implications of parameter uncertainty on soil moisture drought analysis in Germany. *Journal of Hydrometeorology*, *14*(1), 47–68. https://doi.org/10.1175/JHM-D-12-075.1

Save, H., Bettadpur, S., & Center, B. D. T. (2016). High-resolution CSR GRACE RL05 mascons. *AGU: Journal of Geophysical Research, Solid Earth*, *119*(iv), 3076–3095. https://doi.org/10.1002/2016JB013007.Received

Scanlon, B. R., Faunt, C. C., Longuevergne, L., Reedy, R. C., Alley, W. M., McGuire, V. L., & McMahon, P. B. (2012). Groundwater depletion and sustainability of irrigation in the US High Plains and Central Valley. *Proceedings of the National Academy of Sciences of the United States of America*, *109*(24), 9320–9325. https://doi.org/10.1073/pnas.1200311109

Scanlon, B. R., Zhang, Z., Save, H., Sun, A. Y., Schmied, H. M., Van Beek, L. P. H., et al. (2018). Global models underestimate large decadal declining and rising water storage trends relative to GRACE satellite data. *Proceedings of the National Academy of Sciences of the United States of America*, *115*(6), E1080–E1089. https://doi.org/10.1073/pnas.1704665115

Schilling, K. E., Jha, M. K., Zhang, Y. K., Gassman, P. W., & Wolter, C. F. (2008). Impact of land use and land cover change on the water balance of a large agricultural watershed: Historical effects and future directions. *Water Resources Research*, *45*(7), 1–12. https://doi.org/10.1029/2007WR006644

Schmied, H. M., Eisner, S., Franz, D., Wattenbach, M., Portmann, F. T., Flörke, M., & Döll, P. (2014). Sensitivity of simulated global-scale freshwater fluxes and storages to input data, hydrological model structure, human water use and calibration. *Hydrology and Earth System Sciences*, *18*(9), 3511–3538. https://doi.org/10.5194/hess-18-3511-2014

Schreiner-McGraw, A. P., & Ajami, H. (2020). Impact of Uncertainty in Precipitation Forcing Data Sets on the Hydrologic Budget of an Integrated Hydrologic Model in Mountainous Terrain. *Water Resources Research*, *56*(12), 1–21. https://doi.org/10.1029/2020WR027639

Schwalm, C. R., Anderegg, W. R. L., Michalak, A. M., Fisher, J. B., Biondi, F., Koch, G., et al. (2017). Global patterns of drought recovery. *Nature*, *548*(7666), 202–205. https://doi.org/10.1038/nature23021

Sheffield, J., & Wood, E. F. (2008). Projected changes in drought occurrence under future global warming from multi-model, multi-scenario, IPCC AR4 simulations. *Climate Dynamics*, *31*(1), 79–105. https://doi.org/10.1007/s00382-007-0340-z

Sheffield, J., Goteti, G., Wen, F., & Wood, E. F. (2004). A simulated soil moisture based drought analysis for the United States. *Journal of Geophysical Research D: Atmospheres*, *109*(24), 1–19. https://doi.org/10.1029/2004JD005182

Sheffield, J., Wood, E. F., & Roderick, M. L. (2012). Little change in global drought over the past 60 years. *Nature*, *491*(7424), 435–438. https://doi.org/10.1038/nature11575

Shiklomanov, I. A. (2000). Appraisal and Assessment of world water resources. *Water International*, *25*(1), 11–32. https://doi.org/10.1080/02508060008686794

Shin, S., Pokhrel, Y., & Miguez-Macho, G. (2019). High-Resolution Modeling of Reservoir Release and Storage Dynamics at the Continental Scale. *Water Resources Research*, *55*(1), 787–810. https://doi.org/10.1029/2018WR023025

Shin, S., Pokhrel, Y., Yamazaki, D., Huang, X., Torbick, N., Qi, J., et al. (2020). High Resolution Modeling of River-Floodplain-Reservoir Inundation Dynamics in the Mekong River Basin. *Water Resources Research*, *56*(5), 1–23. https://doi.org/10.1029/2019WR026449

Shrestha, B., Babel, M. S., Maskey, S., Van Griensven, A., Uhlenbrook, S., Green, A., & Akkharath, I. (2013). Impact of climate change on sediment yield in the Mekong River basin: A case study of the Nam Ou basin, Lao PDR. *Hydrology and Earth System Sciences*, *17*(1), 1–20. https://doi.org/10.5194/hess-17-1-2013

Shrestha, S., Bach, T. V., & Pandey, V. P. (2016). Climate change impacts on groundwater resources in Mekong Delta under representative concentration pathways (RCPs) scenarios. *Environmental Science and Policy*, *61*, 1–13. https://doi.org/10.1016/j.envsci.2016.03.010

Siebert, S., Kummu, M., Porkka, M., Döll, P., Ramankutty, N., & Scanlon, B. R. (2015). A global data set of the extent of irrigated land from 1900 to 2005. *Hydrology and Earth System Sciences*, *19*(3), 1521–1545. https://doi.org/10.5194/hess-19-1521-2015

Siebert, Stefan, & Döll, P. (2010). Quantifying blue and green virtual water contents in global crop production as well as potential production losses without irrigation. *Journal of Hydrology*, *384*(3–4), 198–217. https://doi.org/10.1016/j.jhydrol.2009.07.031

Singh, A., Reager, J. T., & Behrangi, A. (2021). Estimation of hydrological drought recovery based on precipitation and Gravity Recovery and Climate Experiment (GRACE) water storage deficit. *Hydrology and Earth System Sciences*, *25*(2), 511–526. https://doi.org/10.5194/hess-25-511-2021

Sivapalan, M., Jothityangkoon, C., & Menabde, M. (2002). Linearity and nonlinearity of basin response as a function of scale : Discussion of alternative definitions, *38*(2), 1–5.

Sok, T., Oeurng, C., Ich, I., Sauvage, S., & Sánchez-Pérez, J. M. (2020). Mekong River Basin Using SWAT Model, 1–25.

Sophocleous, M. (2002). Interactions between groundwater and surface water: The state of the science. *Hydrogeology Journal*, *10*(1), 52–67. https://doi.org/10.1007/s10040-001-0170-8

Sridhar, V., Kang, H., & Ali, S. A. (2019). Human-induced alterations to land use and climate and their responses for hydrology and water management in the Mekong River Basin. *Water (Switzerland)*, *11*(6). https://doi.org/10.3390/w11061307

Sun, C., Xiao, Z. N., & Nguyen, M. (2021). Projection on precipitation frequency of different intensities and precipitation amount in the Lancang-Mekong River basin in the 21st century. *Advances in Climate Change Research*, *12*(2), 162–171. https://doi.org/10.1016/j.accre.2021.03.001

Swenson, S. C., & Lawrence, D. M. (2015). A GRACE-based assessment of interannual groundwater dynamics in the Community Land Model. *Water Resources Research*, *51*(11), 8817–8833. https://doi.org/10.1002/2015WR017582

Swenson, Sean C., Clark, M., Fan, Y., Lawrence, D. M., & Perket, J. (2019). Representing Intrahillslope Lateral Subsurface Flow in the Community Land Model. *Journal of Advances in Modeling Earth Systems*, *11*(12), 4044–4065. https://doi.org/10.1029/2019MS001833

Tan, Z., Zhuang, Q., Walter Anthony, K., Wang, M., Larson, V. E., & Ghan, S. J. (2015). Journal of Advances in Modeling Earth Systems. *Journal of Advances in Modeling Earth Systems*, *6*, 513–526. https://doi.org/10.1002/2015MS000526.Received

Tang, G., Long, D., Hong, Y., Gao, J., & Wan, W. (2018). Documentation of multifactorial relationships between precipitation and topography of the Tibetan Plateau using spaceborne precipitation radars. *Remote Sensing of Environment*, *208*(March 2017), 82–96. https://doi.org/10.1016/j.rse.2018.02.007

Tang, X., Zhang, J., Gao, C., Ruben, G. B., & Wang, G. (2019). Assessing the uncertainties of four precipitation products for SWAT modeling in Mekong River Basin. *Remote Sensing*, *11*(3), 1–24. https://doi.org/10.3390/rs11030304

Tatsumi, K., & Yamashiki, Y. (2015). Effect of irrigation water withdrawals on water and energy balance in the Mekong River Basin using an improved VIC land surface model with fewer calibration parameters. *Agricultural Water Management*, *159*, 92–106. https://doi.org/10.1016/j.agwat.2015.05.011

Tegegne, G., Park, D. K., & Kim, Y. (2017). Journal of Hydrology : Regional Studies Comparison of hydrological models for the assessment of water resources in a data-scarce region , the Upper Blue Nile River Basin. *Journal of Hydrology: Regional Studies*, *14*(October), 49–66. https://doi.org/10.1016/j.ejrh.2017.10.002

Thompson, J. R., Green, A. J., Kingston, D. G., & Gosling, S. N. (2013). Assessment of uncertainty in river flow projections for the Mekong River using multiple GCMs and hydrological models. *Journal of Hydrology*, *486*, 1–30. https://doi.org/10.1016/j.jhydrol.2013.01.029

Thompson, J. R., Green, A. J., & Kingston, D. G. (2014). Potential evapotranspiration-related uncertainty in climate change impacts on river flow: An assessment for the Mekong River basin. *Journal of Hydrology*, *510*, 259–279. https://doi.org/10.1016/j.jhydrol.2013.12.010

Tian, W., Liu, X., Wang, K., Bai, P., Liang, K., & Liu, C. (2021). Evaluation of six precipitation products in the Mekong River Basin. *Atmospheric Research*, *255*(August 2020), 105539. https://doi.org/10.1016/j.atmosres.2021.105539

Tijerina, D., Condon, L., FitzGerald, K., Dugger, A., O'Neill, M. M., Sampson, K., et al. (2021). Continental Hydrologic Intercomparison Project (CHIP), Phase 1: A Large-Scale Hydrologic Model Comparison over the Continental United States. *Water Resources Research*, 1–27. https://doi.org/10.1029/2020wr028931

Tran, D. A., Tsujimura, M., Pham, H. V., Nguyen, T. V., Ho, L. H., Le Vo, P., et al. (2022). Intensified salinity intrusion in coastal aquifers due to groundwater overextraction: a case study in the Mekong Delta, Vietnam. *Environmental Science and Pollution Research*, *29*(6), 8996–9010. https://doi.org/10.1007/s11356-021-16282-3

Tu, T. A., Tweed, S., Dan, N. P., Descloitres, M., Quang, K. H., Nemery, J., et al. (2022a). Localized recharge processes in the NE Mekong Delta and implications for groundwater quality. *Science of the Total Environment*, *845*(June). https://doi.org/10.1016/j.scitotenv.2022.157118

Tu, T. A., Tweed, S., Dan, N. P., Descloitres, M., Quang, K. H., Nemery, J., et al. (2022b). Localized recharge processes in the NE Mekong Delta and implications for groundwater quality. *Science of the Total Environment*, *845*(March). https://doi.org/10.1016/j.scitotenv.2022.157118

Vanderkwaak, J. E., & Loague, K. (2001). model S •• dy Site = o • aho •, *37*(4), 999–1013.

Veldkamp, T. I. E., Zhao, F., Ward, P. J., De Moel, H., Aerts, J. C. J. H., Schmied, H. M., et al. (2018). Human impact parameterizations in global hydrological models improve estimates of monthly discharges and hydrological extremes: A multi-model validation study. *Environmental Research Letters*, *13*(5). https://doi.org/10.1088/1748-9326/aab96f

Wada, Y., Wisser, D., & Bierkens, M. F. P. (2014). Global modeling of withdrawal, allocation and consumptive use of surface water and groundwater resources. *Earth System Dynamics*, *5*(1), 15–40. https://doi.org/10.5194/esd-5-15-2014

Wada, Yoshihide, Van Beek, L. P. H., Van Kempen, C. M., Reckman, J. W. T. M., Vasak, S., & Bierkens, M. F. P. (2010). Global depletion of groundwater resources. *Geophysical Research Letters*, *37*(20), 1–5. https://doi.org/10.1029/2010GL044571

Wada, Yoshihide, Wisser, D., Eisner, S., Flörke, M., Gerten, D., Haddeland, I., et al. (2013). Multimodel projections and uncertainties of irrigation water demand under climate change.

Geophysical Research Letters, *40*(17), 4626–4632. https://doi.org/10.1002/grl.50686

Wada, Yoshihide, de Graaf, I. E. M. de G., & Beek, L. P. H. van. (2016). High-resolution modeling of human and climate impacts on global water resources. *Journal of Advances in Modeling Earth Systems*, *8*, 1180–1209. https://doi.org/10.1002/2015MS000618.Received

Wada, Yoshihide, Bierkens, M. F. P., De Roo, A., Dirmeyer, P. A., Famiglietti, J. S., Hanasaki, N., et al. (2017). Human-water interface in hydrological modelling: current status and future directions Human-water interface in hydrological modelling. *Hydrol. Earth Syst. Sci*, *21*, 4169–4193. https://doi.org/10.5194/hess-21-4169-2017

Wang, Wei, Lu, H., Yang, D., Sothea, K., Jiao, Y., Gao, B., et al. (2016). Modelling hydrologic processes in the Mekong River basin using a distributed model driven by satellite precipitation and rain gauge observations. *PLoS ONE*, *11*(3), 1–19. https://doi.org/10.1371/journal.pone.0152229

Wang, Wei, Lu, H., Ruby Leung, L., Li, H. Y., Zhao, J., Tian, F., et al. (2017). Dam Construction in Lancang-Mekong River Basin Could Mitigate Future Flood Risk From Warming-Induced Intensified Rainfall. *Geophysical Research Letters*, *44*(20), 10,378-10,386. https://doi.org/10.1002/2017GL075037

Wang, Wen, Ertsen, M. W., Svoboda, M. D., & Hafeez, M. (2016). Propagation of drought: From meteorological drought to agricultural and hydrological drought. *Advances in Meteorology*, *2016*(4). https://doi.org/10.1155/2016/6547209

Water Resources Research. (1969). *Journal of the American Water Resources Association*, *5*(3), 2–2. https://doi.org/10.1111/j.1752-1688.1969.tb04897.x

Watkins, M. M., Wiese, D. N., Yuan, D.-N., Carmen Boening, & Landerer, F. W. (2014). Improved methods for observing Earth's time variable mass distribution with GRACE using spherical cap mascons Michael. *AGU: Journal of Geophysical Research, Solid Earth*, *119*(iv), 3076–3095. https://doi.org/10.1002/2014JB011547.Received

Weedon, G. P., Balsamo, G., Bellouin, N., Gomes, S., Best, M. J., & Viterbo, P. (2014). Data methodology applied to ERA-Interim reanalysis data. *Water Resources Research*, *50*, 7505–7514. https://doi.org/10.1002/2014WR015638.Received

Wiese, D. N., Landerer, F. W., & Watkins, M. M. (2016). Water Resources Research Institute. *Wyo Univ Water Resour Res Inst Water Resour Ser*, (44), 7490–7502. https://doi.org/10.1002/2016WR019344.Received

Wu, J., Chen, X., Yao, H., Liu, Z., & Zhang, D. (2018). Hydrological Drought Instantaneous Propagation Speed Based on the Variable Motion Relationship of Speed-Time Process. *Water Resources Research*, *54*(11), 9549–9565. https://doi.org/10.1029/2018WR023120

Wu, J., Chen, X., Yu, Z., Yao, H., Li, W., & Zhang, D. (2019). Assessing the impact of human regulations on hydrological drought development and recovery based on a 'simulated-observed' comparison of the SWAT model. *Journal of Hydrology*, *577*(July), 123990.

https://doi.org/10.1016/j.jhydrol.2019.123990

Wu, J., Chen, X., Love, C. A., Yao, H., Chen, X., & AghaKouchak, A. (2020). Determination of water required to recover from hydrological drought: Perspective from drought propagation and non-standardized indices. *Journal of Hydrology*, *590*(January), 125227. https://doi.org/10.1016/j.jhydrol.2020.125227

Wu, W., Clark, J. S., & Vose, J. M. (2010). Assimilating multi-source uncertainties of a parsimonious conceptual hydrological model using hierarchical Bayesian modeling. *Journal of Hydrology*, *394*(3–4), 436–446. https://doi.org/10.1016/j.jhydrol.2010.09.017

Xue, Z., Liu, J. P., & Ge, Q. (2011). Changes in hydrology and sediment delivery of the Mekong River in the last 50 years: Connection to damming, monsoon, and ENSO. *Earth Surface Processes and Landforms*, *36*(3), 296–308. https://doi.org/10.1002/esp.2036

Yamazaki, D., Kanae, S., Kim, H., & Oki, T. (2011). A physically based description of floodplain inundation dynamics in a global river routing model. *Water Resources Research*, *47*(4), 1–21. https://doi.org/10.1029/2010WR009726

Yamazaki, D., Sato, T., Kanae, S., Hirabayashi, Y., & Bates, P. D. (2014). Geophysical Research Letters. *Geophysical Research Letters RESEARCH*, (April), 6413–6419. https://doi.org/10.1002/2014GL061184.Received

Yeh, P J F, & Eltahir, E. A. B. (2005). Representation of water table dynamics in a land surface scheme. Part I: Model development. *Journal of Climate*, *18*(12), 1861–1880.

Yeh, Pat J.F., & Eltahir, E. A. B. (2005). Representation of water table dynamics in a land surface scheme. Part II: Subgrid variability. *Journal of Climate*, *18*(12), 1881–1901. https://doi.org/10.1175/JCLI3331.1

Yin, J., Gentine, P., Slater, L., Gu, L., Pokhrel, Y., Hanasaki, N., et al. (2023). *Future socio-ecosystem productivity threatened by compound drought–heatwave events*. *Nature Sustainability*. Springer US. https://doi.org/10.1038/s41893-022-01024-1

Yuan, E., Nie, W., & Sanders, E. (2014). Problems and prospects of SWAT model application on an arid/semi-arid watershed in Arizona. *SEDHYD 2014 Joint Conference*.

Yun, X., Tang, Q., Wang, J., Liu, X., Zhang, Y., Lu, H., et al. (2020). Impacts of climate change and reservoir operation on streamflow and flood characteristics in the Lancang-Mekong River Basin. *Journal of Hydrology*, *590*(June), 125472. https://doi.org/10.1016/j.jhydrol.2020.125472

Yun, X., Tang, Q., Li, J., Lu, H., Zhang, L., & Chen, D. (2021). Can reservoir regulation mitigate future climate change induced hydrological extremes in the Lancang-Mekong River Basin? *Science of the Total Environment*, *785*, 147322. https://doi.org/10.1016/j.scitotenv.2021.147322

Yuting, Y., McVicar, T. R., Donohue, R. J., Zhang, Y., Roderick, M. L., Chiew, F. H. S., et al.

(2017). Lags in hydrologic recovery following an extreme drought: Assessing the roles of climate and catchment characteristics. *Journal of the American Water Resources Association*, *53*, *4821–4*. https://doi.org/10.1111/j.1752-1688.1969.tb04897.x

Zaherpour, J., Gosling, S. N., Mount, N., Schmied, H. M., Veldkamp, T. I. E., Dankers, R., et al. (2018). Worldwide evaluation of mean and extreme runoff from six global-scale hydrological models that account for human impacts. *Environmental Research Letters*, *13*(6). https://doi.org/10.1088/1748-9326/aac547

Zeng, Y., Zhenghui, X., Yan, Y., Shuang, L., Linying, W., Jing, Z., et al. (2016). Journal of Advances in Modeling Earth Systems. *Journal of Advances in Modeling Earth Systems*, *8*, 1358–1375. https://doi.org/10.1002/2016MS000625

Zeng, Y., Xie, Z., Liu, S., Xie, J., Jia, B., Qin, P., & Gao, J. (2018). Global Land Surface Modeling Including Lateral Groundwater Flow. *Journal of Advances in Modeling Earth Systems*, *10*(8), 1882–1900. https://doi.org/10.1029/2018MS001304

Zhang, R., Kim, S., & Sharma, A. (2019). A comprehensive validation of the SMAP Enhanced Level-3 Soil Moisture product using ground measurements over varied climates and landscapes. *Remote Sensing of Environment*, *223*(January), 82–94. https://doi.org/10.1016/j.rse.2019.01.015

Ziv, G., Baran, E., Nam, S., Rodríguez-Iturbe, I., & Levin, S. A. (2012). Trading-off fish biodiversity, food security, and hydropower in the Mekong River Basin. *Proceedings of the National Academy of Sciences of the United States of America*, *109*(15), 5609–5614. https://doi.org/10.1073/pnas.1201423109